Evolutionary Ecology of Loricariid Catfishes

by

Corinthia Ray Black

A dissertation submitted to the Graduate Faculty of
Auburn University
in partial fulfillment of the
requirements for the Degree of
Doctor of Philosophy

Auburn, Alabama
August 6, 2022

Keywords: morphology, geometric morphometrics, modularity, phylogenetic comparative methods, stable isotopes, South America

Approved by

Jonathan W. Armbruster, Chair, Professor of Biological Sciences and Director of Auburn University Museum of Natural History
Moises A. Bernal, Assistant Professor of Biological Sciences
Jamie R. Oaks, Assistant Professor of Biological Sciences
Daniel A. Warner, Associate Professor of Biological Sciences

Abstract

How extrinsic (like functional constrains and ecological interactions) and intrinsic (like modularity and integration) interactions drive diversification is a formative area of evolutionary biology. In this dissertation, I explore the phenotypic diversification of the armored catfishes using geometric morphometrics, stable isotope analyses, and phylogenetic comparative methods. I found that the armored catfish body is highly modularized, with varying degrees of integration between each module, suggesting that interactions within and between modules influence morphological evolution. Additionally, slight changes in modularity and integration patterns in clades may have allowed for diversification along a specific trajectory. When focused on the oral jaw shape, I found that traditional and automated processes captured shape more effectively when all jaw components were combined. Although ecological traits do not play a role in jaw shape, there was a correlation between clades with diverse diets and fast evolutionary rates of shape. These results suggest that shape is not constrained to diet and that similarly shaped jaws coupled with different types of teeth could allow the fishes to feed on a wide range of materials. Finally, I built a vector-based analysis, baseline-standardized isotopic vector analysis (BaSIVA) to visualize dietary variation while accounting for isotopic discrepancies between locations. Results from BaSIVA delineate trophic groups better than traditional trophic positioning methods while accounting for variation in basal resources, suggesting BaSIVA should be the standard for vector-based stable isotope analysis in riverine environments with similar baseline resources.

Acknowledgements

During my Ph.D. I have heard others say that you cannot complete a dissertation without the help of many others. I cannot overstate how true this is. To Dr. Steve O'Kane, whether you know it or not, you were the first to introduce me to the concept of evolution and push me to think more about how life on this planet diversified. To Drs Peter Berendzen and Jonathan Armbruster, you both took a risk accepting me into graduate programs despite my poor undergraduate performance. You both provided me with the freedom to explore my academic interests. My committee members, Drs Moises Bernal, Jamie Oaks, and Daniel Warner have pushed me to think creatively about solutions when projects did not go as planned.

Many colleagues have taken the time to discuss ideas and contribute to the work in this dissertation. This includes, but is not limited to, Milton Tan, Aaron Olsen, Nathan Lujan, Vanessa Meza Vargas, Dario Faustino, Junior Chuctaya, David Werneke, Erling Holm, David Brooks, Edward Burress, and Beth Brainerd. Many friends and lab members kept me grounded and provided a much-needed social network, including Akila Abesinghe, Courtney Weyand, Dan Akin, Dave Werneke, Malorie Hayes, and Charles Stephen. The Red Wolf School of Martial Arts and those I trained with are responsible for fostering a life-long love of Muay Thai while providing me an outlet to burn off excess stress and anxiety. I want to give special thanks to Coach Dude for believing in me and pushing me outside of my comfort zone.

Thank you, to my parents and sister, for always believing I would make it this far. My cats have provided unconditional love and warmth throughout these years, and I will miss the ones we have lost during my Ph.D. I will miss the ones we lost over the years and continue to love the ones we still have. Special thanks to my partner of fifteen years, Jared Wheetley. This

path would have been more difficult if I had gone it alone. Your love, support, and patience have allowed me to fulfill my goal of becoming the biologist I am today.

Table of Contents

List of Abbreviations

3D	Three-dimensional
ACSIVA	Assemblage centroid-standardized isotope vector analysis
BaSIVA	Baseline-standardized isotopic vector analysis
CR	Covariance ratio
CSD	circular standard deviation
GM	Geometric Morphometrics
GPA	Generalized least squares Procrustes superimposition
MS-222	tricaine methanesulfonate
MYA	Million years ago
PaCA	Phylogenetically-aligned component analysis
PCA	Principal component analyses
PGLS	Phylogenetic generalized least squares
PLS	Partial least squares
SS	Sums of squares

List of Tables

List of Figures

Chapter 1

Chapter 2

General Introduction

Identifying the evolutionary forces driving form has been a significant part of evolutionary biology. Across taxa, evolutionary biologists have discovered that form is influenced by extrinsic and intrinsic factors, like biomechanical constraints, natural selection, ecological interactions, modularity, and integration (Wake and Larson 1987; Gould 2002; Adams and Nistri 2010; Sanger et al. 2012; Du et al. 2019; Evans et al. 2019). Yet, questions of how certain groups of animals have diversified remain. For example, catfishes make up 10% of all fishes but have been understudied. The most species-rich family in the order of Siluriformes is the Loricariidae. Commonly called the suckermouth armored catfishes, the group comprises over 1000 recognized species in 100 genera (Armbruster et al. 2018; Fricke et al. 2022). Within some small geographic regions local diversity is substantial, with upwards of 30 interacting species. Three traits allow the identification of this Neotropical family; ossified dermal plates that cover the body, integumentary teeth known as odontodes on bony plates and fin rays, and a ventral oral disk used in feeding and adhering to objects in their habitats (Adriaens et al. 2009; Garg et al. 2010; Geerinckx et al. 2011; Lujan and Armbruster 2012a). Widespread throughout Costa Rica, Panama, and tropical to subtropical South America, the ecomorphologically diverse family is a fascinating group for analyses of shape evolution.

The common thread of this dissertation is to examine the factors that lead to the considerable morphological diversity in loricariid catfishes. In chapter 1 – *Integration and modularity in the diversity of the suckermouth armored catfishes*, I use three-dimensional geometric morphometrics, phylogenetic comparative methods, and modularity and integration tests to visualize body shape and its relationship to extrinsic and intrinsic factors. Schaefer and

Lauder (1986, 1996) postulated that the loss of biomechanical couples led to increasing diversity of loricariid oral jaws. The decoupling of the interoperculo-mandibular ligament suggests there has been an increase in morphological modules that may evolve somewhat independently of one another, helping to drive diversification within the group. Since this discovery by Schaefer and Lauder (1986, 1996), our knowledge of the phylogenetic relationships of loricariid catfishes has increased along with new methods to study shape, modularity and integration tests, and phylogenetic comparative methods have allowed me to examine loricariid body shape in three dimensions and whether modularity may be a cause of loricariid diversity.

Chapter 2 – *Chew on this: Oral jaw shape is not correlated with diet type in Loricariid catfishes,* further explores the relationship between diet and jaw shape using three-dimensional oral jaw shape from CT scans. The oral jaws are highly variable in loricariid catfishes, with the jaws ranging from no teeth to over 200. Being both complex morphologically and biomechanically, and it has been difficult to study the anatomy of the oral jaws in loricariids. In chapter 2, I devise a method to examine loricariid jaws in three dimensions. Results suggest that the jaws evolve independently to diet type suggesting that different jaw shapes are capable of eating different foods depending on the types of teeth that they have. The Hypostominae, where greater trophic diversity is observed, has faster rates of oral jaw evolution suggesting that jaws can change quickly to accommodate different diets.

In chapter 3 – *New method of isotopic analysis: Baseline-standardized isotope Vector analysis show trophic partitioning in loricariids*, I develop a new approach to analyze stable isotopes in difficult to partition species with similar diets. One issue with studying loricariids is that gut content analysis is not particularly useful. Most loricariid guts contain an amorphous mix of materials that is difficult to identify. Additionally, if the food is identifiable, it may not be

what loricariids are assimilating into their body. For example, some loricariids consume wood but have been shown to be incapable of digesting it. Instead, loricariids are consuming the microorganisms that live in and consume the wood (German 2009; McCauley et al. 2020). Lujan et al. (2012) attempted to solve this issue by examining stable isotopes to categorize diets among loricariids. Stable isotopes detect what has been assimilated by the organisms, but they are not comparable across locations due to differences in the baseline level of nutrients in the environment. The ACSIVA approach by Lujan et al. (2012) allowed for comparison of different communities, but it had flaws that kept the method from being used. In chapter 3, I present a refinement of the technique, BaSIVA, that takes into account the basal resources available to the fishes. This technique provides the possibility of comparing diets of loricariids across their range.

Taken all together, this dissertation integrates diet, morphology, and phylogeny to understand the diversification of loricariid catfishes. It builds upon studies to discern the causes of diversity that began with Schaefer and Lauder (1986, 1996), Lujan and Armbruster (2012), and Lujan et al. (2012); however, there is still more to explore and will require broader phylogenies and more morphological and ecological data.

References

Adams DC, Nistri A. 2010. Ontogenetic convergence and evolution of foot morphology in European cave salamanders (Family: Plethodontidae). BMC Evol Biol 10:216.

Adriaens D, Geerinckx T, Vlassenbroeck J, Van Hoorebeke L, Herrel A. 2009. Extensive Jaw Mobility in Suckermouth Armored Catfishes (Loricariidae): A Morphological and Kinematic Analysis of Substrate Scraping Mode of Feeding. Physiological and Biochemical Zoology 82:51–62.

Armbruster JW, van der Sleen P, Lujan NK. 2018. Family Loricariidae - Suckermouth Armored Catfishes. In: van der Sleen P, Albert JS, editors. Field Guide to the Fishes of the Amazon, Orinoco, & Guianas Princeton University Press. p. 253–54.

Du TY, Tissandier SC, Larsson HCE. 2019. Integration and modularity of teleostean pectoral fin shape and its role in the diversification of acanthomorph fishes. Evolution 73:401–11.

Evans KM, Vidal-García M, Tagliacollo VA, Taylor SJ, Fenolio DB. 2019. Bony Patchwork: Mosaic Patterns of Evolution in the Skull of Electric Fishes (Apteronotidae: Gymnotiformes). Integrative and Comparative Biology 59:420–31.

Fricke R, Eschmeyer WN, Fong J. 2022. Eschmeyer's Catalog of Fishes. (http://researcharchive.calacademy.org/research/ichthyology/catalog/SpeciesByFamily).

Garg TK, Valdez Domingos FX, Almeida-Val VMF, Val AL. 2010. Histochemistry and functional organization of the dorsal skin of Ancistrus dolichopterus (Siluriformes: Loricariidae). Neotropical Ichthyology.

Geerinckx T, Herrel A, Adriaens D. 2011. Suckermouth armored catfish resolve the paradox of simultaneous respiration and suction attachment: a kinematic study of Pterygoplichthys

disjunctivus. Journal of Experimental Zoology Part A: Ecological Genetics and Physiology.

German DP. 2009. Inside the guts of wood-eating catfishes: Can they digest wood? Journal of Comparative Physiology B: Biochemical, Systemic, and Environmental Physiology 179:1011–23.

Gould SJ. 2002. The structure of evolutionary theory Cambridge: Harvard University Press.

Lujan NK, Armbruster JW. 2012. Morphological and functional diversity of the mandible in suckermouth armored catfishes (Siluriformes: Loricariidae). Journal of Morphology 273:24–39.

Lujan NK, Winemiller KO, Armbruster JW. 2012. Trophic diversity in the evolution and community assembly of loricariid catfishes. BMC Evolutionary Biology 12:124.

McCauley M, German DP, Lujan NK, Jackson CR. 2020. Gut microbiomes of sympatric Amazonian wood-eating catfishes (Loricariidae) reflect host identity and little role in wood digestion. Ecology and Evolution 10:7117–28.

Sanger TJ, Mahler DL, Abzhanov A, Losos JB. 2012. Roles for modularity and constraint in the evolution of cranial diversity among *anolis* lizards: *anolis* skull shape and modularity. Evolution 66:1525–42.

Schaefer SA, Lauder GV. 1986. Historical Transformation of Functional Design: Evolutionary Morphology of Feeding Mechanisms in Loricarioid Catfishes. Systematic Zoology 35:489–508.

Schaefer SA, Lauder GV. 1996. Testing historical hypotheses of morphological change: biomechanical decoupling in loricarioid catfishes. 50:1661–75.

Wake DB, Larson A. 1987. Multidimensional Analysis of an Evolving Lineage. Science 238:42–48.

Chapter 1 – Integration and modularity in the diversity of the suckermouth armored catfishes

Submitted to Royal Society Open Science

Abstract

The evolution of morphological diversity has held a long-standing fascination among scientists. In particular, do bodies evolve as single, integrative units, or do different body parts evolve semi-independently (modules). Suckermouth armored catfishes have a unique morphology that lends nicely to modularity and integration studies. In addition to a ventrally facing oral jaw that directly contacts surfaces, the neurocranium and pectoral girdle are fused, which limits movement of the anterior part of the body. Jaw operation includes both losses of and novel biomechanical connections, which allow jaw rami to operate separately. With food manipulation primarily located within the head, it would seem likely that the head and body may act as separate modules that can evolve independently; for example, similar jaw morphologies may be found in different body shapes or vice versa. If true, one would expect to see a two or three-module system where the head and body are morphologically distinct. To test this hypothesis, we quantified shape using geometric morphometric analysis and assessed the degree of modularity across functionally important regions. Body shape was highly correlated to phylogenetic relationships, although subfamilies diverged from one another early in their evolutionary history. Within each subfamily, there are various levels of diversification. Surprisingly, we found that the armored catfish body is highly modularized, with varying degrees of integration between each module. Within subfamilies, there are different patterns of modularity and integration, suggesting that the various patterns may have driven diversification along a single trajectory in each

subfamily. This study suggests the evolution of armored catfish diversification is complex, with morphological evolution influenced by interactions within and between modules.

Introduction

The evolution of morphological diversity is often influenced by extrinsic factors, like functional constrains and ecological interactions [1–3]. However, intrinsic properties, such as modularity and integration, have been shown to enhance or constrain the evolution of form [4–6]. Modularity and integration are closely related concepts that investigate how different units within an organism correlate to one another [7]. Although these concepts are closely related, modularity refers to how parts of the body change as independent units, whereas integration describes the coordinated interactions between parts of the body where changes in one area effect the changes in another [8]. Modularity has been hypothesized to accelerate diversification, as independent modules have the ability to evolve separately from one another. Integration, on the other hand, has been hypothesized to constrain the evolution of form due to the tight interactions of parts that prevent rapid changes; however, it has been linked to increased diversity along a single trajectory [9].

Additionally, integration and modularity are not all or nothing concepts, but more a matter of degree. For example, Klingenberg et al. [10] discovered that the lower jaw of the mouse skull has distinct modules, however they are not completely independent of each other. Although the alveolar region is distinct from the ramus, changes in one will affect changes in the other to some degree. This type of relationship has been seen in fishes, where African cichlids, a clade known for rapid radiation, shows integration between the oral and pharyngeal jaws. Integration between modules was previously hypothesized to limit the evolvability of

morphology but seems to work as a feature to promote radiations in cichlids [11]. Integration of modules may mean that changes to accommodate one life history function, such as feeding, may have broad effects across the morphology of the organism. This subsequently may allow for broader ecological change stemming from a simple change in one module. Such modularity and integration would suggest that convergence in one module may lead to corresponding similar changes throughout the integrated modules.

Geography and subsequent changes of said geography can also attribute to diversification within animals. In South America, highland areas include the very old Brazilian and Guiana Shields (part of the Amazon craton) and the much younger Andes mountains, which are separated from one another by lowlands that have been occasionally flooded by marine incursions. With limited dispersal for upland fauna between the Brazilian and Guiana shields and between the shields and Andes, the interplay of modularity and integration sets up a system whereby convergence in body form is likely to occur.

One group of neotropical fishes that are incredibly diverse in morphology and ecology, are the suckermouth armored catfishes, or the family Loricariidae. Consisting of over 1000 species in 100 genera, loricariids are considered the most species-rich family in the order of Siluriformes [12]. Many new species are described each year, making the loricariid catfishes a dynamic and growing group of freshwater fishes. The family is monophyletic and united by three traits; ossified dermal plates that cover the body, integumentary teeth known as odontodes on bony plates and fin spines, and a ventral oral disk used in feeding and to adhere to objects in their habitats [13–16].

The unique morphology and evolutionary history of armored catfishes lends nicely to modularity and integration studies. Most loricariids feed by scraping their jaws along surfaces to

remove attached particles or to comb for loose bits of food. The jaws are remarkably diverse with some species lacking teeth, whereas others have teeth ranging from just one large tooth per jaw ramus to over 200 small teeth. The shape of the teeth are normally villiform, but some are spoon-shaped that are used for scraping bits of wood, whereas others are elongate that may be used to scoop snails or caddis flies from their shells.

Schaefer and Lauder [17,18] proposed a set of significant decouplings (as well as new biomechanical couples) in loricariid catfishes. These changes are hypothesized to have functionally decoupled the jaws; a new division of the adductor mandibulae operates the premaxillae, and the left and right lower jaws are decoupled from one another and can move independently. Furthermore, the jaws lost a coupling of the opercular complex (interopercular-mandibular ligament), although that couple appears to have re-evolved multiple times [19]. In addition to a ventrally facing oral jaw that directly attaches to surfaces, the neurocranium and pectoral girdle are fused, which limits movement of the anterior part of the body.

With the jaws ability to move independent of the skull and the limitations to movement within the neurocranium and pectoral girdle, it would appear that changes in jaw, head, and postcranial morphology could act as separate modules that could evolve somewhat independently of one another. This gives the possibility of swapping jaw modules without considerable changes to much of the rest of the anatomy. However, integration may still play a role, as there are limitations to form. For example, a long dentary bone in a narrow head would not logically be possible. This suggests that changes in jaw morphology could lead to a series of changes elsewhere in the body. To test for the degree of modularity and integration across functionally important regions within the armored catfishes, we quantified shape using geometric

morphometric analysis and found that loricariids are highly modular with varying degrees of integration between the modules.

Materials and methods

Data collection

A total of 209 specimens representing 71 species within the Loricariidae were photographed from various fish collections. Four subfamilies were represented by the following number of species; Hypoptopomatinae *n* = 6 (255 total species), Hypostominae *n* = 50 (498 total species), Lithogeninae *n* = 1 (3 total species), and Loricariinae *n* = 13 (258 total species). Thirty-three landmarks that capture overall body shape were modified from Armbruster [20] (Fig. 1). The landmarks were reconstructed into a three-dimensional (3D) space using stereo camera reconstruction in the R package StereoMorph for three to five individuals per species (Table 1) [21]. Two cameras (Nikon D90 DSLR attached to a copy stand and a Canon Rebel XSi DSLR attached to a tripod) were positioned at an approximately 35-degree angle from one another and calibrated in space using an 8x6, 180-pixel checkerboard. To avoid movement of the camera positions, photos were taken using a wireless remote and autofocus was turned off for the session. Specimens were held in place using molding clay to avoid movement of the specimen and align the specimen properly. Each specimen was photographed in two aspects, a dorsal and ventral view, to capture the maximum shape variation with landmarks.

Shape analysis

Specimens were superimposed using a generalized least squares Procrustes superimposition to remove non-shape related information (orientation, translation, size) in the R package geomorph ver. 4.0.1 [22,23]. Superimposed landmarks were averaged in the base

package in R [24] for each species and a multivariate analysis was performed through a principal component analysis (PCA). The significant axes were found using the broken stick method in the R package PCDimension and principal component backtransformations were generated for significant axes to view the theoretical shape of the morphospace for both ventral and lateral views [25–29].

Phylomorphospaces for two well supported phylogenies [30,31] were generated in the R package geomorph to explore the evolutionary trends in the loricariid body shape [22,23]. This method projects evolutionary relationships onto a shape space and estimates the ancestral shapes for the nodes to help visualize patterns in shape change across a phylogeny [32]. Phylogenies were downloaded from the respective supplemental materials and non-corresponding specimens were pruned from each tree in the R package ape [33]. Significant axes were found and backtransformations to visualize shape change were generated for each phylogeny. After pruning, the phylogeny generated by Lujan and others [30] had 49 corresponding species, covering four subfamilies, whereas the phylogeny generated by Roxo and others [31] had 30 corresponding species covering three subfamilies. Although the Lujan et al. [30] phylogeny had better coverage, the Roxo et al. [31] phylogeny is time-calibrated and represents a majority of species variation. The phylogenetic signal for each phylogeny was calculated using the Kmult method in geomorph, and the phylogenetic signal for each subfamily was found for the Lujan et al. [30] phylogeny [22,23].

Because the Lujan et al. [30] phylogeny covered a broader number of species, we assessed convergence and ecological correlation across the phylomorphospace. To determine if closely placed species converged in shape, we identified a group of species from different clades (*Corumbataia tocantinensis*, *Isorineloricaria spinosissima*, *Exastilithoxus* sp., and *Lithogenes*

villosus) in the morphospace and preformed convergence tests in convevol in R [34]. Using the function convnum, an ellipse was placed around the convergent taxa and the number of times a lineage crossed the ellipse was calculated. If a lineage (node to the tip of the phylogeny) crosses the ellipse, the respective taxa are suggested to be convergent [34]. To estimate the probability that shape variation is attributed to ecological factors, we collected ecological data from primary literature and aquarist websites and preformed phylogenetic generalized least squares (PGLS) for all specimens and each subfamily in geomorph using the procD.pgls function [22,35,36]. Ecological factors included diet, type of vegetation the species was found in, type of riverine habitat, and if the species is found primarily on sand or not. Due to inconsistencies in diet type between the literature and hobby aquarists, we included both in analyses. Because PGLS uses permutation tests instead of the standard variance-covariance matrix to generate p-values, collinearity between factors does not cause variance inflation. This means we can include both diet type from the primary literature and diet type from aquarists in our linear models without discrepancies in p-values [22,35,36]. Our linear models used type III (marginal) sums of squares (SS) as the order of factors in the linear model does not affect the outcome because the effect of each variable is evaluated after other factors.

To understand how morphological disparity changed over time, we calculated distance based morphological disparity using code modified from Stanley [37] at thirty-one time points along the time calibrated phylogeny [31]. Subfamilies were isolated and morphological disparity was calculated for these subsets. To calculate the disparity through time, ancestral shapes were reconstructed within a chronophylomorphospace, where the distance between the nodes were used to estimate ancestral disparity. Based on the overall disparity scores in the clade, an

increase of divergence greater than ten between two subsequent time points was determined to be a burst of divergence.

Modularity and integration

We tested ten *a priori* modularity model structures that ranged from fully integrated (one module) to highly parameterized (seven modules, Fig 1). Hypotheses were based on an understanding of armored catfish morphology and previous modular hypotheses for similar fishes (Table S1) [38]. To investigate patterns of modularity across the loricariid body, we used two approaches: a phylogenetically corrected Evaluating Modularity with Maximum Likelihood (EMMLiv2) and a covariance ratio (CR) analysis [39–41]. All further analyses used the Lujan et al. [30] phylogeny. EMMLiv2 uses maximum likelihood to test different modularity hypotheses and calculates the between and within-module correlations for the best fit model to evaluate the degree of interrelatedness [41–43]. However, EMMLi has been found to favor parameterized models over smaller ones, and does not explicitly test modularity hypotheses, so to support these findings, we used a CR method. Covariance ratio measures covariation between hypothesized modules [38,39]. Using the compare.CR function in geomorph, we tested for the best model and observed phylogenetically corrected patterns of modularity by using the phylo.modularity function for the best supported model for all species and each subfamily [39]. An evolutionary rate ratio was used to calculate evolutionary rates among modules. Phylo.modularity calculates a ratio between multivariate rates, which are estimated for each module by replicating datasets along a phylogeny using a single rate Brownian motion model [38,44,45]. Lower values suggest greater modularity, where a CR = 1 suggests no modularity. Values above one mean covariance between modules exceed the covariance within the modules. To test for integration between modules, we ran a phylogenetically corrected patterns of integration using phylo.integration for

the best supported model for the whole family and each subfamily [39]. Phylo.integration calculates the average pairwise partial least squares (PLS) under a Brownian motion model. rPLS closer to 0 suggests there is no integration between modules, whereas values closer to one suggest there is full integration between modules.

We used the compare.multi.evol.rates function in geomorph to test for the evolutionary rates of each module for the best supported model for the family and each subfamily. To further understand the evolutionary rates of morphological change for each species and their ancestors, we performed a phylogenetically-aligned component analysis (PaCA) to identify shape changes related to phylogenetic signal for the whole family. PaCA aligns shape data to the axis of greatest phylogenetic signal, maximizing shape variation related to phylogenic relationships on the first component [46]. This allowed us to maximize evolutionary rates along the first component. Evolutionary rates were calculated for significant PaCA axes (determined with the same broken stick method mentioned above) using a penalized-likelihood model in the R package, phytools. This model uses Brownian motion with a penalty term that is equal to the log-transformed probability density multiplied by an intermediate smoothing coefficient ($\lambda = 1$) to calculate evolutionary rates [47,48]. The evolutionary rates were calculated across the Lujan et al. [30] phylogeny for the total shape and each separate module to test for differences among modules.

Results

(A) Shape is driven by phylogenetic relationships

The morphospace of loricariids showed clear separation between subfamilies, with the broken stick method finding two significant axes of shape variation (~72.0% of variation) (Fig

2). The first axis described ~63.0% of the variation in shape, where individuals on the negative end had thicker, deeper bodies, thicker caudal peduncles, larger oral disks, and larger eyes. Individuals on the positive end of the first axis were slim and dorsoventrally compressed, with long, thin caudal peduncles, a smaller oral disk, and smaller eyes. The second axis described ~9.0% of the overall variation in shape, which explained the placement of the eye. On the negative end, the eyes were placed more dorsally on the head, generally facing upwards, whereas the eyes on the negative end of the second axis were laterally placed, toward the middle of the head. The subfamily, Hypostominae grouped together toward the negative ends of both axes, whereas the Loricariinae grouped together toward the positive end of the first axis and negative end of the second axis. The Hypoptopomatinae were the most widespread subfamily across the morphospace, but primarily grouped toward the positive end of the second axis. The subfamily, Lithogeninae was represented by one species which fell close to the intermediate shape (~x = 0.05, and y = 0) on the morphospace.

When the morphospace was trimmed to fit phylogenetic hypotheses, the broken stick methods found three significant axes for the Lujan et al. [30] phylogeny and two significant axes for the Roxo et al. [31] phylogeny (Fig 3, S1-S4). Shape variation across both phylomorphospaces were similar to the morphospace described above; however, the phylomorphospace based on the Lujan et al. [30] phylogeny showed additional changes in shape on the third axis, with the body shape being more compressed but thicker with smaller eyes on the dorsal part of the head and a wider oral disk on the negative end (Fig S3). On the positive end of the third axis, individuals were deeper bodied and thinner with larger more laterally placed eyes and a smaller oral disk (Fig S3). The observed phylogenetic signal for both phylogenies were significantly strong; The Lujan et al. [30] phylogeny had a K value of 1.1134 (p = 0.001)

and the Roxo et al. [31] phylogeny had a K value of 1.1846 (p = 0.001). Within subfamilies, there were varying levels of phylogenetic signal for the Lujan et al. [30] phylogeny. The Hypostominae had a significant observed phylogenetic signal of K = 0.54 (p = 0.001), whereas Hypoptopomatinae and Loricariinae had insignificant K values of K = 0.96 (p = 0.1235) and K = 1.25 (p = 0.062) respectively.

Although subfamilies tend to cluster together, a few species from different clades seemed to converge in the intermediate shape space. The ellipsis covered an area of 3.797^{e-4} with all four species (*Corumbataia tocantinensis*, *Isorineloricaria spinosissima*, *Exastilithoxus* sp., and *Lithogenes villosus*) crossing the ellipsis (Fig S5). Convergent evolution was quantified using the C1, C2, C3, and C4 measures as described by Stayton (2015) where the observed values are as follows; C1 = 0.737 (p = 0), C2 = 0.081 (p = 0), C3 = 0.348 (p = 0), and C4 = 0.035 (p = 0). To further explore convergent evolution between and within the subfamilies, we performed a PGLS for all specimens and for each subfamily. Phylogenetic linear models showed no significant correlation between ecological traits and shape for all specimens, just Hypostominae, just Hypoptopomatinae, and just Loricariinae (Table S2).

(B) Between subfamily divergence was fast

Overall, there were three major bursts of shape divergence across all species (Fig 4, Table S3). The first happened primarily in the Oligocene, ~36–23 million years ago (MYA), when the subfamily Loricariinae diverged from the other subfamilies, Hypoptopomatinae and Hypostominae. This was followed by two bursts in disparity in the middle Miocene, ~14 and 11–10 MYA. Within the subfamilies, change in disparity varied in timing and speed. The Hypoptopomatinae was the earliest family to diverge ~28 MYA, with two quick bursts of disparity at ~27 (disparity = 13.37) and 23 MYA (disparity = 12.08) followed by a slow

divergence for a total disparity of 30.46. This was followed by the Loricariinae which began to diverge ~23 MYA. Whereas the Hypoptopomatinae underwent fast changes in disparity, the Loricariinae experienced slow changes over time, steadily increasing to an overall disparity of 15.39. The Hypostominae was the latest to diverge ~14 MYA, experiencing a steady increase in diversity, followed by one major burst in disparity at about 10 MYA (disparity = 11.87) and a subsequent steady increase for a total disparity of 43.4. Overall the Loricariinae was the least disparate, whereas the Hypostominae was the most disparate subfamily.

(C) Integration between modules may drive diversification

Family Level. Phylogenetically corrected EMMLi analyses recovered the seven separate modules model as the best supported (Table S4). The pelvic fins (0.77), cloaca (0.84), and caudal peduncle (0.91) had strong within covariance, whereas the anal area and caudal peduncle (0.81) had strong between covariance (Fig 5a, Table S5). Because EMMLi tends to prefer the most parametrized model, we further tested model fit using a CR based method which recovered the seven-module model as the best supported. Modularity tests recovered a slightly modular morphology (CR = 0.79, p = 0.001) (Fig S6). Pairwise CR suggest that the majority of the modules show some modularity; however, the caudal peduncle had high covariance with four separate modules, the opercula (CR = 1.04), the pectoral and dorsal fins (CR = 1.25), the pelvic fins (CR = 1.1), and the anal area (CR = 1.4). As these values are greater than one, this suggests the covariance between modules exceeds covariance within each module, which suggest modules are highly integrated (Table S6). Integration tests for the best supported model found that there was some integration between modules (r-PLS = 0.73, p = 0.001). All pairwise r-PLS were significant (p = 0.001-0.002) and show varying amounts of integration between modules (Table S6). Most modules have an intermediate amount of integration. Some modules show strong

integration; the mouth and head (r-PLS = 0.77, p = 0.001), the head and opercula (r-PLS = 0.81, p = 0.001), the head and pectoral/dorsal fin (r-PLS = 0.86, p = 0.001), the opercula and pectoral/dorsal fin (r-PLS = 0.81, p = 0.001), and the caudal peduncle with all modules (mouth at r-PLS = 0.76; head at r-PLS = 0.76; opercula at r-PLS = 0.81; pectoral/dorsal fin at r-PLS = 0.88; pelvic fins at r-PLS = 0.82; and the anal area at r-PLS = 0.86). The evolutionary rates for each module were similar to one another, with the exception of the caudal peduncle that was unusually high at a rate of 2.02^{e-05}. The mouth (4.10^{e-06}), head (4.29^{e-06}), and opercula (3.21^{e-06}) had the lowest rates, followed by the pectoral and dorsal fins (6.55^{e-06}), pelvic fins (4.96^{e-06}), and anal area (6.57^{e-06}) (Fig S7).

Subfamily level. To examine modularity and integration patterns within subfamilies, we tested model fit using a CR based method. The subfamily Hypostominae recovered a four-module model as the best supported (CR = 0.78, p = 0.001); where module 1 = mouth, module 2 = head and opercula, module 3 = pectoral, dorsal, and pelvic fins, and module 4 = anal area and caudal peduncle. Pairwise CR suggest most modules show some modularity with the exception of the tail and midbody which had high covariance (CR = 1.07) (Table S7). Integration tests for the best supported model found that there was some integration between modules (r-PLS = 0.797, p = 0.001). All pairwise r-PLS were significant (p = 0.001-0.006). Some modules show strong integration; the mouth with the tail region (rPLS = 0.76), the head/opercula with the tail (rPLS = 0.78), and the midbody with the tail (rPLS = 0.92). Evolutionary rates for each module were similar to one another, with the exception of the tail region that was high at a rate of 1.28e-05 (p = 0.014). The mouth (4.31e-06), head/opercula (4.44e-06), and midbody (5.95e-06) had the lowest rates (Fig S7).

The best supported model for the subfamily Hypoptopomatinae was a seven-module model (CR = 0.88, p = 0.001), the same model that was found to be best supported across the family. Pairwise CR suggest most modules show some modularity between one another, and many modules had very high covariance. The pectoral and dorsal fins had high covariance with the head (CR = 1.03) and the opercula (CR = 1.07), and the pelvic fins had high covariance with the anal area (CR = 1.05). Additionally, the caudal peduncle had high covariance with the pectoral and dorsal fins (CR = 1.13) and the anal area (CR = 1.21) (Table S8). Modules that had low covariance, suggesting stronger modularity between modules, were the mouth with the anal area (CR = 0.56) and the caudle peduncle (CR = 0.44). Integration tests for the best supported model were insignificant (r-PLS = 0.83, p = 0.21), with only one pairwise r-PLS values as significant (caudal peduncle with the anal area with a rPLS = 0.95, p = 0.047). The evolutionary rates for each module were similar to one another with the exception of the caudal peduncle; however, these observed rates were not significant (p = 0.47).

For the subfamily Loricariinae, the best supported model was the seven-module model (CR = 0.88, p = 0.001), the same model that was found to be best supported for Hypoptopomatinae and the whole family. Pairwise CR suggests most modules show some modularity, yet some modules had high covariance. The pectoral and dorsal fins had high covariance with the head (CR = 1.05) and with the pelvic fins (CR = 1.07). The caudal peduncle had high covariance with the mouth (CR = 1.12), the opercula (CR = 1.07), and the anal area (CR = 1.13) (Table S9). Modules that had low covariance were the anal area with the pectoral and dorsal fins (CR = 0.52) and the pelvic fins (CR = 0.48). Integration tests for the best supported model found that there was some integration between modules (r-PLS = 0.808, p = 0.002). Some pairwise r-PLS were significant and show high integration between modules;

mouth with the anal area (rPLS = 0.90, p = 0.018) and caudal peduncle (rPLS = 0.95, p = 0.008); the head with the pectoral and dorsal fins (rPLS = 0.95, p = 0.003) and pelvic fins (rPLS = 0.96, p = 0.003); the opercula with the pectoral and dorsal fins (rPLS = 0.82, p = 0.028), the pelvic fins (rPLS = 0.86, p = 0.037), and the caudal peduncle (rPLS = 0.90, p = 0.012); the pectoral and dorsal fins with the pelvic fins (rPLS = 0.92, p = 0.006); the pelvic fins with the caudal peduncle (rPLS = 0.81, p = 0.050); and the anal area with the caudle peduncle (rPLS = 0.88, p = 0.003). Evolutionary rates show the most variability between modules than all other subfamilies, including the total family (Fig. S7). The modules with the fastest evolutionary rates were the anal area (9.61e-06) and the caudal peduncle (1.10e-05). The pectoral and dorsal fins (4.72e-06) were similar to the pelvic fins (2.87e-06), with a moderately fast evolutionary rate. The modules with the slowest rates were the mouth (2.26e-06), the head (7.88e-07), and the opercula (1.32e-06).

Species level. To further explore evolutionary rates of each species we maximized evolutionary rates along the first component though PaCA. Shape variation was similar to previous PCAs; however, this method placed 97.6% and 98.2% of the total shape variation on the first axis for the Lujan et al. [30] and Roxo et al. [31] phylogenies respectively (Fig S9). There was no unique pattern to evolutionary rates for the total shape nor the rates for each module. For the total shape *Oxyropsis acutirostra* had the highest rate (2.2^{e-03}), whereas *Lithogenes villosus* had the lowest (4.3^{e-10}) (Fig S10, Table S10). *Lithogenes villosus* had the slowest rates for each module (mouth = 2.8^{e-10}, head = 1.5^{e-10}, opercula = 6.9^{e-12}, pectoral and dorsal fins = 1.4^{e-11}, pelvic fins = 2.8^{e-10}, caudal peduncle = 4.0^{e-10}), except for the anal area where *Lasiancistrus schomburgkii* was the slowest (4.4^{e-08}). The species with the highest rates varied for each module: for the mouth *Farlowella curtirostra* at 3.7^{e-04}, for the head *Hypostomus niceforoi* at 5.8^{e-04}, for the opercula *Oxyropsis acutirostra* at 1.9^{e-04} , for the pectoral and dorsal

fins *Farlowella curtirostra* at 3.7^{e-04}, for the anal area *Isorineloricaria spinosissima* at 3.0^{e-04}, and for the caudal peduncle *Oxyropsis acutirostra* at 8.7^{e-04} (Fig S11, Table S10).

Discussion

The armored catfish body shape is highly correlated to phylogenetic relationships across the family but show different patterns of evolution within subfamilies. The loricariid subfamilies diverged early from one another and show various levels of diversification within. Surprisingly, we found that the armored catfish body is highly modularized, with varying degrees of integration between each module, which suggests the evolution of armored catfish diversification is complex and morphological evolution is influenced by interactions within and between modules.

Body shape is diverse within the Loricariidae, with shape ranging from dorsoventrally compressed with small eyes and a thin caudal peduncle to deep bodied with large eyes and a thick caudal peduncle. Additionally, we saw changes in the oral disk shape and size across the morphospace, with some species having wide and large oral disks whereas others had thin, small oral disks. The shape within the family is driven by phylogenetic relationships, however within subfamilies there were mixed results. Although Hypoptopomatinae and Loricariinae had strong but insignificant phylogenetic signals, Hypostominae had a weak phylogenetic signal ($K = 0.54$, $p=0.001$), suggesting that phylogeny may drive some shape variation, but not all. For example, a handful of species fell in the middle of the morphospace close to the root of the phylogeny (Fig 3a). This suggests that *Corumbataia tocantinensis*, *Isorineloricaria spinosissima*, *Exastilithoxus* sp., and *Lithogenes villosus* retain the ancestral characteristics of the most common ancestor to the loricariids. Yet, we were unable to find correlating ecological traits to suggest that these

shapes converged due to ecological interactions. However, there are shortcomings to our ecological dataset. For one, some ecologies are not well known for specific species and are inferred based on the closest relative. Additionally, using discrete ecological traits may lead to bias in correlation models, as continuous trait data has been shown to be better at identifying correlations between shape and ecological traits [49].

Nevertheless, we found interesting patterns of divergence across the loricariids and within each subfamily (Fig. 4). Across the family, there were three quick bursts of morphological divergence, starting with the Loricariinae splitting from the other subfamilies around 36–23 MYA. During this time, there were many geological changes occurring in South America that may have contributed to the diversification and speciation of the loricariids. Around this time the central and northern Andes began to uplift and the sub-Andean trunk river flowed south to north into the Atlantic Ocean [50]. Although there are some loricariines at high elevation, loricariines tend to be more diverse in the lowlands, and the early orogeny of the Andes may have allowed for greater isolation of foreland basins. Interestingly, there was a second and third burst of morphological disparity around the middle Miocene (~14–10 MYA). This time is referred to as the middle Miocene disruption, which is associated with global cooling and aquatic extinctions, yet South America experienced even more drastic changes with the orogeny of the Andes and the formation of the Amazonian river system which flows west to east. Many groups of fishes, other than the loricariids, have undergone similar diversification patterns which are documented in many marine fishes [51,52]. Increased extinction rates in addition to the formation of new habitats may have led to the further diversification of the armored catfishes. For example, the rise of the Andes allowed for diversification of high montane taxa in subbasins as well as differentiation between species in cis- vs trans-Andean basins (cis- refers to areas east and south

of the Andes and trans- for areas west and north). The developing Amazon River began to capture other river systems, as can be seen today with the Casiquiare River (which drains much of the upper Orinoco into the Amazon) and the Rupununi Portal (which seasonally connects the Amazon and Essequibo rivers). These major shifts in river basins allowed for isolation of formerly connected habitats as well as movement of Amazonian fauna into other river systems, which have continued to accelerate speciation in Neotropical fishes [50,53,54].

Within the subfamilies, different patterns of morphological disparity emerged. The subfamily Hypoptopomatinae began to diversify around 28 MYA with two bursts in shape resulting in a moderate variation in body shape. Admittedly, this family is represented by few species in our dataset, so the patterns in disparity may be exaggerated. The least disparate subfamily was the Loricariinae, which began to diverge and steadily diversify around 23 MYA. This subfamily occupied a small region of the morphospace, which suggests shape evolves more gradually than in other subfamilies. This may be because of limitations enforced by the extreme dorsoventral flattening in loricariines (Fig. 2-3). The Hypostominae experienced a steady increase in disparity, starting around 14 MYA, resulting in the subfamily becoming the most disparate group of the loricariids. The hypostomine body form seems less constrained than that of hypoptopomatines or loricariines. Hypostomines have a broader range of size disparity in addition to shape disparity when compared to all other loricariid subfamilies. Hypostominae includes species nearly as elongate as loricariines (*Isorineloricaria* was named because of its similarity in form to loricariines [55,56]; as well as species approaching the small sizes of some hypoptopomatines [54] and some amongst the largest of loricariids [57]. Biogeography likely plays a role in diversity as well. Hypoptopomatines are more diverse in species and morphology in the shorter Atlantic drainages of Brazil, and these smaller river systems do not provide the

breadth of habitats available elsewhere where hypostomines are dominant [58,59]. Hypostomines and loricariines share similar continental ranges, but hypostomines are diverse in both uplands and lowlands whereas loricariine diversity in uplands is lower (Armbruster pers. obs.).

Independently evolving modules may allow for greater morphological diversification, and we found that loricariids are highly modularized, with varying degrees of integration between each module (Fig 5). Both likelihood and covariation ratio models returned a seven-module system across the family of armored catfishes, giving the fishes many areas to adapt with some degree of independence from one another; however, varying degrees of integration between the modules means that changes within one module will likely lead to cascading changes across the body. Specifically, morphological changes in the caudal peduncle are highly integrated with the rest of the body. This means if shape changes occur in the caudal peduncle, for example if the caudal peduncle becomes thinner, the rest of the body will experience morphological changes to some degree. We also found the head, opercula, and pectoral/dorsal fins had a strong degree of integration, which could explain the relatively small and weak fins and heads of loricariines vs. the broader, deeper heads and larger fins of hypostomines. As integration and modularity are not all of nothing concepts, this suggests that each module is separate from one another to some degree, but not completely independent of one another [10]. The interplay of modularity and integration within the loricariid body may attribute to the high degree of diversity that is seen within these fishes.

Within the subfamilies, we found similar patterns of modularity and integration, however there were slight differences, which may explain why subfamilies occupy their own area of the morphospace. Both the Hypoptopomatinae and the Loricariinae were highly modular yet have differences in what modules are more covariant with one another. The Hypoptopomatinae show

high covariation of the pectoral, dorsal, and pelvic fins with the anal area, whereas the Loricariinae had little covariation between those modules. Conversely, the Loricariinae have high covariation between the mouth, the anal area, and the caudle peduncle, where the Hypoptopomatinae had little covariation of the modules. These slight changes in modularity and integration patterns may have allowed for different interactions of parts to increase diversity along the subfamilies trajectory as seen in Hedrick et al. [9].

Interestingly, the Hypostominae has less modularity than the other subfamilies, with a four-module system. Our data suggests that the mouth acts as a module separate from the head and opercula. Furthermore, the pectoral, dorsal, and pelvic fins act as a module and the anal area and caudal peduncle acts as the final module. Although there were high amounts of integration between modules, this separation of mouth from other parts of body may allow for changes to the body while retaining similar feeding modes.

When confronted with the dizzying array of morphological diversity proscribed by groups of organisms like loricariids, it is difficult to understand how such diversity has evolved. Loricariids are especially problematic as most eat an unidentifiable mixture of organic compounds and biofilm that make dietary description difficult. Stable isotopic studies have not shown great diversity in what loricariids assimilate from the environment making the array of forms within the family particularly confounding [60,61]. Although ecological reasons for diversity of form are still elusive, the great number of morphological modules found in this study demonstrate a proximate reason such morphological diversity has formed. Those morphological modules have some evolutionary independence from one another to evolve separately and varying degrees of integration between modules means that evolutionary pressures to change one part of the body will have concomitant changes across the body. This tight interplay between

many integrated modules allows for the morphological disparity observed and explains patterns such as that demonstrated by *Peckoltia lujani* and *P. wernekei* which differ in jaw shape (long and nearly straight dentaries vs. short, angled dentaries), tooth number and size (many small vs. few larger), and body shape (elongate and narrow vs. short and stout) despite having little genetic differentiation [62]. Phylogeny was found to be a driving factor for disparity of the family, but not within subfamilies, meaning that convergence likely plays a major role in the evolution of form and integrated modules may further prompt convergence of morphologies. Our study was necessarily limited by the scope of phylogenies available, and as knowledge proceeds, a study such as this will be able to capture more of the morphological variation present within the family.

References

1. Wake DB, Larson A. 1987 Multidimensional Analysis of an Evolving Lineage. *Science* **238**, 42–48.
2. Gould SJ. 2002 *The structure of evolutionary theory*. Cambridge: Harvard University Press.
3. Adams DC, Nistri A. 2010 Ontogenetic convergence and evolution of foot morphology in European cave salamanders (Family: Plethodontidae). *BMC Evol Biol* **10**, 216. (doi:10.1186/1471-2148-10-216)
4. Sanger TJ, Mahler DL, Abzhanov A, Losos JB. 2012 ROLES FOR MODULARITY AND CONSTRAINT IN THE EVOLUTION OF CRANIAL DIVERSITY AMONG *ANOLIS* LIZARDS: *ANOLIS* SKULL SHAPE AND MODULARITY. *Evolution* **66**, 1525–1542. (doi:10.1111/j.1558-5646.2011.01519.x)
5. Du TY, Tissandier SC, Larsson HCE. 2019 Integration and modularity of teleostean pectoral fin shape and its role in the diversification of acanthomorph fishes. *Evolution* **73**, 401–411. (doi:10.1111/evo.13669)
6. Evans KM, Vidal-García M, Tagliacollo VA, Taylor SJ, Fenolio DB. 2019 Bony Patchwork: Mosaic Patterns of Evolution in the Skull of Electric Fishes (Apteronotidae: Gymnotiformes). *Integrative and Comparative Biology* **59**, 420–431. (doi:10.1093/icb/icz026)
7. Klingenberg CP. 2008 Morphological Integration and Developmental Modularity. *Annual Review of Ecology, Evolution, and Systematics* **39**, 115–132. (doi:10.1146/annurev.ecolsys.37.091305.110054)

8. Goswami A, Polly PD. 2010 Methods for Studying Morphological Integration and Modularity. *Paleontol. Soc. pap.* **16**, 213–243. (doi:10.1017/S1089332600001881)

9. Hedrick BP, Mutumi GL, Munteanu VD, Sadier A, Davies KTJ, Rossiter SJ, Sears KE, Dávalos LM, Dumont E. 2020 Morphological Diversification under High Integration in a Hyper Diverse Mammal Clade. *J Mammal Evol* **27**, 563–575. (doi:10.1007/s10914-019-09472-x)

10. Klingenberg CP, Mebus K, Auffray J-C. 2003 Developmental integration in a complex morphological structure: how distinct are the modules in the mouse mandible? *Evolution and Development* **5**, 522–531.

11. Conith AJ, Albertson RC. 2021 The cichlid oral and pharyngeal jaws are evolutionarily and genetically coupled. *Nat Commun* **12**, 5477. (doi:10.1038/s41467-021-25755-5)

12. Fricke R, Eschmeyer WN, Fong J. 2022 Eschmeyer's Catalog of Fishes. See http://researcharchive.calacademy.org/research/ichthyology/catalog/SpeciesByFamily.asp (accessed on 23 February 2019).

13. Adriaens D, Geerinckx T, Vlassenbroeck J, Van Hoorebeke L, Herrel A. 2009 Extensive Jaw Mobility in Suckermouth Armored Catfishes (Loricariidae): A Morphological and Kinematic Analysis of Substrate Scraping Mode of Feeding. *Physiological and Biochemical Zoology* **82**, 51–62. (doi:10.1086/594378)

14. Garg TK, Valdez Domingos FX, Almeida-Val VMF, Val AL. 2010 Histochemistry and functional organization of the dorsal skin of Ancistrus dolichopterus (Siluriformes: Loricariidae). *Neotropical Ichthyology* (doi:10.1590/S1679-62252010000400018)

15. Geerinckx T, Herrel A, Adriaens D. 2011 Suckermouth armored catfish resolve the paradox of simultaneous respiration and suction attachment: a kinematic study of

Pterygoplichthys disjunctivus. *Journal of Experimental Zoology Part A: Ecological Genetics and Physiology* (doi:10.1002/jez.656)

16. Lujan NK, Armbruster JW. 2012 Morphological and functional diversity of the mandible in suckermouth armored catfishes (Siluriformes: Loricariidae). *Journal of Morphology* **273**, 24–39. (doi:10.1002/jmor.11003)
17. Schaefer SA, Lauder GV. 1986 Historical Transformation of Functional Design: Evolutionary Morphology of Feeding Mechanisms in Loricarioid Catfishes. *Systematic Zoology* **35**, 489–508. (doi:10.2307/2413111)
18. Schaefer SA, Lauder GV. 1996 TESTING HISTORICAL HYPOTHESES OF MORPHOLOGICAL CHANGE : BIOMECHANICAL DECOUPLING IN LORICARIOID CATFISHES. **50**, 1661–1675.
19. Armbruster JW. 2004 Phylogenetic relationships of the suckermouth armoured catfishes (Loricariidae) with emphasis on the Hypostominae and the Ancistrinae. *Zoological Journal of the Linnean Society* **141**, 1–80. (doi:10.1111/j.1096-3642.2004.00109.x)
20. Armbruster JW. 2003 Peckoltia sabaji, a new species from the Guyana Shield (Siluriformes: Loricariidae). *Zootaxa* **344**, 1–12.
21. Olsen AM, Westneat MW. 2015 StereoMorph: An R package for the collection of 3D landmarks and curves using a stereo camera set-up. *Methods in Ecology and Evolution* **6**, 351–356. (doi:10.1111/2041-210X.12326)
22. Adams DC, Collyer ML, Kaliontzopoulou A, Baken EK. 2021 *Geomorph: Software for geometric morphometric analyses*. See https://cran.r-project.org/package=geomorph.

23. Baken EK, Collyer ML, Kaliontzopoulou A, Adams DC. 2021 gmShiny and geomorph v4.0: new graphical interface and enhanced analytics for a comprehensive morphometric experience. *Methods in Ecology and Evolution*

24. R Core Team. 2020 *R: A language and environment for statistical computing.* R Foundation for Statistical Computing, Vienna, Austria. See https://www.R-project.org/.

25. Frontier S. 1976 Study of the decay of eigenvalues in a principal component analysis: Comparison with the broken stick model. *Journal of Experimental Marine Biology and Ecology* **25**, 67–75. (doi:10.1016/0022-0981(76)90076-9)

26. Jackson DA. 1993 Stopping Rules in Principal Components Analysis: A Comparison of Heuristical and Statistical Approaches. *Ecology* **74**, 2204–2214. (doi:10.2307/1939574)

27. Legendre P, Legendre L. 2012 *Numerical Ecology*. Elsevier.

28. Olsen AM. 2017 Feeding ecology is the primary driver of beak shape diversification in waterfowl. *Functional Ecology* (doi:10.1111/1365-2435.12890)

29. Coombes KR, Wang M. 2019 *PCDimension: Finding the Number of Significant Principal Components.* See https://CRAN.R-project.org/package=PCDimension.

30. Lujan NK, Armbruster JW, Lovejoy NR, López-Fernández H. 2015 Multilocus molecular phylogeny of the suckermouth armored catfishes (Siluriformes: Loricariidae) with a focus on subfamily Hypostominae. *Molecular Phylogenetics and Evolution* **82**, 269–288. (doi:10.1016/j.ympev.2014.08.020)

31. Roxo FF *et al.* 2019 Phylogenomic reappraisal of the Neotropical catfish family Loricariidae (Teleostei: Siluriformes) using ultraconserved elements. *Molecular Phylogenetics and Evolution* **135**, 148–165. (doi:10.1016/j.ympev.2019.02.017)

32. Sidlauskas B. 2008 Continuous and arrested morphological diversification in sister clades of characiform fishes: A phylomorphospace approach. *Evolution* **62**, 3135–3156. (doi:10.1111/j.1558-5646.2008.00519.x)

33. Paradis E, Claude J, Strimmer K. 2004 APE: Analyses of Phylogenetics and Evolution in R language. *Bioinformatics* **20**, 289–290. (doi:10.1093/bioinformatics/btg412)

34. Stayton CT. 2015 The definition, recognition, and interpretation of convergent evolution, and two new measures for quantifying and assessing the significance of convergence: DEFINITIONS AND MEASURES OF CONVERGENT EVOLUTION. *Evolution* **69**, 2140–2153. (doi:10.1111/evo.12729)

35. Collyer ML, Adams DC. 2018 RRPP: An r package for fitting linear models to high-dimensional data using residual randomization. *Methods in Ecology and Evolution* **9**, 1772–1779. (doi:10.1111/2041-210X.13029)

36. Collyer ML, Adams DC. 2021 *RRPP: Linear Model Evaluation with Randomized Residuals in a Permutation Procedure*. See https://cran.r-project.org/web/packages/RRPP.

37. Stanley E. 2020 *Disparity Through Time Functions*.

38. Larouche O, Zelditch ML, Cloutier R. 2018 Modularity promotes morphological divergence in ray-finned fishes. *Sci Rep* **8**, 7278. (doi:10.1038/s41598-018-25715-y)

39. Adams DC. 2016 Evaluating modularity in morphometric data: challenges with the RV coefficient and a new test measure. *Methods Ecol Evol* **7**, 565–572. (doi:10.1111/2041-210X.12511)

40. Goswami A, Finarelli JA. 2016 EMMLi: A maximum likelihood approach to the analysis of modularity: MAXIMUM LIKELIHOOD ANALYSIS OF MODULARITY. *Evolution* **70**, 1622–1637. (doi:10.1111/evo.12956)

41. Goswami A, Lucas T, Ferguson-Gow H, Sivasubramaniam P, Finarelli J. 2019 *EMMLiv2: A Maximum Likelihood Approach to the Analysis of Modularity*. See https://github.com/hferg/EMMLiv2.

42. Felice RN, Goswami A. 2018 Developmental origins of mosaic evolution in the avian cranium. *Proc. Natl. Acad. Sci. U.S.A.* **115**, 555–560. (doi:10.1073/pnas.1716437115)

43. Marshall AF, Bardua C, Gower DJ, Wilkinson M, Sherratt E, Goswami A. 2019 High-density three-dimensional morphometric analyses support conserved static (intraspecific) modularity in caecilian (Amphibia: Gymnophiona) crania. *Biological Journal of the Linnean Society* **126**, 721–742. (doi:10.1093/biolinnean/blz001)

44. Adams DC. 2014 Quantifying and Comparing Phylogenetic Evolutionary Rates for Shape and Other High-Dimensional Phenotypic Data. *Systematic Biology* **63**, 166–177. (doi:10.1093/sysbio/syt105)

45. Denton JSS, Adams DC. 2015 A new phylogenetic test for comparing multiple high-dimensional evolutionary rates suggests interplay of evolutionary rates and modularity in lanternfishes (Myctophiformes; Myctophidae): RATES AND MODULARITY IN LANTERNFISHES. *Evolution* **69**, 2425–2440. (doi:10.1111/evo.12743)

46. Collyer ML, Adams DC. 2021 Phylogenetically aligned component analysis. *Methods Ecol Evol* **12**, 359–372. (doi:10.1111/2041-210X.13515)

47. Revell LJ. 2012 phytools: An R package for phylogenetic comparative biology (and other things). *Methods in Ecology and Evolution* (doi:10.1111/j.2041-210X.2011.00169.x)

48. Revell LJ. 2021 A variable-rate quantitative trait evolution model using penalized-likelihood. *bioRxiv* , 2021.04.17.440282.

49. Feilich KL, López-Fernández H. 2019 When Does Form Reflect Function? Acknowledging and Supporting Ecomorphological Assumptions. *Integrative and Comparative Biology* **59**, 358–370. (doi:10.1093/icb/icz070)

50. Hoorn C, Wesselingh FP. 2010 *Amazonia: landscape and species evolution a look into the past*. Hoboken: Wiley.

51. Black CR, Berendzen PB. 2020 Shared ecological traits influence shape of the skeleton in flatfishes (Pleuronectiformes). *PeerJ* **8**, e8919. (doi:10.7717/peerj.8919)

52. Siqueira AC, Morais RA, Bellwood DR, Cowman PF. 2020 Trophic innovations fuel reef fish diversification. *Nat Commun* **11**, 2669. (doi:10.1038/s41467-020-16498-w)

53. Albert JS, Reis RE. 2011 *Historical biogeography of neotropical freshwater fishes*. Berkeley: University of California Press.

54. Lujan NK, Armbruster JW. 2011 Two New Genera and Species of Ancistrini (Siluriformes: Loricariidae) from the Western Guiana Shield. *Copeia* **2011**, 216–225.

55. Isbrücker. 1980 Classification and catalogue of the mailed Loricariidae (Pisces, Siluriformes). *Verslagen en Technische Gegevens* **22**, 1–181.

56. Ray CK, Armbruster JW. 2016 The genera Isorineloricaria and Aphanotorulus (Siluriformes: Loricariidae) with description of a new species. *Zootaxa* **4072**, 501. (doi:10.11646/zootaxa.4072.5.1)

57. Chamon CC. 2016 Redescription of Acanthicus hystrix Agassiz, 1829 (Siluriformes: Loricariidae), with comments on the systematics and distribution of the genus. *Zootaxa* **4088**, 395. (doi:10.11646/zootaxa.4088.3.5)

58. Schaefer SA. 1991 Phylogenetic analysis of the loricariid subfamily Hypoptopomatinae (Pisces: Siluroidei: Loricariidae), with comments on generic diagnoses and geographic distribution. *Zoological Journal of the Linnean Society* **102**, 1–41. (doi:10.1111/j.1096-3642.1991.tb01535.x)

59. Chiachio MC, Oliveira C, Montoya-Burgos JI. 2008 Molecular systematic and historical biogeography of the armored Neotropical catfishes Hypoptopomatinae and Neoplecostominae (Siluriformes: Loricariidae). *Molecular Phylogenetics and Evolution* **49**, 606–617. (doi:10.1016/j.ympev.2008.08.013)

60. Lujan NK, Winemiller KO, Armbruster JW. 2012 Trophic diversity in the evolution and community assembly of loricariid catfishes. *BMC Evolutionary Biology* **12**, 124. (doi:10.1186/1471-2148-12-124)

61. Black CR, Armbruster JW. 2021 New method of isotopic analysis: baseline-standardized isotope vector analysis shows trophic partitioning in loricariids. *Ecosphere* **12**. (doi:10.1002/ecs2.3503)

62. Armbruster JW, Lujan NK. 2016 A new species of Peckoltia from the Upper Orinoco (Siluriformes, Loricariidae). *Zookeys* , 105–121. (doi:10.3897/zookeys.569.6630)

Tables

Table 1. Specimens used in this study.

Taxon	Abbr. in Fig.	Catalog Number	In Roxo et al. (congener)	In Lujan et al. (congener)
Loricariidae				
Hypoptopomatinae				
Corumbataia tocantinensis	*C. toc*	AUM45418, AUM45418, AUM45418, AUM45418	yes (*Corumbataia cuestae* 17210)	yes (*Corumbataia cuestae*)
Hypoptopoma gulare	*H. gul*	AUM66085	yes (*Hypoptopoma psilogaster* 22980)	yes (*Hypoptopoma spectabile*)
Hypoptopoma thoracatum	*H. tho*	AUM47901, AUM47901	yes	no
Otocinclus vestitus	*O. ves*	AUM22715	yes (*Otocinclus vittatus* 26232)	yes (*Otocinclus vittatus*)
Oxyropsis acutirostra	*O. acu*	AUM56739	no	yes (*Oxyropsis ephippia*)
Parotocinclus eppleyi	*P. epp*	AUM56697	yes (*Parotocinclus* cf. *bahiensis* 34692)	yes (*Parotocinclus bidentatus*)
Hypostominae				
Ancistrus bufonius	*A. buf*	AUM46276	no	no
Ancistrus chagresi	*A. cha*	AUM32114	no	no
Ancistrus damasceni	*A. dam*	AUM20700	no	no
Ancistrus leucostictus	*A. leu*	AUM48762	no	yes
Ancistrus lithurgicus	*A. lit*	AUM38182, AUM38821	no	no
Ancistrus macrophthalmus	*A. mac*	AUM53526	no	yes
Ancistrus marcapatae	*A. mar*	AUM51152	no	no
Ancistrus nudiceps	*A. nud*	AUM35624, AUM47720, AUM50295	no	no
Ancistrus triradiatus	*A. tri*	AUM22190, AUM22297, AUM54016, AUM54047	no	no
Aphanotorulus ammophilus	*A. amm*	AUM27705	yes *(Aphanotorulus unicolor* 19719)	yes
Baryancistrus beggini	*B. beg*	AUM54990	yes (*Baryancistrus beggini* 39227)	yes
Chaetostoma lineopunctatum	*C. lin*	AUM51201, AUM51341	yes (*Chaetostoma jegui*)	yes
Cordylancistrus sp.	*C. sp.*	AUM71150, AUM71168	no	yes (*Cordylancistrus torbesensis*)
Corymbophanes kaiei	*C. kai*	AUM62801	no	yes
Dekeyseria scaphirhynchus	*D. sca*	AUM44111, AUM54474	no	yes
Dolichancistrus cobrensis	*D. cob*	AUM46306	yes (*Dolichancistrus carnegiei* 189598)	yes (*Dolichancistrus carnegiei* 6647)

Taxon	Abbr. in Fig.	Catalog Number	In Roxo et al. (congener)	In Lujan et al. (congener)
Exastilithoxus sp.	*E. sp.*	AUM54450	yes (*Exastilithoxus hoedemani* 42177)	yes (*Exastilithoxus* nsp Ventuari T09667)
Hemiancistrus guahiborum	*H. gua*	AUM53523, AUM53821, AUM56668	yes (*Hemiancistrus punctulatus* 60931)	yes
Hemiancistrus lujani	*H. luj*	ANSP162174, AUM43008	yes (*Hemiancistrus fuliginosus* 61299)	no
Hypancistrus debilittera	*H. deb*	AUM53528	yes (*Hypancistrus* sp. 61759)	no
Hypancistrus furunculus	*H. fur*	AUM54463	no	yes
Hypancistrus lunaorum	*H. lun*	AUM42120, AUM44315	no	yes
Hypostomus niceforoi	*H. nic*	AUM45519, AUM57497	no	yes
Hypostomus robinii	*H. rob*	AUM22244, AUM36436	no	yes
Isorineloricaria spinosissima	*I. spi*	AUM4251	no	yes
Lasiancistrus schomburgkii	*L. sch*	AUM45574, AUM45627	yes (*Lasiancistrus saetiger* 42517)	yes
Lasiancistrus tentaculatus	*L. ten*	AUM39278, AUM53761	no	yes
Leporacanthicus cf. galaxias	*L. gal*	AUM54029	yes	yes
Lithoxus lithoides	*L. lit*	AUM39040	no	yes
Micracanthicus vandragti	*M. van*	AUM54991	yes	no
Neblinichthys yaravi	*N. yar*	AUM36633	no	yes (*Neblinichthys echinasus* T06066)
Panaque bathyphilus	*P. bat*	AUM45504	yes (*Panaque cochliodon* 19170)	yes
Panaque maccus	*P. mac*	AUM22665	no	yes
Paralithoxus bovallii	*P. bov*	AUM67039, AUM67039, AUM67039, AUM67039, AUM67039	no	yes
Peckoltia braueri	*P. bra*	AUM48093	yes	yes
Peckoltia ephippiata	*P. eph*	ANSP197614, AUM42662, AUM65116, MCP48395, UF237091	no	no
Peckoltia greedoi	*P. gre*	ANSP197617, AUM21972, MCP21972, MNRJ42663	no	no
Peckoltia lineola	*P. lin*	AUM54033	no	yes
Peckoltia n.sp.	*P. n.s*	AUM21972	no	no
Peckoltia sabaji	*P. sab*	AUM35733, AUM38259,	no	yes

Taxon	Abbr. in Fig.	Catalog Number	In Roxo et al. (congener)	In Lujan et al. (congener)
		AUM39835, AUM48767		
Peckoltia sp.	*P. sp.*	MCBXXXXX	no	no
Peckoltia vittata	*P. vit*	AUM39313, AUM54314	no	yes
Peckoltia wernekei	*P. wer*	AUM39313	no	yes
Peckoltichthys bachi	*P. bac*	AUM45592, AUM66083	no	yes
Pseudacanthicus leopardus	*P. leo*	AUM35738	yes (*Pseudacanthicus* sp 64046)	yes
Pseudancistrus barbatus	*P. bar*	AUM38023	yes (*Pseudancistrus pectegenitor* 43192)	yes
Pseudancistrus nigrescens	*P. nig*	AUM44594, AUM45299	no	yes
Pseudancistrus sidereus	*P. sid*	AUM42168, AUM42180, AUM43443, AUM54310	no	yes
Pseudolithoxus dumus	*P. dum*	AUM39589, AUM42118	yes (*Pseudolithoxus tigris* 185263)	yes
Pterygoplichthys gibbiceps	*P. gib*	AUM41441	yes (*Pterygoplichthys multiradiatus* 47289)	yes
Lithogeninae				
Lithogenes villosus	*L. vil*	AUM62909	no	yes
Loricariinae				
Crossoloricaria bahuaji	*C. bah*	AUM51403	yes (*Crossoloricaria cephalaspis* 5106)	no
Farlowella curtirostra	*F. cur*	AUM46301	yes (*Farlowella oxyrryncha* 11509)	yes (*Farlowella acus*)
Harttia platystoma	*H. pla*	AUM35643, AUM38789	yes	yes (*Harttia loricariformis*)
Hemiodontichthys acipenserinus	*H. aci*	AUM44413, AUM51464	no	no
Loricaria simillima	*L. sim*	AUM57811	yes (*Loricaria prolixa* 34926)	yes (*Loricaria clavipinna*)
Paraloricaria sp.(Dientes cortos)	*P. sp.*	AUM39899	no	no
Planiloricaria cryptodon	*P. cry*	AUM57837	yes	no
Pseudohemiodon sp.	*P. sp.*	AUM41498, AUM27708, AUM39848	yes (*Pseudohemiodon lamina* 23059)	yes (*Pseudohemiodon laticeps*)
Pseudoloricaria laeviuscula	*P. lae*	AUM38888	yes	no
Rineloricaria fallax	*R. fal*	AUM47892	yes (*Rineloricaria maackii* 51110)	yes
Rineloricaria stewarti	*R. ste*	AUM44491	no	no
Spatuloricaria puganensis	*S. pug*	AUM45611, AUM46619	yes (*Spatuloricaria* sp 16145)	yes

Taxon	Abbr. in Fig.	Catalog Number	In Roxo et al. (congener)	In Lujan et al. (congener)
Sturisoma monopelte	*S. mon*	AUM47971, AUM48752	yes (*Sturisoma barbatum* 42452)	yes (*Sturisoma* cf. *monopelte*)

Figures

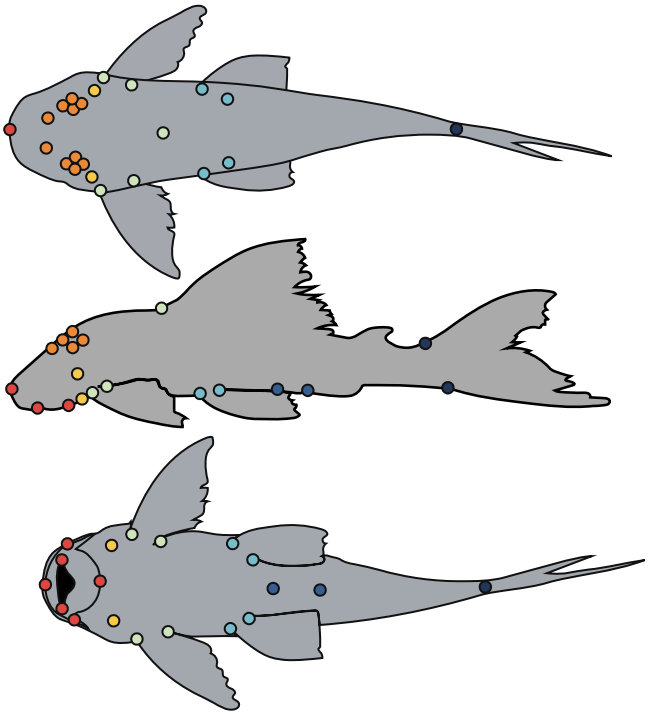

Figure 1. Landmark scheme and modules on a representative catfish in dorsal, left lateral, and ventral views. Colors correspond to body regions of distinct modules: red = mouth (tip of snout, left and right lateral joints of mouth, and most lateral and posterior parts of the oral disk), orange = head (left and right naris, anterior, dorsal, posterior, and ventral points of the eyes), yellow = opercula (most ventral and dorsal slits of opercula), light green = pectoral and dorsal fins (origin and insertion of the pectoral fins and origin of dorsal fin), light blue = pelvic fins (origin and insertion of the pelvic fins), dark blue = anal area (cloaca and anal-fin origin), dark purple = caudal peduncle (dorsal and ventral points of the caudal peduncle).

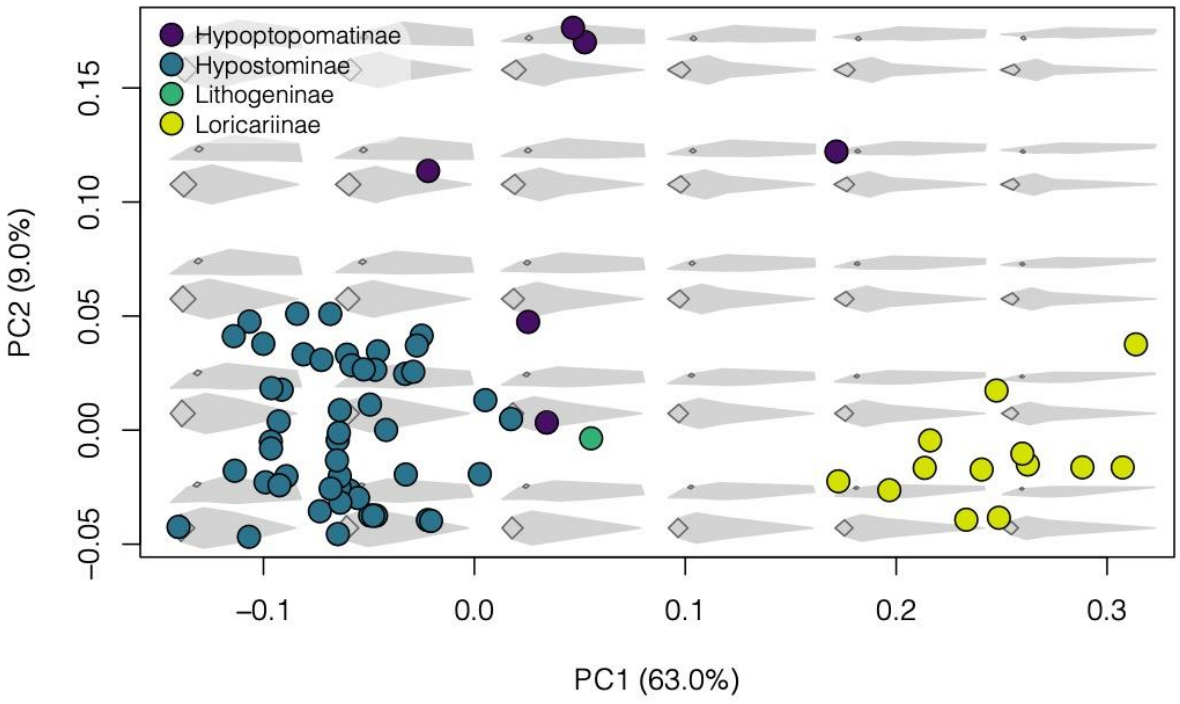

Figure 2. Body shape variation within loricariids. The morphospace of PC1 and PC2 represent ~70% of the body shape variation. Each point indicates the mean of a species which colors match the subfamilies denoted in the key. Backtransformed shapes (in gray with black outlined eyes and oral disks) portray shape variation throughout the morphospace.

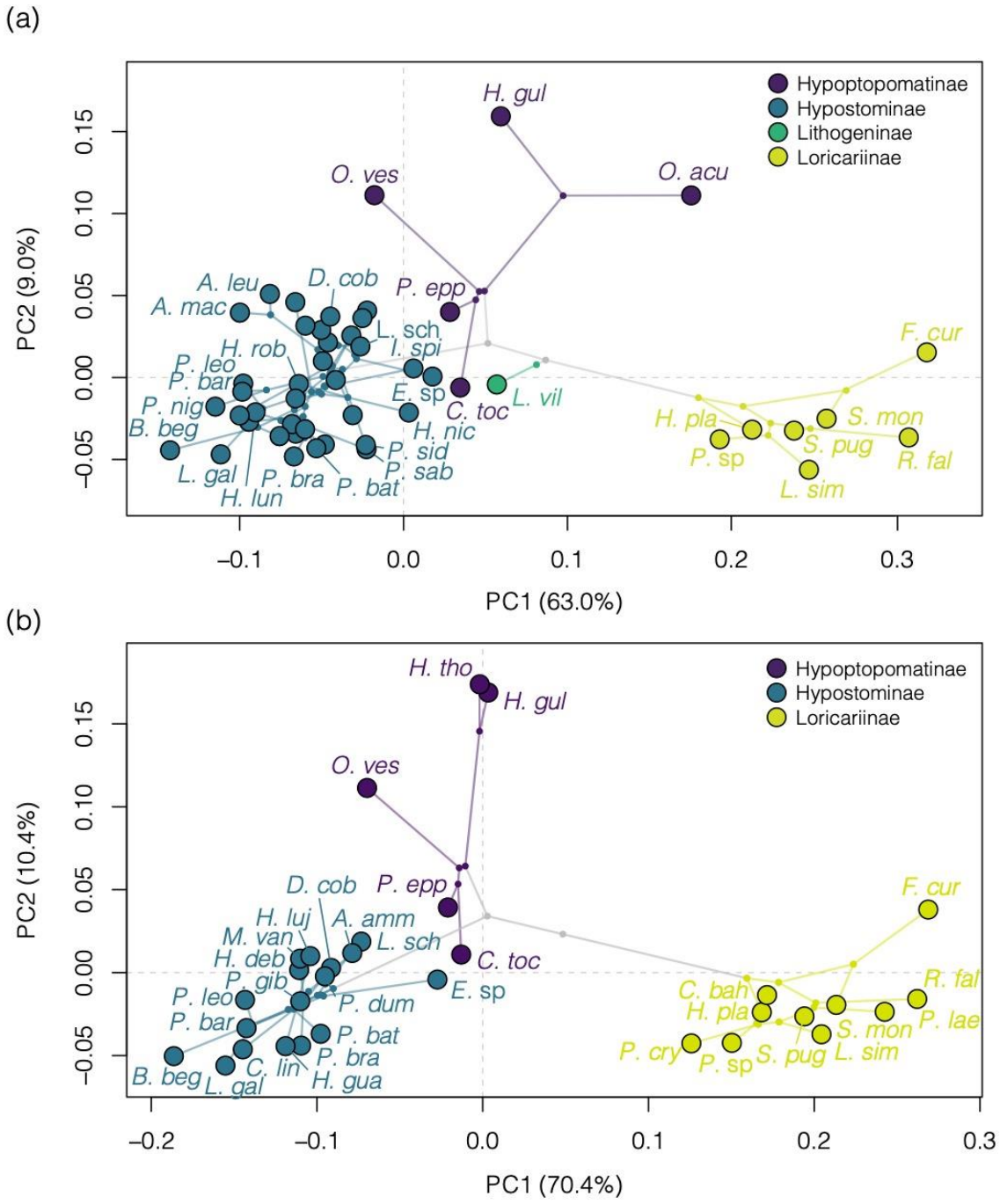

Figure 3. Phylomorphospaces of body shape across the loricariids. Phylogenetic relationships from (a) Lujan et al. 2015 and (b) Roxo et al. 2019 are projected onto the morphospace to demonstrate evolutionary relationships. Colored points represent the mean of a species with ancestral nodes represented by small grey circles.

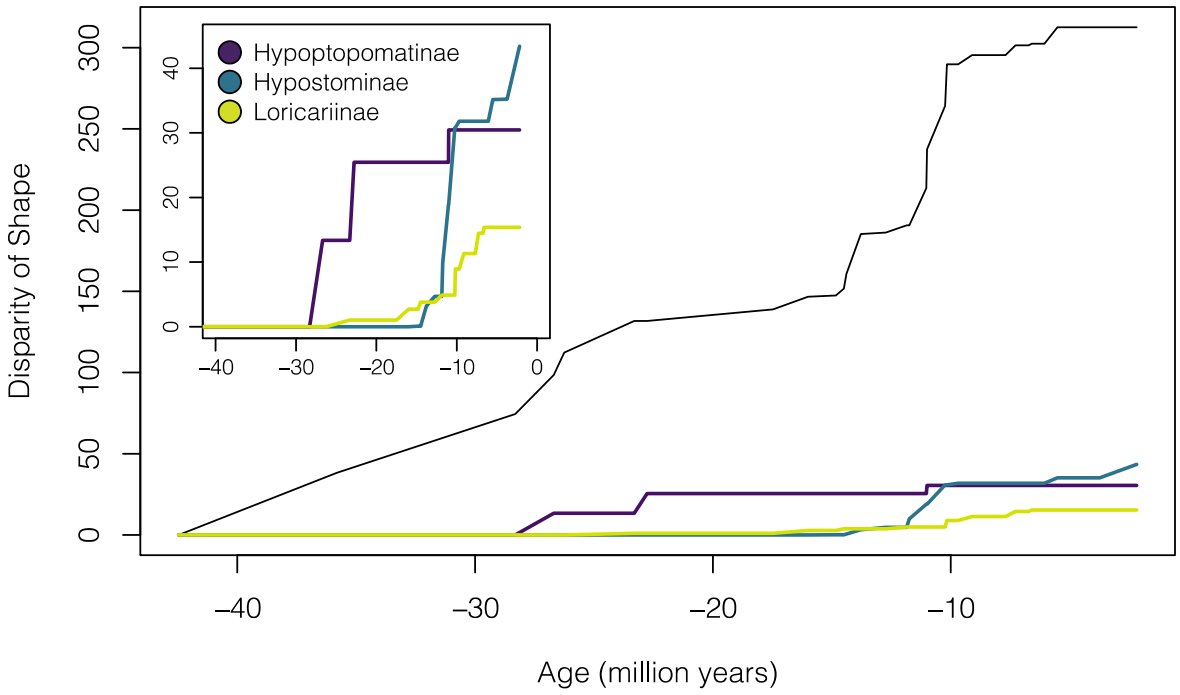

Figure 4. Disparity through time for loricariid family and separate subfamilies (inset) on the phylogenomic phylogeny (Roxo et al. 2019).

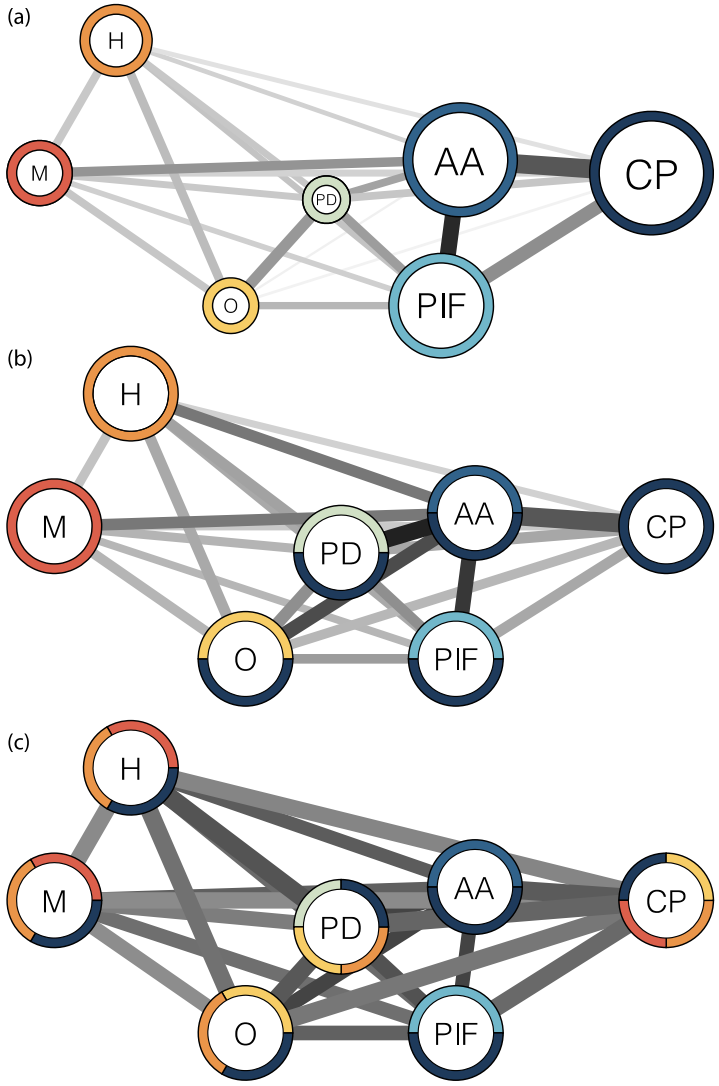

Figure 5. Modularity networks for the Loricariidae where lines represent between module integration. (a) Phylogenetically corrected modules found by EMMLi where the size of circles indicated within modular integration. (b) Covariation ratios of modularity and (c) r-PLS integration tests are standardized to within modular integration, so size of the circles do not matter. For each subfigure, colors represent high covariation (CR ≥ 1.00) or high integration (r-PLS ≥ 0.75) between modules where M represents the mouth (red) , H the head (orange), O the opercula (yellow), PD the pectoral and dorsal fins (green), PIF the pelvic fins (light blue), AA the anal area (medium blue), and CP the caudal peduncle (dark blue).

Chapter 1 Supplemental Materials

Supplemental Tables

Table S1. Modularity hypotheses based on functionally important regions of the loricariid body and previously tested hypotheses from Larouche et al. 2018.

Landmark	None	7mod	6mod	4mod	3mod	2mod	2A.Larouche	2B.Larouche	2C.Larouche	3.Larouche
Anal-fin-anterior	1	7	6	4	3	2	2	2	2	3
Caudal-fin-dorsal	1	6	5	3	2	2	2	1	2	3
Caudal-fin-ventral	1	6	5	3	2	2	2	1	2	3
Cloaca	1	7	6	4	3	2	2	1	2	3
Dorsal-fin-anterior	1	4	3	3	2	2	2	2	2	2
Eye-anterior_R	1	2	2	2	1	1	1	1	1	1
Eye-anterior_L	1	2	2	2	1	1	1	1	1	1
Eye-lateral_R	1	2	2	2	1	1	1	1	1	1
Eye-lateral_L	1	2	2	2	1	1	1	1	1	1
Eye-medial_R	1	2	2	2	1	1	1	1	1	1
Eye-medial_L	1	2	2	2	1	1	1	1	1	1
Eye-posterior_R	1	2	2	2	1	1	1	1	1	1
Eye-posterior_L	1	2	2	2	1	1	1	1	1	1
Mouth-lateral_R	1	1	1	1	1	1	1	1	1	1
Mouth-lateral_L	1	1	1	1	1	1	1	1	1	1
Naris_R	1	2	2	2	1	1	1	1	1	1
Naris_L	1	2	2	2	1	1	1	1	1	1
Opercle-dorsal_R	1	3	2	2	1	1	1	1	1	1
Opercle-dorsal_L	1	3	2	2	1	1	1	1	1	1
Opercle-ventral_R	1	3	2	2	1	1	1	1	1	1
Opercle-ventral_L	1	3	2	2	1	1	1	1	1	1
Oral-disk-lateral_R	1	1	1	1	1	1	1	1	1	1
Oral-disk-lateral_L	1	1	1	1	1	1	1	1	1	1
Oral-disk-posterior	1	1	1	1	1	1	1	1	1	1
Pectoral-fin-anterior_R	1	4	3	3	2	2	1	1	1	2
Pectoral-fin-anterior_L	1	4	3	3	2	2	1	1	1	2
Pectoral-fin-posterior_R	1	4	3	3	2	2	1	1	1	2
Pectoral-fin-posterior_L	1	4	3	3	2	2	1	1	1	2
Pelvic-fin-anterior_R	1	5	4	3	2	2	1	1	2	2
Pelvic-fin-anterior_L	1	5	4	3	2	2	1	1	2	2
Pelvic-fin-posterior_R	1	5	4	3	2	2	1	1	2	2
Pelvic-fin-posterior_L	1	5	4	3	2	2	1	1	2	2
Tip-of-snout	1	1	1	1	1	1	1	1	1	1

Table S2. Ecological trait correlation of shape for the whole family and each subfamily separately.

PGLS Model	Df	SS	MS	Rsq	F	Z	Pr(>F)
All Subfamilies							
Shape~Habitat.Albert	7	0.003	0.000	0.092	0.579	-1.731	0.959
Shape~Vegetation.Albert	2	0.001	0.001	0.053	1.164	0.563	0.282
Shape~Diet.Adult	4	0.002	0.001	0.083	0.916	0.068	0.454
Shape~Diet.Albert	1	0.000	0.000	0.017	0.752	-0.020	0.51
Shape~Sand	1	0.000	0.000	0.018	0.775	-0.066	0.513
Hypostominae							
Shape~Habitat.Albert	7	0.002	0.000	0.105	0.464	-1.929	0.978
Shape~Vegetation.Albert	1	0.000	0.000	0.015	0.450	-0.630	0.740
Shape~Diet.Adult	4	0.002	0.000	0.093	0.717	-0.376	0.628
Shape~Diet.Albert	1	0.000	0.000	0.024	0.732	0.115	0.443
Shape~Sand	NA	NA	NA	NA	NA	NA	NA
Hypoptopomatinae							
Shape~Habitat.Albert	2	0.001	0.001	0.569	0.910	-0.202	0.575
Shape~Vegetation.Albert	NA	NA	NA	NA	NA	NA	NA
Shape~Diet.Adult	1	0.000	0.000	0.161	0.516	-0.190	0.667
Shape~Diet.Albert	NA	NA	NA	NA	NA	NA	NA
Shape~Sand	NA	NA	NA	NA	NA	NA	NA
Loricariinae							
Shape~Habitat.Albert	4	0.001	0.000	0.510	0.673	-0.672	0.703
Shape~Vegetation.Albert	2	0.001	0.000	0.237	0.625	-0.600	0.743
Shape~Diet.Adult	1	0.000	0.000	0.119	0.626	-0.441	0.670
Shape~Diet.Albert	NA	NA	NA	NA	NA	NA	NA
Shape~Sand	NA	NA	NA	NA	NA	NA	NA

Table S3. Detailed disparity through time for each subfamily and the family.

Age (MYA)	Hypoptopomatinae	Hypostominae	Loricariinae	Total Disparity
-42.5	0.00	0.00	0.00	0.00
-35.8	0.00	0.00	0.00	38.27
-28.3	0.00	0.00	0.00	74.39
-26.7	13.37	0.00	0.00	98.47
-26.3	13.37	0.00	0.00	112.26
-23.3	13.37	0.00	1.02	131.74
-22.8	25.45	0.00	1.02	131.74
-17.5	25.45	0.00	1.02	138.85
-16.0	25.45	0.00	2.73	146.71
-14.8	25.45	0.07	2.73	147.47
-14.5	25.45	0.07	3.79	151.61
-14.4	25.45	0.49	3.79	160.70
-13.8	25.45	3.21	3.79	185.30
-12.7	25.45	4.69	3.79	186.19
-11.9	25.45	4.69	4.88	190.64
-11.7	25.45	9.86	4.88	190.64
-11.0	25.45	18.93	4.88	213.53
-11.0	30.46	18.93	4.88	237.50
-10.2	30.46	30.80	4.88	264.17
-10.2	30.46	30.80	8.94	289.73
-9.7	30.46	31.81	8.94	289.73
-9.1	30.46	31.81	11.33	295.50
-7.7	30.46	31.81	11.33	295.50
-7.3	30.46	31.81	14.45	301.52
-6.7	30.46	31.81	14.45	301.52
-6.6	30.46	31.81	15.39	302.50
-6.1	30.46	31.81	15.39	302.50
-5.5	30.46	35.16	15.39	312.58
-3.7	30.46	35.22	15.39	312.58
-2.2	30.46	43.40	15.39	312.58

Table S4. AICc weights for modularity hypothesis as proposed by EMMLi.

	MaxL	K	AICc	dAICc	Model_L	Post_Pob
7.mod.sep.Mod + sep.between	**198.23**	**29**	**-336.83**	**0.00**	**1.00**	**1.00**
6.mod.sep.Mod + sep.between	149.89	22	-254.82	82.00	0.00	0.00
7.mod.same.Mod + sep.between	126.44	23	-205.85	130.98	0.00	0.00
6.mod.same.Mod + sep.between	71.08	17	-107.59	229.23	0.00	0.00
2C.Larouche.sep.Mod + same.between	16.15	4	-24.27	312.56	0.00	0.00
3.Larouche.sep.Mod + sep.between	7.89	7	-1.68	335.15	0.00	0.00
4.mod.sep.Mod + sep.between	-7.08	11	36.40	373.23	0.00	0.00
7.mod.sep.Mod + same.between	-15.95	9	50.06	386.89	0.00	0.00
3.mod.sep.Mod + sep.between	-35.29	7	84.69	421.51	0.00	0.00
4.mod.same.Mod + sep.between	-34.31	8	84.76	421.58	0.00	0.00
6.mod.sep.Mod + same.between	-39.26	8	94.65	431.48	0.00	0.00
3.Larouche.sep.Mod + same.between	-45.42	5	100.89	437.72	0.00	0.00
2.mod.sep.Mod + same.between	-65.66	4	139.35	476.18	0.00	0.00
4.mod.sep.Mod + same.between	-70.34	6	152.75	489.58	0.00	0.00
3.mod.same.Mod + sep.between	-73.28	5	156.62	493.45	0.00	0.00
3.Larouche.same.Mod + sep.between	-76.39	5	162.84	499.66	0.00	0.00
2.mod.same.Mod + same.between	-87.08	3	180.19	517.01	0.00	0.00
7.mod.same.Mod + same.between	-87.74	3	181.50	518.33	0.00	0.00
2C.Larouche.same.Mod + same.between	-91.97	3	189.97	526.79	0.00	0.00
3.mod.sep.Mod + same.between	-90.19	5	190.44	527.26	0.00	0.00
4.mod.same.Mod + same.between	-97.57	3	201.16	537.99	0.00	0.00
6.mod.same.Mod + same.between	-118.06	3	242.15	578.98	0.00	0.00
3.mod.same.Mod + same.between	-128.18	3	262.39	599.21	0.00	0.00
3.Larouche.same.Mod + same.between	-129.70	3	265.42	602.25	0.00	0.00
2A.Larouche.sep.Mod + same.between	-136.17	4	280.38	617.21	0.00	0.00
2A.Larouche.same.Mod + same.between	-187.24	3	380.51	717.33	0.00	0.00
2B.Larouche.same.Mod + same.between	-209.04	3	424.10	760.93	0.00	0.00
2B.Larouche.sep.Mod + same.between	-209.04	4	426.12	762.94	0.00	0.00
No.modules.default	-212.06	2	428.13	764.96	0.00	0.00

Table S5. Results of modularity within (highlighted gray) and between regions as proposed by EMMLi.

	Mouth	Head	Opercula	Pec&Dor Fins	Pelvic Fins	Anal Area	Caudal Peduncle
Mouth	0.48						
Head	0.33	0.53					
Opercula	0.31	0.35	0.41				
Pec&Dor Fins	0.26	0.26	0.46	0.35			
Pelvic Fins	0.2	0.24	0.28	0.37	0.77		
Anal Area	0.38	0.16	0.05	0.3	0.68	0.84	
Caudal Peduncle	0.27	0.17	0.07	0.3	0.57	0.81	0.91

Table S6. Pairwise comparisons of modularity and integration tests across the loricariids. Above the diagonal are pairwise CR values where bold variables are ≥ 1.00 (p-values are not calculated for individual pairwise CR, but are the same as the empirically calculated p-value from resampling procedures of the total model). Below the diagonal are r-PLS values where bold variables are ≥ 0.75 and p-value is denoted as follows, ***p < 0.001, **p < 0.01, *p <0.05.

	Mouth	Head	Opercula	Pec&Dor Fins	Pelvic Fins	Anal Area	Caudal Peduncle
Mouth		0.64	0.7	0.63	0.52	0.56	0.83
Head	**0.77*** **		0.78	0.75	0.6	0.46	0.81
Opercula	0.68**	**0.81*** **		0.87	0.67	0.68	**1.04**
Pec&Dor Fins	0.68***	**0.86*** **	**0.81*** **		0.73	0.8	**1.25**
Pelvic Fins	0.65***	0.65***	0.67***	**0.71*** **		0.76	**1.1**
Anal Area	0.61***	0.61***	0.68***	0.66***	0.65***		**1.4**
Caudal Peduncle	**0.76*** **	**0.76*** **	**0.81*** **	**0.88*** **	**0.82*** **	**0.86*** **	

Table S7. Pairwise comparisons of modularity and integration tests for the Hypostominae only. Above the diagonal are pairwise CR values where bold variables are ≥ 1.00 (p-values are not calculated for individual pairwise CR, but are the same as the empirically calculated p-value from resampling procedures of the total model). Below the diagonal are r-PLS values where bold variables are ≥ 0.75 and p-value is denoted as follows, ***p < 0.001, **p < 0.01, *p <0.05.

	Mouth	Head& Opercula	MidBody	Tail
Mouth		0.68	0.63	0.72
Head&Opercula	0.72**		0.83	0.75
MidBody	0.69**	**0.86*** **		**1.07**
Tail	**0.76*** **	**0.78*** **	**0.92*** **	

Table S8. Pairwise comparisons of modularity and integration tests for the Hypoptopomatinae only. Above the diagonal are pairwise CR values where bold variables are ≥ 1.00 (p-values are not calculated for individual pairwise CR, but are the same as the empirically calculated p-value from resampling procedures of the total model). Below the diagonal are r-PLS values where bold variables are ≥ 0.75 and p-value is denoted as follows, ***p < 0.001, **p < 0.01, *p <0.05.

	Mouth	Head	Opercula	Pec&Dor Fins	Pelvic Fins	Anal Area	Caudal Peduncle
Mouth		0.82	0.96	0.76	0.76	0.56	0.44
Head	**0.92**		0.90	**1.03**	0.89	0.78	0.91
Opercula	**0.92**	**0.94**		**1.07**	0.73	0.83	0.91
Pec&Dor Fins	**0.77**	**0.96**	**0.90**		0.80	0.92	**1.13**
Pelvic Fins	**0.86**	**0.82**	0.71	0.72		**1.05**	0.97
Anal Area	0.55	**0.90**	**0.77**	**0.75**	**0.91**		**1.21**
Caudal Peduncle	0.55	**0.95**	**0.84**	**0.90**	**0.89**	**0.95***	

Table S9. Pairwise comparisons of modularity and integration tests for the Loricariinae only. Above the diagonal are pairwise CR values where bold variables are ≥ 1.00 (p-values are not calculated for individual pairwise CR, but are the same as the empirically calculated p-value from resampling procedures of the total model). Below the diagonal are r-PLS values where bold variables are ≥ 0.75 and p-value is denoted as follows, ***p < 0.001, **p < 0.01, *p <0.05.

	Mouth	Head	Opercula	Pec&Dor Fins	Pelvic Fins	Anal Area	Caudal Peduncle
Mouth		0.80	0.88	0.72	0.77	0.97	**1.12**
Head	0.72		0.85	**1.05**	0.96	0.74	0.88
Opercula	**0.82**	**0.85**		0.92	0.92	0.85	**1.07**
Pec&Dor Fins	0.65	**0.95****	**0.82***		**1.07**	0.52	0.87
Pelvic Fins	**0.76**	**0.96****	**0.86***	**0.92****		0.48	0.89
Anal Area	**0.90***	**0.89**	**0.75**	0.49	0.51		**1.13**
Caudal Peduncle	**0.95****	**0.85**	**0.90***	**0.75**	**0.81***	**0.88****	

Table S10. The evolutionary rates of total shape and each module for all species. Bold values denote the fastest rate among species, and bold and italicized values denote the slowest rates.

	Total Shape	**Mouth**	**Head**	**Opercula**	**Pec Dorsal Fins**	**Pelvic Fins**	**Anal Area**	**Caudal Peduncle**
Peckoltia vittata	4.5E-05	5.3E-06	4.1E-05	1.5E-05	4.2E-06	1.6E-05	1.6E-06	6.3E-06
Peckoltia lineola	7.0E-06	5.3E-06	2.5E-05	5.5E-06	1.3E-06	1.0E-05	3.1E-06	2.2E-06
Peckoltia braueri	7.6E-06	3.6E-05	2.1E-05	3.1E-06	1.2E-06	5.9E-06	1.2E-06	2.0E-06
Peckoltia sabaji	3.3E-04	2.7E-06	2.6E-05	2.0E-05	1.7E-04	1.4E-05	8.0E-07	1.2E-04
Peckoltia wernekei	1.1E-05	1.1E-05	7.8E-06	3.7E-06	3.3E-06	6.4E-05	8.1E-07	8.1E-06
Panaque maccus	1.4E-04	9.6E-06	5.2E-05	3.2E-05	1.3E-05	6.1E-06	2.0E-05	5.0E-05
Hypancistrus lunaorum	5.4E-04	1.1E-05	6.7E-05	7.1E-06	6.6E-05	1.2E-04	2.2E-04	3.7E-04
Hypancistrus furunculus	5.3E-04	1.0E-05	6.9E-05	6.9E-06	6.7E-05	1.1E-04	2.2E-04	3.6E-04
Peckoltichthys bachi	7.4E-06	3.1E-05	1.4E-05	9.8E-06	1.8E-05	2.7E-05	1.1E-06	3.4E-06
Isorineloricaria spinosissima	6.4E-04	1.4E-05	2.6E-05	5.6E-07	2.1E-05	4.2E-05	**3.0E-04**	3.8E-04
Aphanotorulus ammophilus	6.6E-05	1.1E-04	2.1E-04	1.5E-06	1.3E-04	3.2E-05	3.9E-06	1.7E-06
Hypostomus niceforoi	6.8E-04	3.3E-05	**5.8E-04**	2.6E-05	5.3E-05	7.3E-06	3.5E-06	2.1E-04
Hypostomus robinii	1.4E-04	2.4E-05	2.0E-04	1.9E-05	2.0E-05	4.9E-06	2.6E-06	4.1E-05
Pterygoplichthys gibbiceps	8.0E-06	9.4E-06	2.5E-05	8.4E-06	1.3E-05	4.2E-05	5.3E-05	4.3E-06
Baryancistrus beggini	9.0E-04	9.0E-05	4.1E-04	1.8E-04	2.1E-04	2.1E-06	1.1E-06	1.9E-04
Hemiancistrus guahiborum	1.9E-05	4.9E-06	7.7E-06	2.1E-06	6.0E-06	7.9E-07	1.0E-05	6.2E-06
Panaque bathyphilus	3.3E-06	3.8E-06	3.3E-05	3.7E-05	4.8E-05	6.7E-04	1.4E-06	1.1E-05
Leporacanthicus-cf. galaxias	9.8E-05	2.5E-04	1.2E-05	9.9E-07	1.2E-05	7.6E-06	2.6E-07	4.8E-05
Pseudacanthicus leopardus	3.9E-05	7.6E-06	1.5E-06	8.3E-06	8.2E-06	2.9E-05	1.4E-07	3.5E-05
Corymbophanes kaiei	4.5E-06	2.3E-04	3.9E-07	1.2E-04	1.2E-04	1.2E-07	1.6E-05	5.3E-07
Dekeyseria scaphirhynchus	2.0E-05	2.8E-06	8.0E-05	5.4E-05	8.5E-06	9.7E-07	2.0E-07	6.2E-06
Ancistrus macrophthalmus	1.2E-04	8.9E-07	3.6E-05	4.1E-05	3.1E-04	1.1E-06	6.7E-06	3.1E-05
Ancistrus leucostictus	3.9E-05	5.1E-07	1.9E-05	6.0E-06	9.7E-06	3.6E-06	1.6E-04	2.3E-05
Lasiancistrus schomburgkii	3.7E-05	2.5E-07	3.5E-06	2.7E-06	5.6E-07	1.8E-05	4.4E-08	2.8E-05

	Total Shape	**Mouth**	**Head**	**Opercula**	**Pec Dorsal Fins**	**Pelvic Fins**	**Anal Area**	**Caudal Peduncle**
Lasiancistrus tentaculatus	1.1E-05	4.3E-07	1.8E-05	1.4E-06	4.4E-07	8.0E-06	5.1E-08	4.5E-06
Pseudolithoxus dumus	1.5E-06	1.6E-06	5.8E-06	5.3E-06	1.6E-05	2.6E-05	2.6E-06	2.7E-07
Pseudancistrus barbatus	7.7E-05	1.4E-05	1.9E-06	2.1E-05	4.8E-05	7.5E-07	3.8E-07	1.3E-05
Pseudancistrus nigrescens	1.9E-04	1.2E-05	2.0E-05	1.3E-05	2.8E-05	2.8E-05	6.6E-06	6.3E-05
Neblinichthys yaravi	1.3E-06	2.2E-07	1.7E-06	5.3E-07	8.5E-07	6.0E-06	4.5E-08	1.2E-06
Exastilithoxus sp	3.5E-04	7.6E-07	1.2E-05	8.5E-06	3.1E-06	1.1E-05	1.8E-04	1.8E-04
Lithoxus lithoides	1.1E-05	2.4E-06	7.5E-05	8.2E-06	7.1E-07	1.6E-04	4.0E-06	2.3E-05
Paralithoxus bovallii	1.2E-05	9.6E-06	1.0E-05	3.6E-07	8.3E-06	2.1E-06	9.4E-06	1.5E-06
Pseudancistrus sidereus	1.3E-05	3.5E-07	6.4E-06	1.8E-06	1.4E-06	2.7E-07	8.5E-08	3.3E-05
Chaetostoma lineopunctatum	2.3E-04	4.0E-05	9.6E-07	7.7E-05	9.6E-05	3.1E-07	8.2E-08	4.3E-05
Dolichancistrus cobrensis	4.3E-06	1.3E-06	5.1E-04	7.2E-08	2.8E-06	5.2E-07	1.5E-06	1.3E-08
Cordylancistrus sp	1.1E-05	3.6E-06	3.5E-06	5.5E-08	1.6E-05	2.3E-05	7.6E-05	1.4E-08
Corumbataia tocantinensis	7.9E-07	3.3E-07	3.5E-05	1.7E-05	1.3E-05	8.1E-07	1.3E-06	7.5E-06
Parotocinclus eppleyi	6.4E-07	1.6E-05	1.5E-06	1.2E-05	4.4E-07	7.6E-07	8.2E-07	1.1E-06
Otocinclus vestitus	1.6E-04	4.5E-07	2.6E-06	7.3E-07	2.1E-07	1.5E-04	3.9E-05	1.3E-04
Hypoptopoma gulare	2.6E-05	8.8E-06	2.3E-05	4.6E-06	1.6E-05	2.4E-06	3.5E-06	7.3E-06
Oxyropsis acutirostra	**2.2E-03**	4.7E-05	2.6E-04	**1.9E-04**	3.7E-04	6.5E-05	8.4E-05	**8.7E-04**
Rineloricaria fallax	4.9E-04	1.0E-04	1.7E-05	6.7E-05	2.3E-05	4.8E-05	1.0E-04	2.2E-04
Spatuloricaria puganensis	1.3E-05	2.2E-06	1.5E-07	1.1E-06	1.7E-06	4.9E-06	1.3E-06	5.2E-06
Pseudohemiodon sp	1.8E-04	9.4E-09	3.1E-08	2.2E-06	8.1E-06	3.7E-05	1.5E-05	1.1E-04
Loricaria simillima	1.4E-05	9.9E-09	1.8E-08	4.3E-05	5.5E-07	1.1E-06	9.9E-06	5.8E-06
Sturisoma monopelte	4.4E-05	1.2E-05	4.9E-07	1.3E-05	3.5E-05	7.0E-06	1.8E-06	1.2E-05
Farlowella curtirostra	3.4E-04	**1.6E-06**	2.7E-06	5.2E-05	**3.7E-04**	3.9E-04	2.2E-05	8.8E-05
Harttia platystoma	2.2E-05	2.9E-07	6.2E-06	2.2E-07	3.8E-07	4.0E-07	3.0E-07	5.5E-06
Lithogenes villosus	***4.3E-10***	***2.8E-10***	***1.5E-10***	***6.9E-12***	***1.4E-11***	***2.8E-10***	2.4E-04	***4.0E-10***

Supplemental Figures

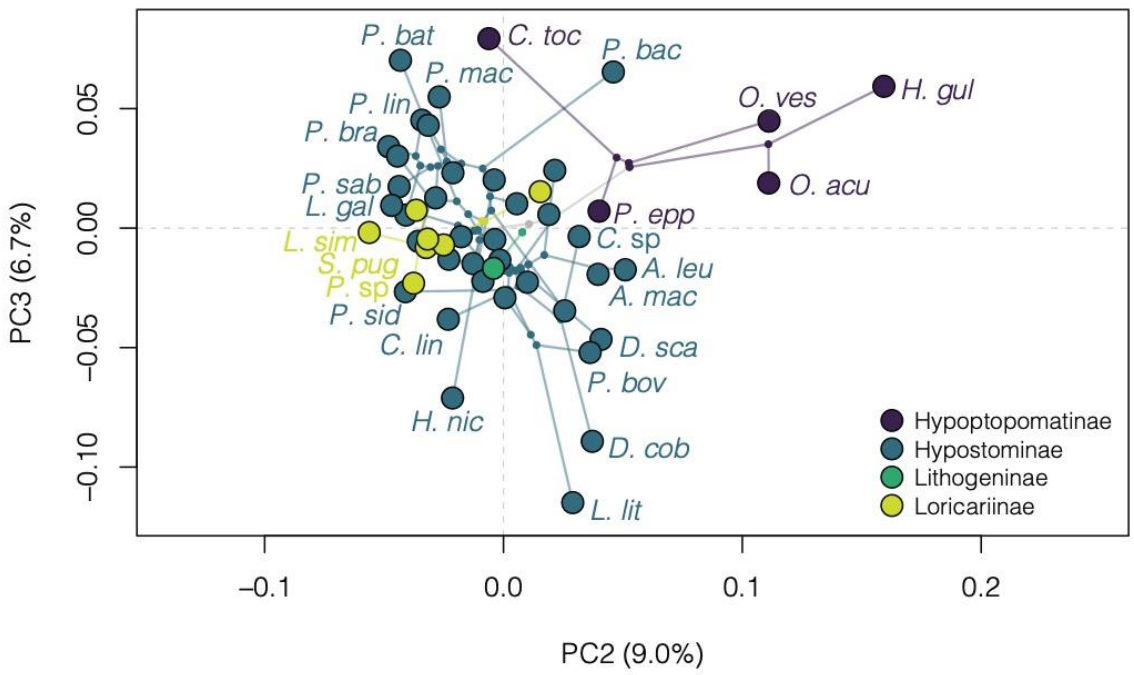

Figure S1. Phylomorphospace of body shape across the loricariids for PC2 and PC3 on Lujan et al. 2015. Colored points represent the mean of a species with ancestral nodes represented by small grey circles.

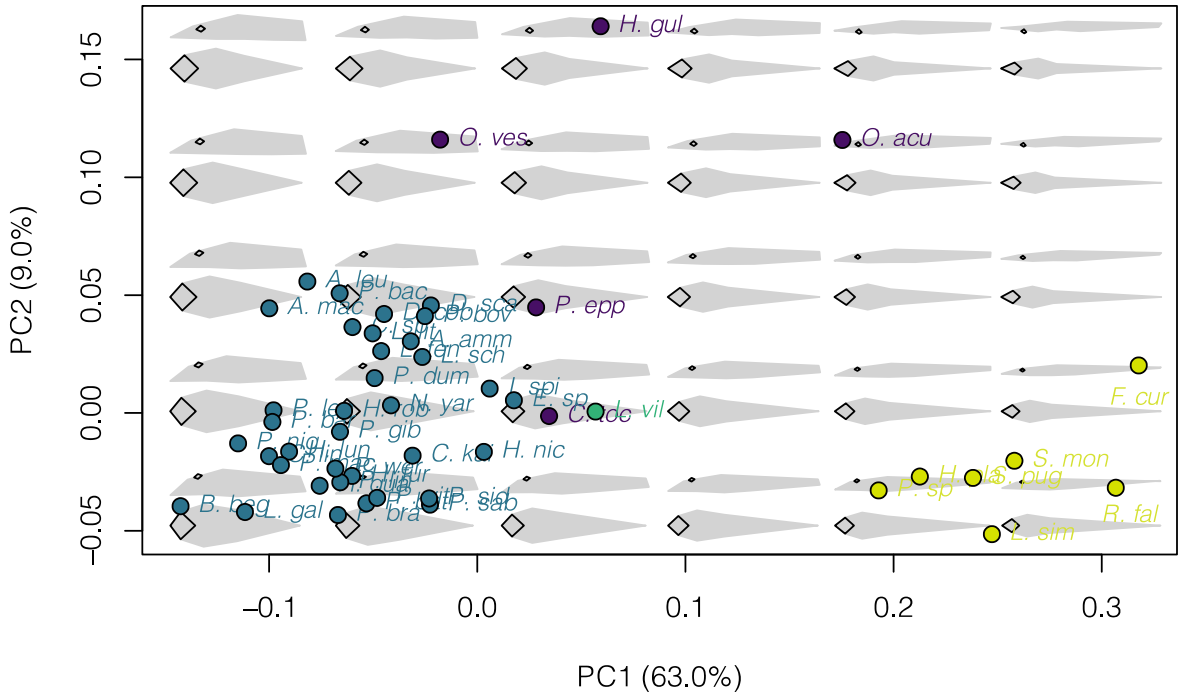

Figure S2. Body shape variation within loricariids for the Lujan et al. 2015 phylomorphospace. Each point indicates the mean of a species which colors match the subfamilies denoted in figure 2. Backtransformed shapes (in gray with black outlined eyes and oral disks) portray shape variation throughout the morphospace.

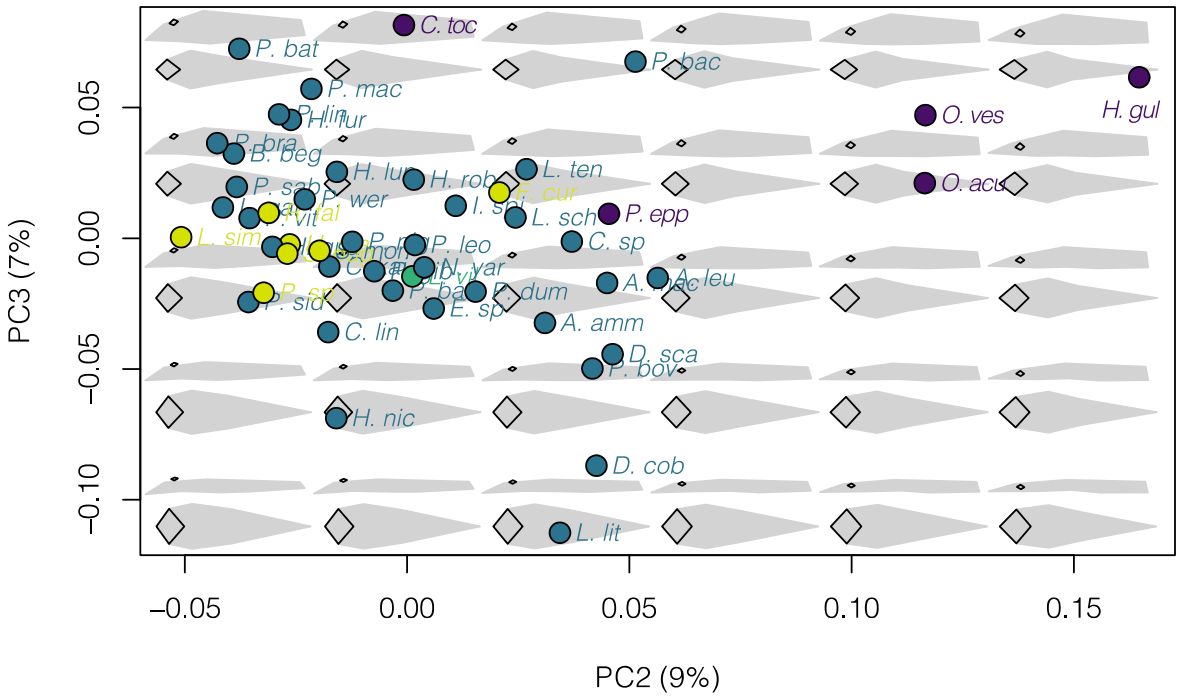

Figure S3. Body shape variation within loricariids for PC2 and PC3 on the Lujan et al. 2015 phylomorphospace. Each point indicates the mean of a species which colors match the subfamilies denoted in figure 2. Backtransformed shapes (in gray with black outlined eyes and oral disks) portray shape variation throughout the morphospace.

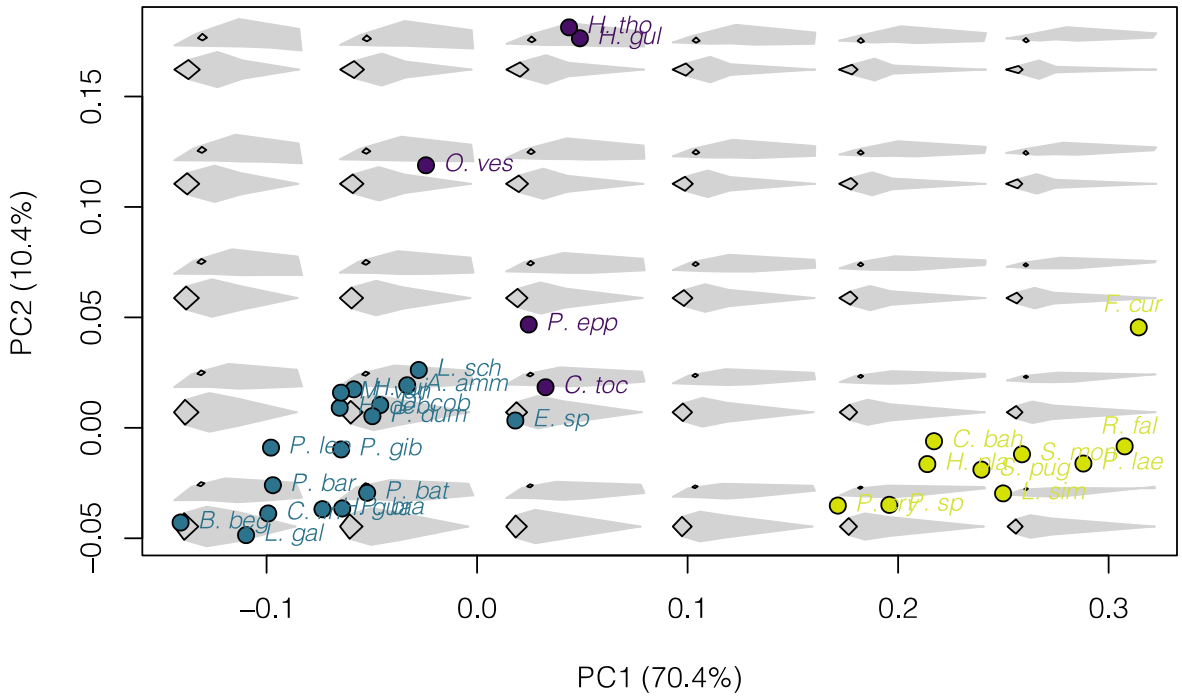

Figure S4. Body shape variation within loricariids for the Roxo et al. 2019 phylomorphospace. Each point indicates the mean of a species which colors match the subfamilies denoted in figure 2. Backtransformed shapes (in gray with black outlined eyes and oral disks) portray shape variation throughout the morphospace.

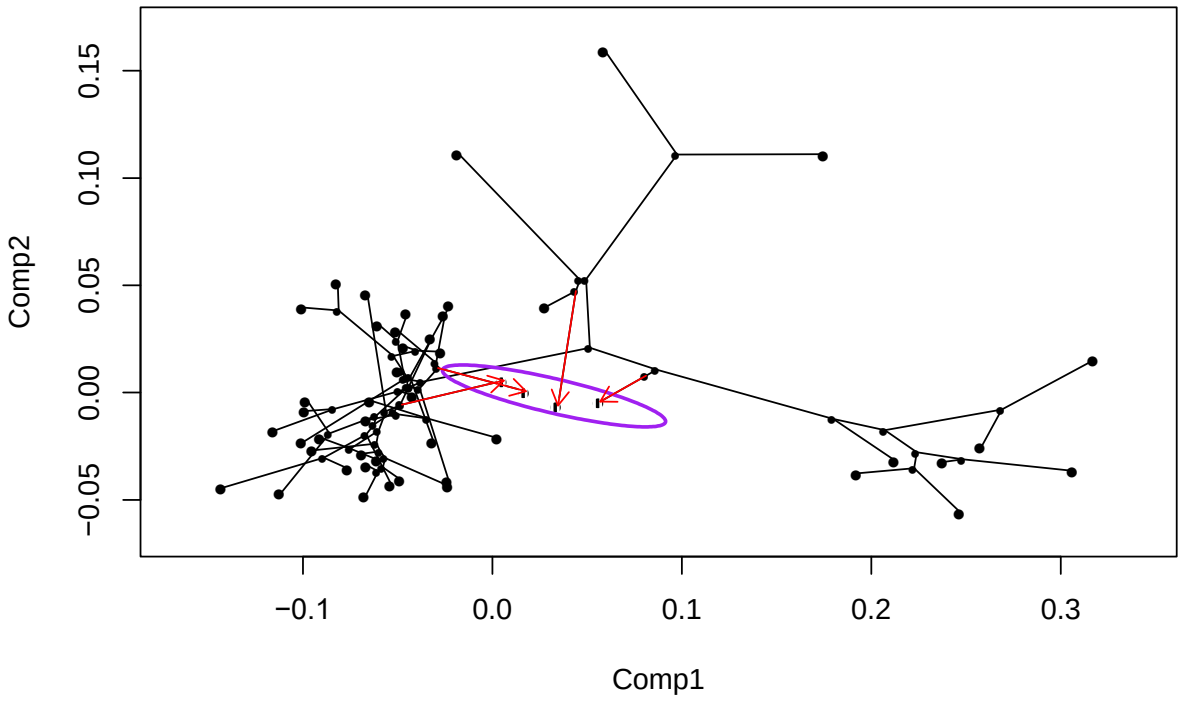

Figure S5. Convergence of taxa crossing the ellipsis for the Lujan et al. 2015 phylomorphospace. Highlighted points represent *Isorineloricaria spinosissima*, *Exastilithoxus* sp, *Corumbataia tocantinensis*, and *Lithogenes villosus*.

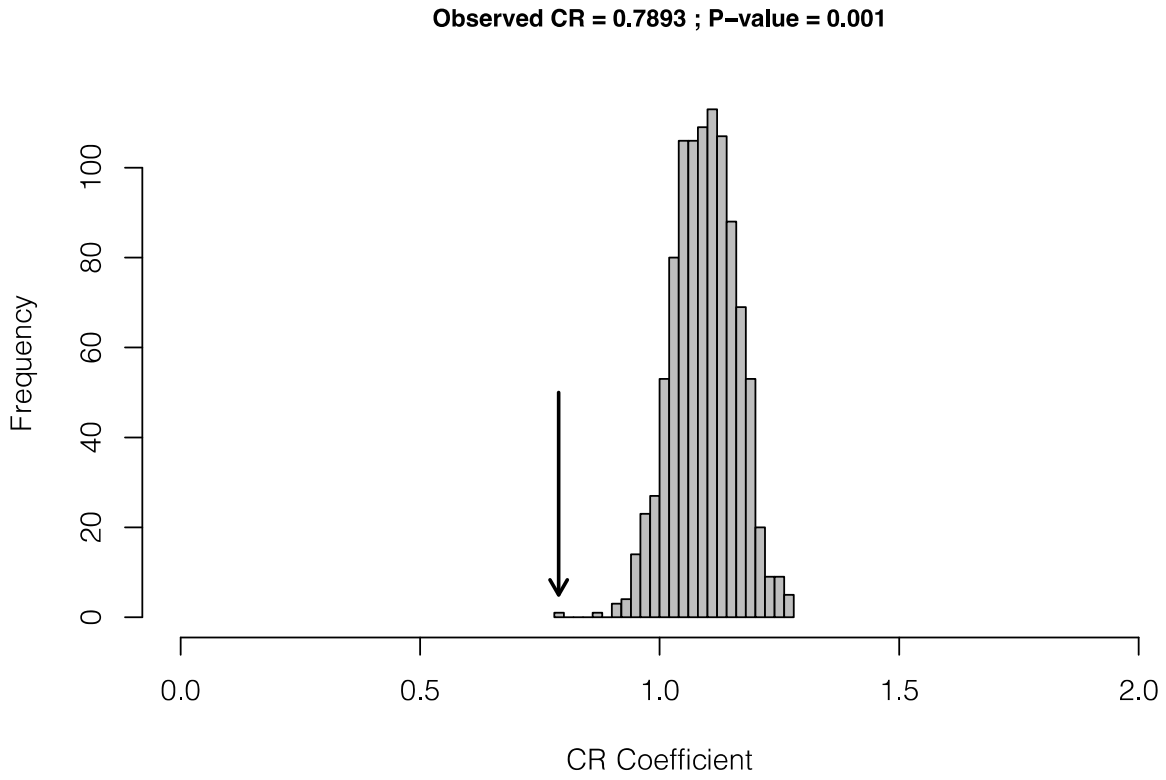

Figure S6. Observed covariation rates which fall outside the normal range, indicating significant modularity for the loricariids.

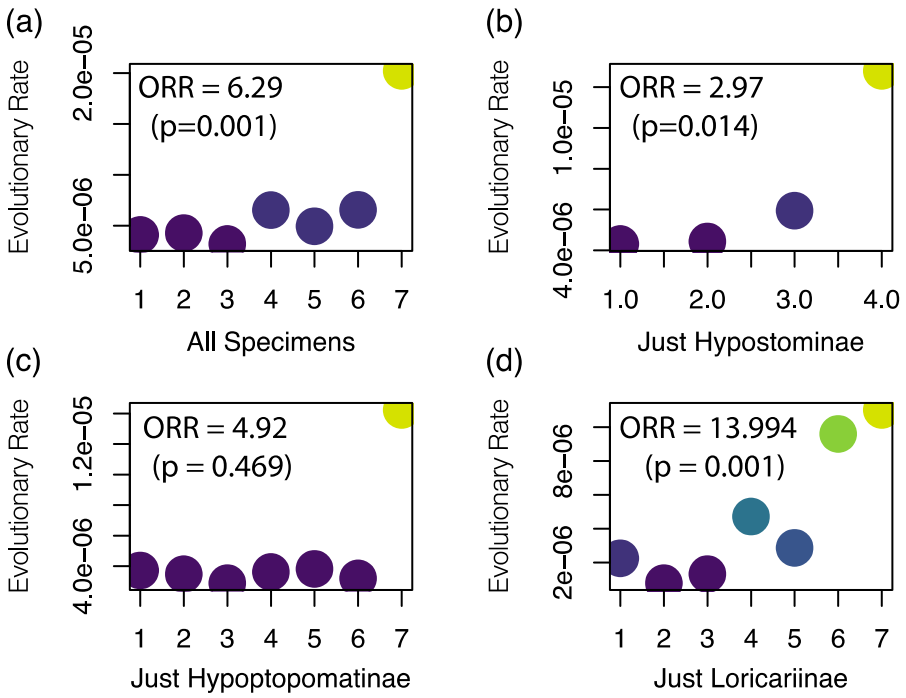

Figure S7. Evolutionary rates of each module for (a) all specimens, (b) only hypostominae, (c) only Hypoptopomatinae, and (d) only Loricariinae. The observed rate ratios (ORR) are indicated for each modularity hypothesis within the plot.

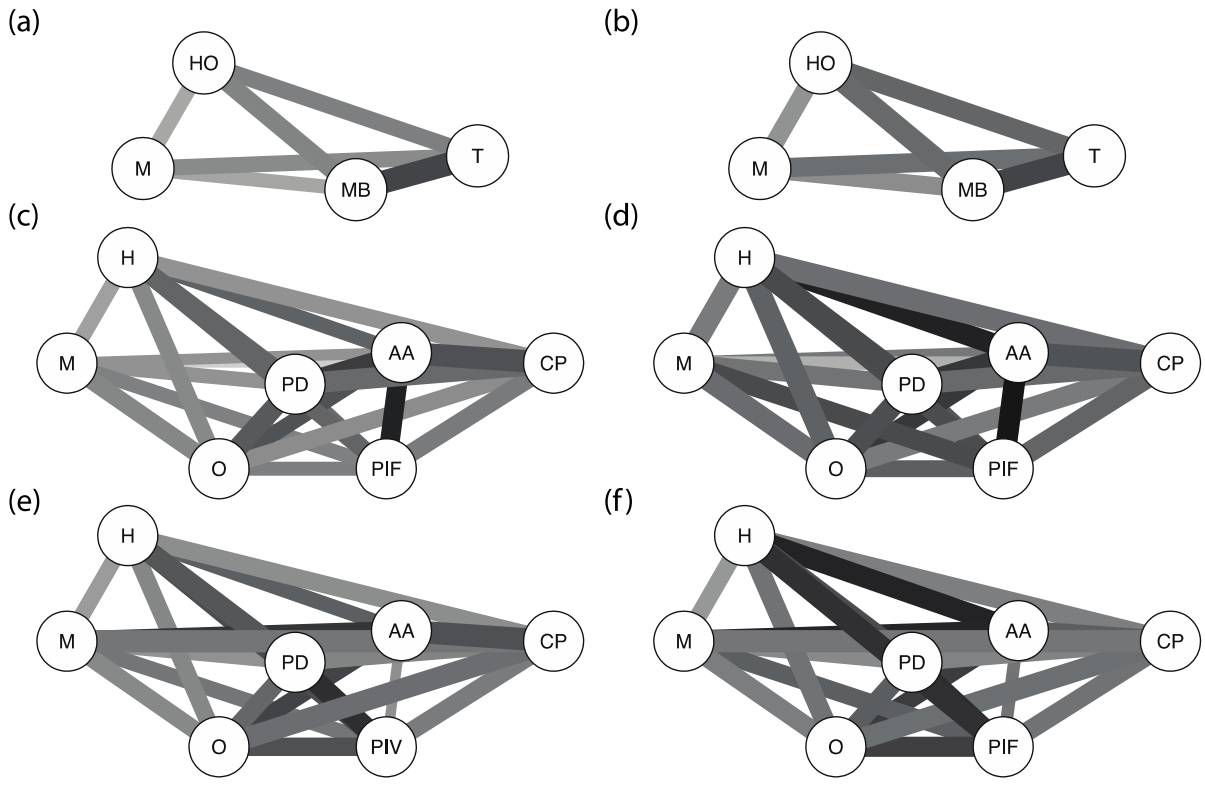

Figure S8. Modularity networks of Loricariidae subfamilies where lines represent between module integration for (a) modularity tests and (b) integration tests of the Hypostominae, (c) modularity tests and (d) integration tests of the Hypoptopomatinae, and (e) modularity tests and (f) integration tests of the Loricariinae. (a-b) M = mouth, HO = head and opercula, MB = midbody (pectoral, dorsal, and pelvic fins), and T = tail (anal area and caudal peduncle). (c-f) M = mouth, H = head, O = opercula, PD = pectoral and dorsal fins, PIF = pelvic fins, AA = anal area, and CP = caudal peduncle.

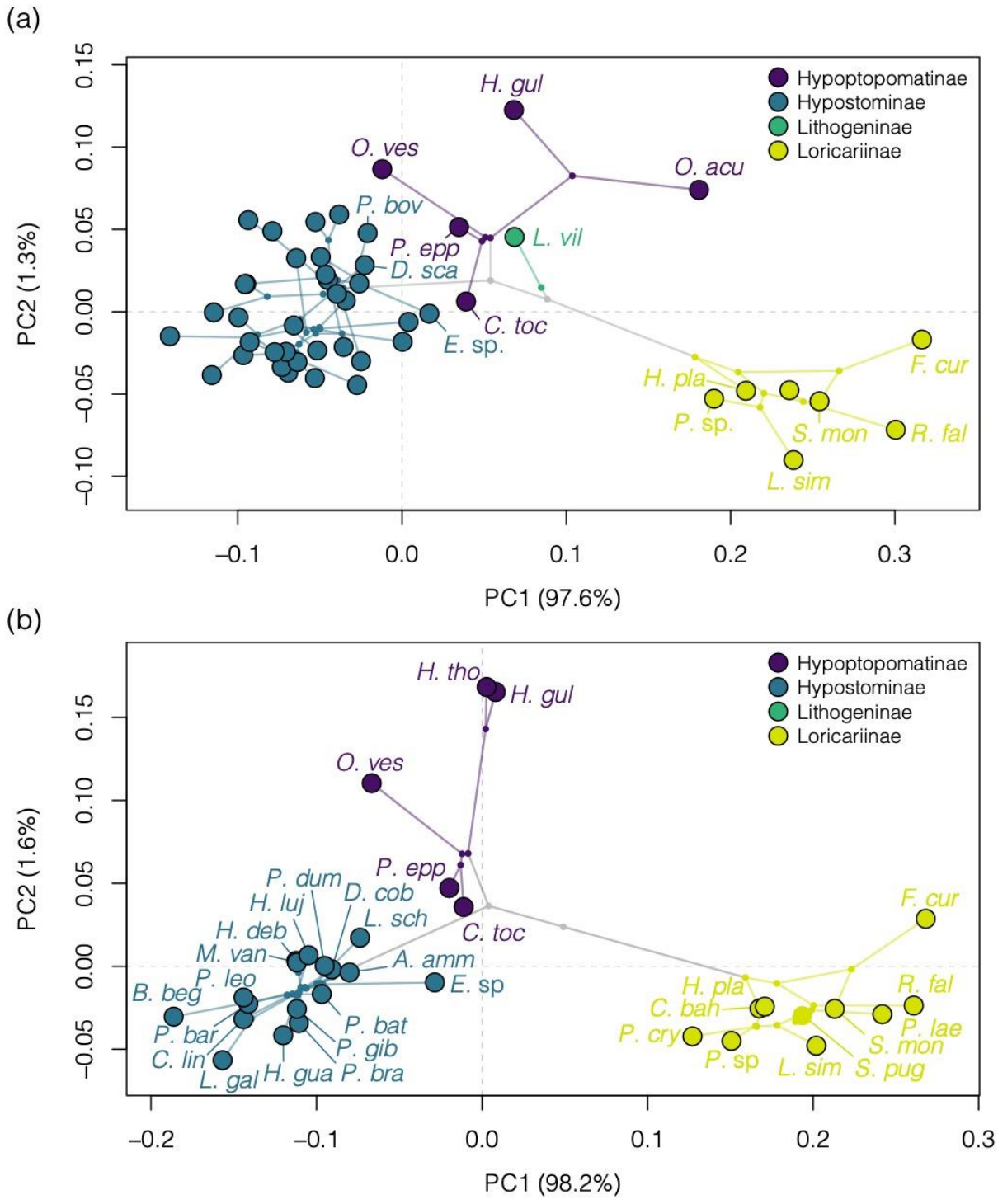

Figure S9. Phylogenetically aligned components (PaCA) for the (a) Lujan et al. 2015 phylogeny and (b) Roxo et al. phylogenomic phylogeny.

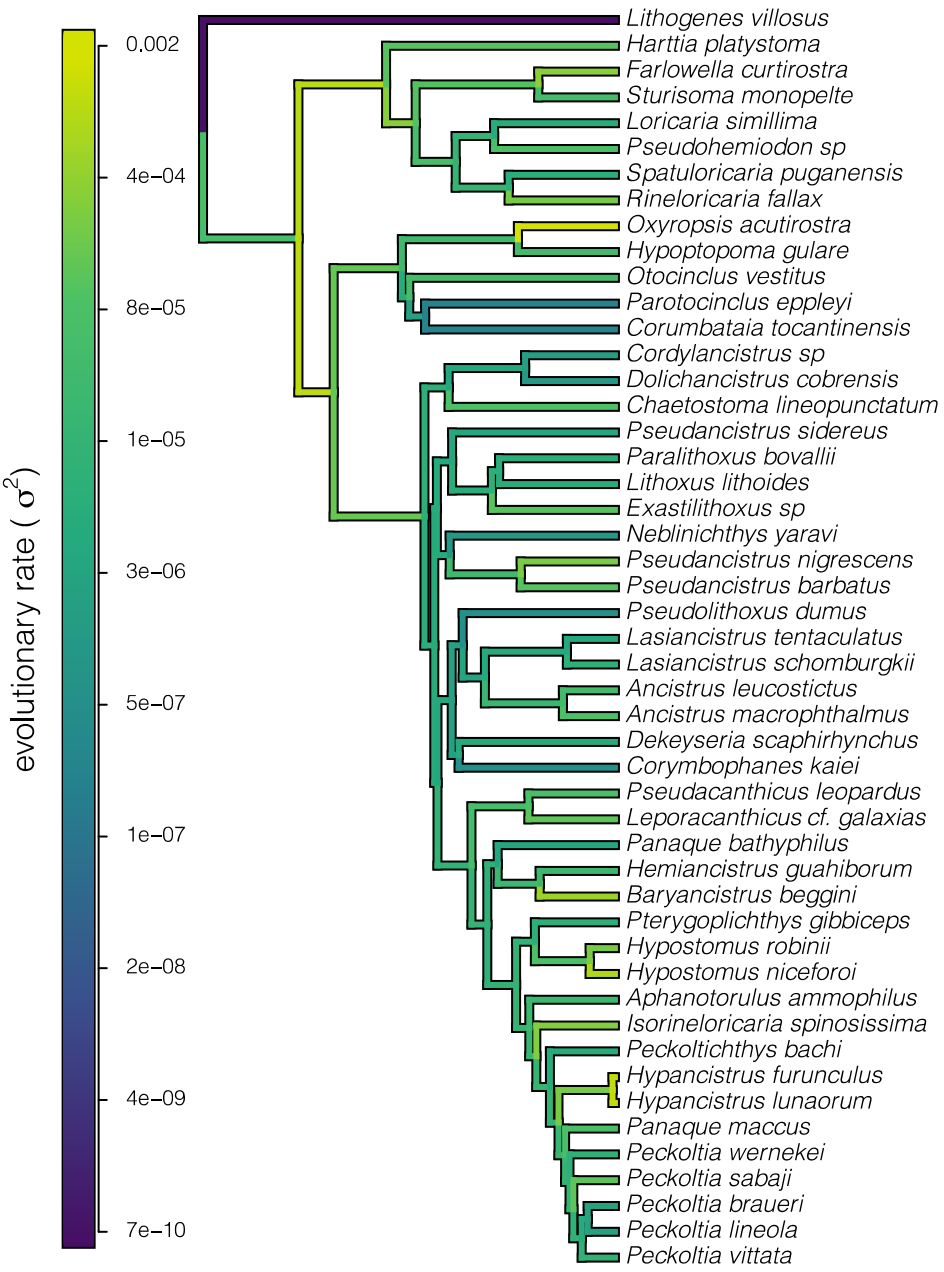

Figure S10. Evolutionary rates of phylogenetically aligned components (PaCA) for loricariid species using a penalized-likelihood model.

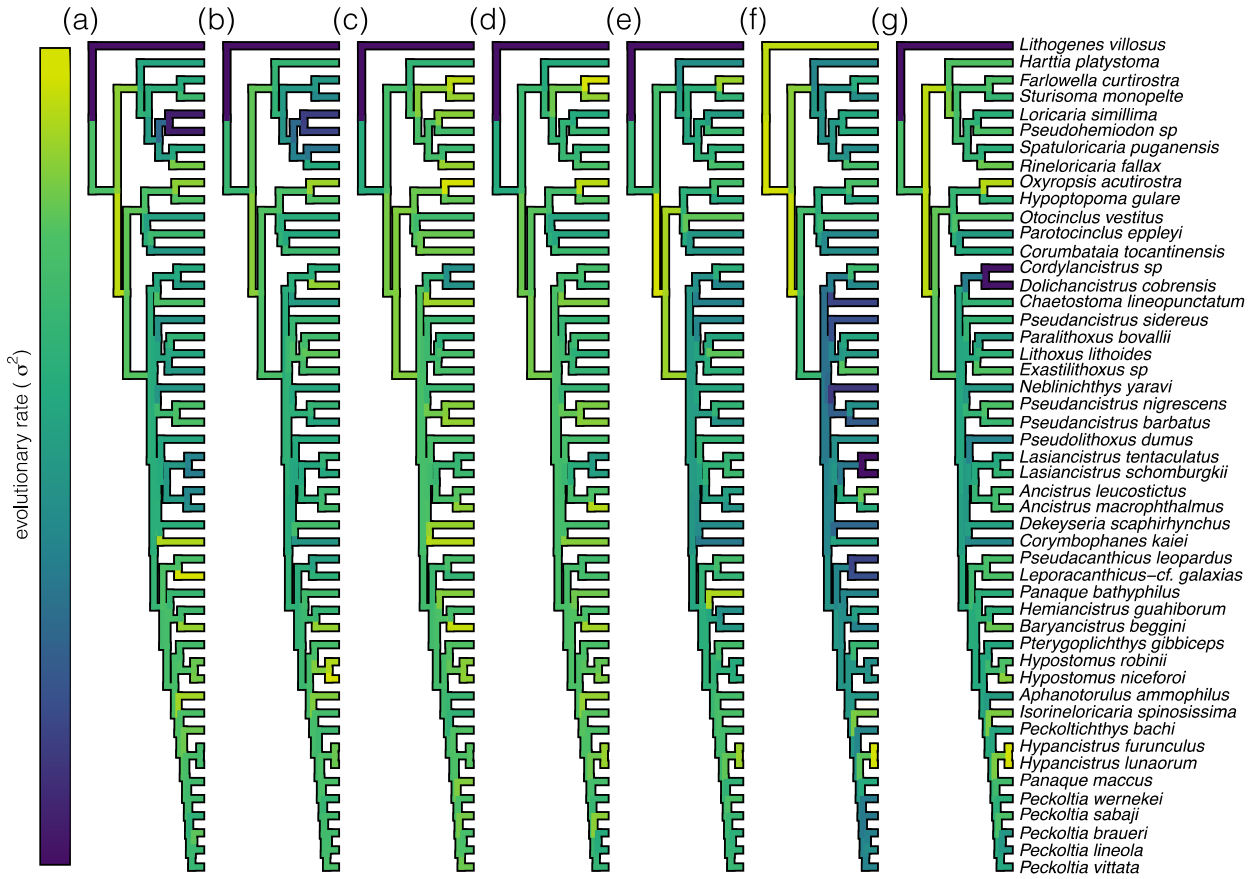

Figure S11. Evolutionary rates of phylogenetically aligned components (PaCA) for each module as described; (a) mouth, (b) head, (c) opercula, (d) pectoral and dorsal fins, (e) pelvic fins, (f) anal area, and (g) caudal peduncle.

Chapter 2 – Chew on this: Oral jaw shape is not correlated with diet type in Loricariid catfishes

Submitted to PLOS ONE

Abstract

The correlation between form and function is influenced by biomechanical constraints, natural selection, and ecological interactions. In many species of suction-feeding fishes, jaw shape has shown to be closely associated with diet. However, these correlations have not been tested in fishes that have more complex jaw functions. For example, the neotropical loricariid catfishes (commonly known as suckermouth armored catfishes or plecos) possess a ventrally facing oral disk, which allows for the oral jaws to adhere to surfaces to conduct feeding. The upper jaw consists of a highly mobile premaxilla. The lower jaw comprises medially separated mandibles that rotate around the long axis within a shallow socket at the anteroventral articulation of the quadrate, and the two jaw rami can be operated independently. Within Loricariidae, oral jaw shape is highly variable and structurally complex, ranging from short jaws with less than five teeth to long jaws with over 200 teeth. To determine if jaw shape is correlated to diet type, we assessed oral jaw shape across 36 species using CT scans. Shape was quantified with traditional and automated landmarking in 3DSlicer, and diet type correlation was calculated using the phylogenetic generalized least squares (PGLS) method. We found that traditional and automated processes captured shape effectively when all jaw components were combined. PGLS found that diet type did not correlate to jaw shape; however, there was a correlation between clades with diverse diets and fast evolutionary rates of shape. These results suggest that shape is not

constrained to diet type, and that similarly shaped jaws coupled with different types of teeth could allow the fishes to feed on a wide range of materials.

Introduction

The correlation between morphology and diet has been demonstrated in many animals from fishes to birds [1–4]. In addition to biomechanical constraints and natural selection, ecological interactions, such as consuming prey, are shown to be important drivers of morphological diversification [5–7]. For example, the lower pharyngeal jaw in neotropical cichlids has diversified with different diet types. Burress [8] found that thinner, more gracile-like pharyngeal jaws typically correlate with species that consume soft-bodied organisms like microscopic zooplankton. In contrast, hypertrophied pharyngeal jaws are found in species that consume hard prey, such as mollusks with thick shells. Pharyngeal jaws are hypothesized to be functionally decoupled from the oral jaws, as they are responsible for the processing of food items, whereas the oral jaws are primarily involved in prey capture [9,10]. In most fishes, the oral jaw quickly opens to create a negative pressure gradient that propels water and prey items into the mouth [11,12]. Because the jaws are not in direct contact with the food items, it is widely believed that oral jaws are optimized for speed, whereas the pharyngeal jaw is optimized for power [10]. However, there are many fishes that do not use their oral jaws in suction feeding, but instead the oral jaws come in direct contact with food items. For example, some reef fishes use a combination of biting and suction feeding to remove prey items from surfaces, placing different functional requirements on their oral jaw anatomy [13–18]. Direct contact between the oral jaws and the substance being fed upon has likely occurred multiple times in fishes, and this has changed the evolutionary pressures on the jaws leading to a diversity of forms [4].

One group of fishes that attaches their oral jaws directly to surfaces to scrape at food particles are the suckermouth armored catfishes, family Loricariidae [19–21]. This large and diverse family of neotropical catfishes consists of over 1000 recognized species and are identified by ossified dermal plates that cover the body and a ventrally located oral disk [22–24]. The oral disk adheres highly mobile and tooth-bearing oral jaws to a surface where the jaws are abducted 180°, then adducted rostrocaudally to scrape, gouge, and pry at a variety of benthic food items [22]. Unlike other catfishes, the premaxilla in loricariids is highly mobile and is controlled by the maxillary motion via a unique branch of the adductor mandibulae [19]. The lower jaw is comprised of medially separated mandibles that rotate around the long axis, like a screwdriver, within a shallow socket at the anteroventral articulation of the quadrate [25]. Most loricariids are assumed to consume an indistinguishable mix of detritus and algae, however some lineages have specialized diets and feed on wood (*Hypostomus cochliodon* species group, *Panaqolus*, and *Panaque*), seeds, and macroinvertebrates [22,26]. Jaw morphologies are varied and range from robust jaws that are used for consuming wood, to small jaws with long thin teeth used to probe crevices for insects, to very long jaws that likely either gouge algae or winnow materials from amongst filamentous algae (Figure 1). Teeth also vary from less than 10 to greater than 200 and from thin, villiform teeth to long, stout, probing teeth, to spoon-shaped, adz-like teeth, Despite the correlation of some morphotypes to dietary specializations, few species-poor studies have examined the convergence of jaw shape and diet [27–29].

One of the most widely used shape analysis methods to explore the evolution of variation is geometric morphometrics (GM). GM has been integral to understanding how form and function has evolved; however, the increasing complexity of capturing homologous landmarks within a 3D space can lead to researcher biases in shape interpretation. In Lujan and Armbruster

[22], the authors attempted to find a single, comparable axis for two-dimensional GM, but various twists in the jaws resulted in no homologous view points across species and standard morphometrics were employed instead. Furthermore, the limited number of homologous landmarks reduces the ability to effectively capture shape in drastically different morphologies, like the oral jaws of loricariids; however, no methods were available at the time to examine these complex structures. Recently designed automated methods allow for the comparison of bones using iterative algorithms to automatically place correspondence points that are effectively homologous to one another across several 3D surface meshes. When compared to traditional 3DGM of primate calcanei, these automated methods produced similar and meaningful shape spaces that avoid researcher errors that are often associated with traditional methods [30]. In this study, we capture the shape of loricariid oral jaws using traditional and automated landmarking methods and test the efficacy of automated methods over traditional. To examine how the shape of the oral jaw evolved, we used phylogenetic comparative methods to test for correlation to diet type, shape relatedness to phylogenic relationships, and evolutionary rates or shape change. We hypothesized that jaw shapes would correlate with diet type, resulting in convergence of shapes.

Materials and methods

Data collection

To capture the shape of the oral jaws in the Loricariidae, CT scans from 36 individuals representing 35 species were downloaded from the online repository, Morphosource, and segmented in SlicerMorph, a 3DSlicer toolkit (Table 1). Four subfamilies were represented by the following number of species: Hypoptopomatinae $n = 13$, Hypostominae $n = 11$, Loricariinae $n = 10$, and Neoplecostominae $n = 1$. Because the oral jaws are highly mobile, the left

premaxilla, maxilla, and lower jaw were individually isolated, and teeth were removed through segmentations in 3D Slicer to avoid issues with automated landmarking. The surface meshes were saved as PLY files and exported for traditional and automated landmarking processes.

Traditional landmarks were captured in SlicerMorph [31] for each skeletal element (Fig. 2 A-B). Premaxillary shape was summarized with six landmarks, denoting the corners of the tooth cup, the most lateral edge of the premaxilla, and the most medial edge of the premaxilla. Maxillary shape was summarized with four landmarks and one curve (20 sliding landmarks), which captured changes in the articulations of the head, the most distal end of the body, and the curvature of the body. Lower jaw shape was summarized by 14 landmarks that denote changes in the tooth cup, height of the crest, articulations of the anguloarticular at the quadrate, and the adductor mandibulae fossa.

Automated pseudolandmarking was completed in the Auto3DGM extension in 3DSlicer [31–33]. Auto3DGM is a homology-free landmarking protocol that places landmarks across the surface of a 3D mesh then uses iterative processes to align meshes to one another so pseudolandmarks are effectively homologous. Shape is represented by 200 pseudolandmarks on the premaxilla, 100 for the maxilla, and 300 for the lower jaw using 1000 iterations for each element (Fig. 2 C-D). The lower jaw consists of two bones, the dentary and anguloarticular. The two bones partially form a suture (sometimes the bones are ankylosed) and partially form a synchondrosis with a cartilaginous section of variable size. These characteristics made it impossible to separate the two bones, and because they operate as a single functional unit, we analyzed the entire lower jaw together. Aligned meshes were imported into Slicermorph to visually check if alignments were correct for automated datasets. Meshes which did not align properly were removed from the dataset. In the premaxilla, six specimens (*Hemiodontichthys*

acipenserinus, *Leporacanthicus joselimai*, *Lithoxus lithoides*, *Loricaria clavipinna*, *Loricariichthys maculatus*, and *Planiloricaria cryptodon*) were removed due to alignment issues and/or lack of a tooth cup. All meshes aligned properly for the maxilla and lower jaw elements.

Analyses

For each jaw element (premaxilla, maxilla, and the lower jaw) the traditional landmarks and automated pseudolandmarks were superimposed for each dataset in the R package, geomorph, using generalized least squares Procrustes superimposition (GPA) resulting in six data sets [34]. Principal component analyses (PCA) were performed for each dataset and theoretical shapes were determined by warping the 3D surface mesh of mean shape to the extremes of the axes. To obtain a mean surface mesh, we found the mean specimen using findMeanSpec in geomorph and used warpRefMesh to warp the surface mesh to the mean shape of the GPA. Once the mean surface mesh was generated, we used warpRefMesh to warp the mean mesh to the extremes of significant axes for each set. To determine the overall shape variation for the oral jaws, the Procrustes aligned landmarks for all jaw elements were combined using combine.subsets for the traditional landmark and automated pseudolandmark data sets in geomorph [35]. We used this method in place of analyzing the entire jaw in vivo because the jaws are highly mobile and can change position during preservation.

To explore evolutionary trends of jaw shape within the Loricariidae, we generated a phylomorphospace by projecting the phylogeny onto the multivariate space for each dataset [36]. Only one species had multiple specimens for which the Procrustes landmarks were averaged. The phylogenomic tree [37] was trimmed to represent the species or their congener in the multivariate dataset in the R package ape (Table 1) [38,39]. Significant axes for each dataset

were found using the broken stick method in the R package PCDimension [40–43]. To identify the shape changes related to phylogenetic signal, we performed a phylogenetically-aligned component analysis (PaCA) for all datasets. Unlike phylogenetic PCA, PaCA aligns shape data to the axis of greatest phylogenetic signal, maximizing the shape variation related to the phylogeny in the first component to reduces errors in phylogenetic signal and maximize evolutionary rates along the first component [44].

To compare traditional to automated data sets we performed a Partial Least Squares (PLS) regression on each phylomorphospace dataset (combined, premaxilla, maxilla, and lower jaw). The phylogenetic signal was calculated for the total shape and significant axes determined by broken stick method for both PCA and PaCA datasets using the K_{mult} method in geomorph. The K_{mult} method uses a Brownian motion model to evaluate the degree of phylogenetic signal in a dataset [34,45,46]. Diet type was collected from the literature and phylogenetic generalized least squares (PGLS) were performed in geomorph using the procD.pgls and pairwise functions [47]. PGLS calculates the probability that shape variation is attributed to ecological factors in a linear model. A linear model (shape coordinates ~ diet) was used to detect relationships between shape and diet. For all PGLS tests, a randomized residual permutation procedure with 1,000 permutations was used.

Evolutionary rates for the PaCA of combined automated landmarks were calculated for significant axes using a penalized-likelihood model in the R package, phytools [48,49]. This method calculates evolutionary rates under a Brownian model using a penalty term equal to the log-transformed probability density and is multiplied by a smoothing coefficient (λ). An intermediate λ ($\lambda = 1$) was used to give equal weights to probabilities. Ancestral state

reconstruction of diet type was caluclated under a Brownian motion model in the R package phytools [48].

Results

(A) Substantial morphological diversity across species.

Morphospaces. All shape analyses show complex variation in oral jaw shape of loricariid catfishes. The broken stick method showed one axis was significant for the morphospace using traditional landmarks on the premaxilla, representing ~71% of the overall variation in shape. Species on the negative end of PC1 have a more elongate premaxilla, whereas species on the positive end had a squarer premaxilla (Fig. S1A). Traditional landmark methods did not effectively separate species from one another, with most species clustered on the positive end of PC1. The only exceptions were *Oxyropsis ephippia* and *Rhadinoloricaria macromystax* which fell on the negative end.

Three axes were significant for the morphospace using traditional landmarks on the maxilla. Principle component one accounted for ~31%, PC2 for ~27%, and PC3 for ~18% of shape variation (Fig. S1C, S2). For all three axes the maxilla was less curved with smaller heads on the negative end and more curved with larger heads toward the positive end of the axes. There was less clustering of species within the morphospace; however, all subfamilies overlapped with one another across each axis.

The broken stick method showed three axes were significant for the morphospace using traditional landmarks on the lower jaw. PC1 accounted for ~48% of the variation, where the anguloarticular crests were taller with more elongated tooth cups on the negative end and shorter processes and tooth cups on positive end. PC2 accounted for ~14% of the variation in shape with

more elongated tooth cups and shorter anguloarticulars on the negative end and shorter tooth cups and longer anguloarticulars on the positive end (Fig. S1E). The third PC accounted for ~12% of the shape variation where lower jaws with smaller processes fell to the negative end and jaws with taller processes were on the positive end (Fig. S3A). Within the morphospace there was a large cluster of species with three species falling to the negative end of PC1 (*Pareiorhaphis cameroni*, *Dentectus barbarmatus*, *Panaqolus* sp.) and two species on the positive end of PC1 (*Cordylancistrus torbesensis*, *Hisonotus maculipinnis*). All subfamilies overlapped with one another across each axis.

Automated landmarking was better able to separate species from one another. Although species were more separated from one another, there was no clear distinction between subfamilies in all automated landmarked morphospaces. For the premaxilla, the broken stick method found two significant axes, representing ~31% for PC1 and ~20% for PC2 (Fig. S1B). On the negative end of PC1, the premaxilla shape was more elongate and became squarer toward the positive end. The opposite was seen on PC2, where premaxilla shape was squarer toward the negative end and became more elongated toward the positive end.

For the maxilla, two significant axes were found. On PC1, ~36% of the overall shape variation was shown, where a more curved, club-like maxilla fell toward the negative end and a less curved, more stick-like maxilla fell on the positive end (Fig. S1D). PC2 accounted for ~12.6% of the shape variation where more curved bodies were placed on the negative end and becoming less curved toward the positive end.

The lower jaw had three significant axes representing about 75% of the total variation; PC1 at ~43%, PC2 at ~20%, and PC3 at ~12% (Figs. S1F, S3B). Across PC1, tooth cups became elongated with a more robust anguloarticular toward the positive end of the axis. On PC2, there

were changes in the anguloarticular crest shape, with crests becoming taller toward the positive end. The PC3 axis primarily represented changes in the anguloarticular length, with shorter anguloarticulars toward the negative end and longer anguloarticulars toward the positive end. Although the lower jaw morphospace using automated landmarks was useful in separating species from one another, there were some misplacement of shape. Because the lower jaw could not be separated into the dentary and anguloarticular due to poor CT scanning quality and anatomical complexity, some species were misplaced in the morphospace. For example, *Cordylancistrus torbesensis*, *Pareiorhaphis cameroni*, and *Chaetostoma milesi* have long tooth cups and small anguloarticulars; however, these species are placed near species in the morphospace with short tooth cups and long anguloarticulars (*Loricariichthys maculatus* and *Dentectus barbarmatus*).

To visualize the total shape variation of the oral jaws, the combined shape was found for the premaxilla, maxilla, and lower jaw. Two axes were significant for traditional landmarks. On PC1, oral jaws with elongate tooth cups, shorter anguloarticulars, and larger maxillary heads were placed on the negative end, whereas oral jaws with shorter tooth cups, elongate anguloarticulars, and smaller maxillary heads were placed on the positive end (Fig. S4A, S5-S7). Along PC2, the bodies of the maxilla and lower jaws were slenderer and became more robust toward the positive end (Fig. S4A, S5-S7).

For automated landmarks, three significant axes were identified through the broken stick method. Along PC1, premaxillary tooth cups were more elongate, processes on the premaxilla and lower jaw were smaller, and the maxilla was slimmer toward the negative end of the axis. On the positive end of the axis, premaxillary tooth cups were shorter, the premaxilla and lower jaw had larger processes, and the maxilla was more robust (Fig. S4B, S5-S7). Across the PC2

axis, premaxillas with elongate tooth cups, smaller maxillary heads, and slenderer anguloarticulars fell on the negative end, whereas on the positive end premaxillas had shorter tooth cups, maxillary heads were larger, and the anguloarticular was more robust (Fig. S4B, S5-S7. The third principle component described only changes in the maxilla and premaxilla, where thinner maxillas and premaxillas with larger processes were placed on the negative end and thicker maxillas and premaxillas with smaller processes were placed on the positive end (Fig. S8, S5-S7).

Phylomorphospaces. When the morphospace was trimmed to fit the phylogeny [37], the broken stick method found fewer significant axes than the traditional landmarked dataset of the lower jaw (2 significant axes), the traditional landmarked combined shape dataset (1 significant axis), and the automated landmarked dataset for the lower jaw (2 significant axes). This suggests some shape data was lost by trimming the dataset to match the phylogenomic data (Fig. S9-S11). Although some shape data was lost, shape was similar to what was seen in the morphospaces (Fig. S12-S14).

All phylomorphospaces had significant overlap of subfamilies with many instances of convergence within the morphospace. Phylogenetic signal was calculated for the total shape and significant axes of each phylomorphospace dataset. The only dataset that was significant for total shape was the automated landmarking for combined jaw shape with K = 0.428 (p = 0.01; Table S1). When restricted to significant axes, the datasets for traditional landmarking and automated landmarking for the combined jaw shape were significant, with K = 0.9452 (p = 0.005) and K = 0.7833 (p = 0.001) respectively (Table S1). To determine if shape was correlated to diet type, PGLS was calculated for all eight datasets, traditional landmarking for premaxilla, maxilla, lower jaw, and combined landmarks, and automated landmarking for premaxilla, maxilla, lower

jaw, and combined landmarks. In all cases, shape was not significantly correlated with diet type (Table S2).

(B) Automated landmarking preforms better than traditional landmarking methods.

To compare how different landmarking schemes preformed to one another, we calculated the PLS between traditional and automated methods (Fig. S15). An r-PLS score of 1 suggests the two datasets are the same, whereas a score of 0 would suggest the datasets are completely different from one another. The traditional and automated landmarks for combined shape showed that traditional and automated landmarking preformed similarly with an r-PLS = 0.942 (p = 0.001; Fig. S15A). However, when traditional and automated landmarking of induvial bones were compared to one another, there was more variation between datasets, with the premaxilla scoring a r-PLS of 0.844 (p = 0.005), the maxilla a r-PLS of 0.75 (p = 0.032), and the lower jaw a r-PLS of 0.923 (p = 0.001; Fig. S15B-D). In addition to differences between the datasets, the warped meshes for traditional landmarking failed to capture realistic shapes, whereas the automated landmarks produced warped meshes that looked representative of loricariid jaws (Fig. S5-7, S11-13).

(C) Diet type correlates with evolutionary rates.

To understand the evolutionary rates of shape change, we calculated evolutionary rates for the PaCA on the combined shape data of automated landmarked specimens (Fig. 4A, S16, Table S3). For evolutionary rates of shape change on the first PC, the fastest evolving species were *Panaque nigrolineatus*, *Panaqolus* sp., and *Micracanthicus vandragti*, with the average of the top three species being 3.6x faster than the average of all species. The slowest species were

Otocinclus vittatus, *Hypoptopoma thoracatum*, and *Lamontichthys filamentosus*, with the average of the bottom three species being 1x slower than the average of all species (Fig. 4A, Table S3). The fastest evolving species for the second PC were *Neoplecostomus microps*, *Pareiorhaphis cameroni*, and *Panaque nigrolineatus*, with the average of the top three species being 2.7x faster than the average of all species. The slowest species for PC2 were *Parotocinclus maculicauda*, *Farlowella acus*, and *Lamontichthys filamentosus*, with the average of the bottom three species being 1.0x slower than the average of all species (Fig. S16, Table S3).

To determine how diet type evolved across the loricariids, we calculated ancestral states for primary diet type of each species. The results showed that the most common ancestor of all loricariids were most likely herbivorous and shifted toward omnivores at the base of the subfamily, Hypostominae. Within the subfamily Hypostominae, there was one reversal to herbivory and two independent shifts to wood eating (Fig. 4.B).

Discussion

This is the first study to use geometric morphometrics to examine the evolution of oral jaw shape in the armored catfishes. In addition to the vast diversity of shape across the species, we found that automated landmarking methods produced more meaningful morphospaces and realistic mesh warps in comparison to traditional landmarks. Shape of the oral jaw does not correlate with phylogeny or diet type, suggesting that neither have an influence on the evolution of the oral jaws in armored catfishes. However, the evolutionary rates of jaw shape correlate with diet type, which may suggest that as loricariids begin to occupy various ecological niches, the oral jaws undergo faster shape changes becoming more disparate in shape. Regardless, the lack of correlation between diet and phylogeny suggests that the loricariid catfishes in our dataset do not

have to have specialized jaws for specific diet types. There are some morphologies that are highly adapted to extreme feeding modes (like wood-eating); however, similarly shaped jaws coupled with different types of teeth could allow the fishes to feed on a wide range of materials.

Automated and traditional landmarking schemes show that suckermouth armored catfishes have a wide diversity of oral jaw shapes, with most changes occurring in the tooth cup and anguloarticular length as well as curvature of the maxilla. Within every shape space, there was considerable overlap between the subfamilies. Although morphospaces between automated and traditional processes were similar in variation, there are dramatic differences in placement within shape spaces. PLS shows significant differences between the automated and traditional landmarks, yet the combined dataset of oral jaw elements is surprisingly close between the two methods (r-PLS = 0.942, $p = 0.001$). This may suggest that a single jaw element may not represent the overall jaw shape well. Even in a decoupled system, it is likely that there is a degree of coordinated evolution between the decoupled structures [50]. For example, the premaxilla and lower jaws of *Leporacanthicus joselimai* are very different. *Leporacanthicus joselimai* is a carnivore likely feeding on snails and caddisflies and has been hypothesized to use the lower jaw to hold the prey item and the upper jaw to scoop them out of their shells or cases [51,52].

Burress and Muñoz [53] found that the pharyngeal jaws can change independently from the oral jaws, but oral jaw changes are always correlated with the pharyngeal jaws. This suggests that capture and processing of food can be decoupled, but the oral jaws cannot be the drivers of such change in cichlids. This has huge implications in functional studies that neglect the oral and pharyngeal jaws as a whole. For example, the biomechanics of loricariid jaw movement has not been successfully modeled and the kinematics are more complex than we have been able to

visualize [22,54]. Loricariids vary in their pharyngeal jaws as well [55] with differences in jaw sizes and shape, tooth number, and tooth size. Seed-feeding loricariids have pharyngeal jaws similar to durophagous cichlids with large, molariform teeth and hypertrophied bones. Future studies should link the oral and pharyngeal jaws together.

In addition to differences in shape spaces, warped 3D meshes were dissimilar between the automated and traditional methods. For extreme warps based on traditional landmarks, the limited number of homologous landmarks produced warps with unnatural shapes, whereas automated processes produced more natural looking warps. This is likely due to the complicated nature of armored catfish oral jaws, which, in addition to articulations and muscle attachments, have complex processes that cannot be captured in traditional landmarking methods. However, automated landmarking methods were limited in the ability to compare wildly different shapes, regardless of the number of intermediates. Boyer et al. [30] found that automated landmarking methods were able to align dissimilar objects to one another if constrained by intermediates, however, we found that despite the number of intermediate shapes, certain jaw shapes did not align correctly. For example, most premaxillas are longer mediolaterally, yet a few species have premaxillas that are longer anteroposteriorly. As the premaxillae are simple, automated methods were unable to differentiate between the two, leading to misalignment of shapes that had to be trimmed from the dataset. We were unable to capture extreme shapes, like *L. joselimai,* in our datasets as automated methods could not align the premaxillae correctly to other loricariids.

To further complicate things, automated methods were not designed to align fused structures such as the lower jaw. The close association of the dentary to the anguloarticular in the lower jaw made separating the two bones difficult. Because of this, there were some misplacements in the morphospace. *Cordylancistrus torbesensis*, *Pareiorhaphis cameroni*, and

Chaetostoma milesi have long tooth cups with a short anguloarticular but grouped with *Loricariichthys maculatus* and *Dentectus barbarmatus* which have short tooth cups and a long anguloarticular (Fig. S1 E-F). However, combining the oral jaws into a single dataset seemed to resolve these issues by including the shape of the premaxilla and maxilla with the lower jaw (Fig. 3, S3). Further research should seek a method that allow automated landmarks to be restricted with traditional landmarks to properly align 3D meshes.

Surprisingly, shape did not correlate with phylogenetic relationships or ecological type. Phylogenetic signal was small or insignificant, which was demonstrated by the notable overlap within the shape space (Fig. 3). In previous studies, it was hypothesized that specific diet types correlated with oral jaw shapes. Long jawed loricariids were thought to feed on detritus and algae, whereas loricariids with robust jaws fed on wood [22]. However, our results suggest that there are more complex relationships between jaw shape and diet. PGLS did not correlate shape to diet type, suggesting that a given oral jaw shape may be used to eat a diversity of materials, and likely depends on shape, number, and size of the teeth associated with the jaws as well as the muscles that operate the jaws. Yet, we did find that morphological evolutionary rates correlated with diet type in loricariids, suggesting that as loricariids begin to occupy various ecological niches, the oral jaw shape evolves faster (Fig. 4). This is consistent to studies in birds, where it was found that diet and skull shape are not closely associated with one another, nor are beak and diet type, but the morphological evolutionary rates did correlate with diet type [56–58].

Still, inadequate evidence of trophic variability across the loricariids may attribute to the lack of shape correlation found in loricariid jaws. Until recently, trophic partitioning in armored catfishes was based solely on gut content analysis, which is difficult as loricariids have fast passage rates and feed on similar looking material [59,60]. This study may benefit from modern

trophic partitioning methods using stable isotope analyses to refine diet type between species, but comparison between specimens collected as disparate localities can be difficult with stable isotopic analyses [61,62]. Sequencing gut contents could be another possibility for better establishing what loricariids feed upon, but loricariids consume mostly indigestible material. For example, although wood-eaters consume wood, they are not likely digesting it [63–65]. Determining what is in the gut of a loricariid may not be reflective of what loricariids are digesting and assimilating. Nonetheless, the lack of correlation between jaw shape, phylogeny, and diet type suggests that oral jaw morphology is not constricted to specific diet types. In other words, there are many ways for loricariids to feed on similar and different food items.

What the examination of adaptive radiations has shown us is that modularity is important in establishing morphological diversity. For loricariid jaws, the shape of the jaw itself is only part of the story. Musculature is clearly important, as muscles can change in strength and mechanical advantage allowing for flexibility in feeding with similar jaw forms [22]. Teeth are likely key to ecological partitioning. Similar jaw morphologies were noted between wood-eaters (*Panaque, Panaqolus*, and the *Hypostomus cochliodon* group), carnivores (*Leporacanthicus* and *Lithoxus* group), and potential spongivores (*Hypancistrus*) [55]. These taxa have very different teeth suggesting that changing teeth with similar jaw morphologies may allow for accessing different food items. Yet, determining diet type remains a problem with loricariids due to indistinguishable gut contents and the quick gut passage rates that limit the important dietary material in the intestinal track [63–65].

Future work will need to include more taxa, as those sampled here represent a very small swath of the diversity of loricariids, and better resolution CT scans are needed to more adequality capture tooth shape. With these data, teeth could be incorporated into the combined analysis to

better parse the shape space. Additionally, the variation in pharyngeal jaws could be incorporated into the dataset. Most pharyngeal jaws are similar across loricariids, nevertheless, there are some specialized pharyngeal jaws in the invertivorous Lithoxini, the granivorous members of the Loricariini, and the algiviorous/detritivrous Rhinelepinae [55,66]. The examination of diversity of catfish pharyngeal jaws has not been undertaken, and their function in the feeding of loricariid catfishes is unknown.

In this study, we have shown the advantages of 3D automated meshes on complex structures like loricariid jaws, but there are limits in the analysis of the premaxilla due to the simple shape (rectangular box) and in the lower jaw due to the inability to separate the two bones. The function of the loricariid jaw mechanism and its integration with ecology still remains elusive, but it would appear that different jaw morphologies can be used to feed upon different objects depending on the teeth and muscular systems associated with those jaws. This flexibly to use different jaw shapes is likely one thing that supports the great diversity of loricariid species.

References

1. Wainwright PC, Bellwood DR, Westneat MW, Grubich JR, Hoey AS. 2004 A functional morphospace for the skull of labrid fishes: patterns of diversity in a complex biomechanical system: Functional skull morphology of labrid fish. *Biological Journal of the Linnean Society* **82**, 1–25. (doi:10.1111/j.1095-8312.2004.00313.x)
2. Metzger KA, Herrel A. 2005 Correlations between lizard cranial shape and diet: a quantitative, phylogenetically informed analysis: Diet and cranial shape in lizards. *Biological Journal of the Linnean Society* **86**, 433–466. (doi:10.1111/j.1095-8312.2005.00546.x)
3. Olsen AM. 2017 Feeding ecology is the primary driver of beak shape diversification in waterfowl. *Functional Ecology* (doi:10.1111/1365-2435.12890)
4. Evans KM, Kim LY, Schubert BA, Albert JS. 2019 Ecomorphology of Neotropical Electric Fishes: An Integrative Approach to Testing the Relationships between Form, Function, and Trophic Ecology. *Integrative Organismal Biology* **1**, obz015. (doi:10.1093/iob/obz015)
5. Wake DB, Larson A. 1987 Multidimensional Analysis of an Evolving Lineage. *Science* **238**, 42–48.
6. Gould SJ. 2002 *The structure of evolutionary theory*. Cambridge: Harvard University Press.
7. Adams DC, Nistri A. 2010 Ontogenetic convergence and evolution of foot morphology in European cave salamanders (Family: Plethodontidae). *BMC Evol Biol* **10**, 216. (doi:10.1186/1471-2148-10-216)

8. Burress ED. 2016 Ecological diversification associated with the pharyngeal jaw diversity of Neotropical cichlid fishes. *J Anim Ecol* **85**, 302–313. (doi:10.1111/1365-2656.12457)

9. Wainwright PC. 2007 Functional Versus Morphological Diversity in Macroevolution. *Annu. Rev. Ecol. Evol. Syst.* **38**, 381–401. (doi:10.1146/annurev.ecolsys.38.091206.095706)

10. Burress ED, Martinez CM, Wainwright PC. 2020 Decoupled jaws promote trophic diversity in cichlid fishes. *Evolution* **74**, 950–961. (doi:10.1111/evo.13971)

11. Ferry-Graham LA, Lauder GV, Hulsey CD. 2001 Aquatic prey capture in ray-finned fishes: A century of progress and new directions. *Journal of Morphology* (doi:10.1002/jmor.1023)

12. Wainwright PC, Day SW. 2007 The forces exerted by aquatic suction feeders on their prey. *Journal of the Royal Society Interface* (doi:10.1098/rsif.2006.0197)

13. Bellwood DR, Choat JH. 1990 A functional analysis of grazing in parrotfishes (family Scaridae): the ecological implications. *Environ Biol Fish* **28**, 189–214. (doi:10.1007/BF00751035)

14. Konow N, Bellwood DR. 2005 Prey-capture in *Pomacanthus semicirculatus* (Teleostei,Pomacanthidae): functional implications of intramandibular joints in marine angelfishes. *Journal of Experimental Biology* **208**, 1421–1433. (doi:10.1242/jeb.01552)

15. Konow N, Bellwood DR, Wainwright PC, Kerr AM. 2008 Evolution of novel jaw joints promote trophic diversity in coral reef fishes: Novel jaw joints in biting reef fishes. *Biological Journal of the Linnean Society* **93**, 545–555. (doi:10.1111/j.1095-8312.2007.00893.x)

16. Ferry LA, Konow N, Gibb AC. 2012 Are Kissing Gourami Specialized for Substrate-Feeding? Prey Capture Kinematics of *Helostoma temminckii* and Other Anabantoid Fishes: Prey capture in anabantoid fishes. *J. Exp. Zool.* **317**, 571–579. (doi:10.1002/jez.1749)

17. Gibb AC, Staab K, Moran C, Ferry LA. 2015 The Teleost Intramandibular Joint: A mechanism That Allows Fish to Obtain Prey Unavailable to Suction Feeders. *Integrative and Comparative Biology* **55**, 85–96. (doi:10.1093/icb/icv042)

18. Corn KA, Martinez CM, Burress ED, Wainwright PC. 2021 A Multifunction Trade-Off has Contrasting Effects on the Evolution of Form and Function. *Systematic Biology* **70**, 681–693. (doi:10.1093/sysbio/syaa091)

19. Schaefer SA, Lauder G V. 1986 Historical Transformation of Functional Design: Evolutionary Morphology of Feeding Mechanisms in Loricarioid Catfishes. *Systematic Zoology* **35**, 489–508. (doi:10.2307/2413111)

20. Herrel A, Adriaens D, Verraes W, Aerts P. 2002 Bite performance in clariid fishes with hypertrophied jaw adductors as deduced by bite modeling. *Journal of Morphology* (doi:10.1002/jmor.1121)

21. Westneat MW. 2004 Evolution of Levers and Linkages in the Feeding Mechanisms of Fishes. *Integrative and Comparative Biology* **44**, 378–389. (doi:10.1093/icb/44.5.378)

22. Lujan NK, Armbruster JW. 2012 Morphological and functional diversity of the mandible in suckermouth armored catfishes (Siluriformes: Loricariidae). *Journal of Morphology* **273**, 24–39. (doi:10.1002/jmor.11003)

23. Armbruster JW, van der Sleen P, Lujan NK. 2018 Family Loricariidae - Suckermouth Armored Catfishes. In *Field Guide to the Fishes of the Amazon, Orinoco, & Guianas* (eds P van der Sleen, JS Albert), pp. 253–254. Princeton University Press.

24. Fricke R, Eschmeyer WN, Fong J. 2022 Eschmeyer's Catalog of Fishes. See http://researcharchive.calacademy.org/research/ichthyology/catalog/SpeciesByFamily.asp (accessed on 23 February 2019).

25. Geerinckx T, Brunain M, Herrel A, Aerts P, Adriaens D. 2007 A head with a suckermouth: A functional-morphological study of the head of the suckermouth armoured catfish Ancistrus cf. triradiatus (Loricariidae, Siluriformes). *Belgian Journal of Zoology* **137**, 47–66.

26. Buck S, Sazima I. 1995 An assemblage of mailed catfish (Loricariidae) in southeastern Brazil: distribution, activity and feeding. *Ichthyological Exploration of Freshwaters* **6**, 325–332. (doi:10.1007/s00410-011-0645-0)

27. Delariva RL, Agostinho AA. 2001 Relationship between morphology and diets of six neotropical loricariids. *Journal of Fish Biology* **58**, 832–847. (doi:10.1006/jfbi.2000.1499)

28. Fugi R, Agostinho AA, Hahn NS. 2005 Trophic morphology of five benthic-feeding fish species of a tropical floodplain. *Revista Brasileira de Biologia* (doi:10.1590/s0034-71082001000100005)

29. de Mérona B, Hugueny B, Tejerina-Garro FL, Gautheret E. 2008 Diet-morphology relationship in a fish assemblage from a medium-sized river of French Guiana: the effect of species taxonomic proximity. *Aquatic Living Resources* (doi:10.1051/alr:2008032)

30. Boyer DM, Puente J, Gladman JT, Glynn C, Mukherjee S, Yapuncich GS, Daubechies I. 2015 A New Fully Automated Approach for Aligning and Comparing Shapes: Automated 3d geometric morphometrics. *Anat. Rec.* **298**, 249–276. (doi:10.1002/ar.23084)

31. Rolfe S *et al.* 2021 SlicerMorph: An open and extensible platform to retrieve, visualize and analyse 3D morphology. *Methods Ecol Evol* **12**, 1816–1825. (doi:10.1111/2041-210X.13669)

32. Kikinis R, Pieper SD, Vosburgh KG. 2014 3D Slicer: A Platform for Subject-Specific Image Analysis, Visualization, and Clinical Support. In *Intraoperative Imaging and Image-Guided Therapy* (ed FA Jolesz), pp. 277–289. New York, NY: Springer New York. (doi:10.1007/978-1-4614-7657-3_19)

33. Aneja D, Vora SR, Camci ED, Shapiro LG, Cox TC. 2015 Automated Detection of 3D Landmarks for the Elimination of Non-Biological Variation in Geometric Morphometric Analyses. In *2015 IEEE 28th International Symposium on Computer-Based Medical Systems*, pp. 78–83. Sao Carlos, Brazil: IEEE. (doi:10.1109/CBMS.2015.86)

34. Adams DC, Otárola-Castillo E. 2013 Geomorph: An r package for the collection and analysis of geometric morphometric shape data. *Methods Ecol Evol* **4**, 393–399. (doi:10.1111/2041-210X.12035)

35. Collyer ML, Davis MA, Adams DC. 2020 Making Heads or Tails of Combined Landmark Configurations in Geometric Morphometric Data. *Evol Biol* **47**, 193–205. (doi:10.1007/s11692-020-09503-z)

36. Sidlauskas B. 2008 Continuous and arrested morphological diversification in sister clades of characiform fishes: A phylomorphospace approach. *Evolution* **62**, 3135–3156. (doi:10.1111/j.1558-5646.2008.00519.x)

37. Roxo FF *et al.* 2019 Phylogenomic reappraisal of the Neotropical catfish family Loricariidae (Teleostei: Siluriformes) using ultraconserved elements. *Molecular Phylogenetics and Evolution* **135**, 148–165. (doi:10.1016/j.ympev.2019.02.017)

38. Paradis E, Claude J, Strimmer K. 2004 APE: Analyses of Phylogenetics and Evolution in R language. *Bioinformatics* **20**, 289–290. (doi:10.1093/bioinformatics/btg412)

39. R Core Team. 2020 *R: A language and environment for statistical computing.* R Foundation for Statistical Computing, Vienna, Austria. See https://www.R-project.org/.

40. Frontier S. 1976 Study of the decay of eigenvalues in a principal component analysis: Comparison with the broken stick model. *Journal of Experimental Marine Biology and Ecology* **25**, 67–75. (doi:10.1016/0022-0981(76)90076-9)

41. Jackson DA. 1993 Stopping Rules in Principal Components Analysis: A Comparison of Heuristical and Statistical Approaches. *Ecology* **74**, 2204–2214. (doi:10.2307/1939574)

42. Legendre P, Legendre L. 2012 *Numerical Ecology*. Elsevier.

43. Coombes KR, Wang M. 2019 *PCDimension: Finding the Number of Significant Principal Components.* See https://CRAN.R-project.org/package=PCDimension.

44. Collyer ML, Adams DC. 2021 Phylogenetically aligned component analysis. *Methods Ecol Evol* **12**, 359–372. (doi:10.1111/2041-210X.13515)

45. Adams DC. 2014 A generalized K statistic for estimating phylogenetic signal from shape and other high-dimensional multivariate data. *Systematic Biology* **63**, 685–697. (doi:10.1093/sysbio/syu030)

46. Collyer ML, Adams DC. 2018 RRPP: An r package for fitting linear models to high-dimensional data using residual randomization. *Methods in Ecology and Evolution* **9**, 1772–1779. (doi:10.1111/2041-210X.13029)

47. Adams DC, Collyer ML. 2018 Phylogenetic ANOVA: Group-clade aggregation, biological challenges, and a refined permutation procedure. *Evolution* **72**, 1204–1215. (doi:10.1111/evo.13492)

48. Revell LJ. 2012 phytools: An R package for phylogenetic comparative biology (and other things). *Methods in Ecology and Evolution* (doi:10.1111/j.2041-210X.2011.00169.x)

49. Revell LJ. 2021 A variable-rate quantitative trait evolution model using penalized-likelihood. *bioRxiv* , 2021.04.17.440282.

50. Conith AJ, Albertson RC. 2021 The cichlid oral and pharyngeal jaws are evolutionarily and genetically coupled. *Nat Commun* **12**, 5477. (doi:10.1038/s41467-021-25755-5)

51. Lujan NK, Armbruster JW. 2011 Two New Genera and Species of Ancistrini (Siluriformes: Loricariidae) from the Western Guiana Shield. *Copeia* **2011**, 216–225.

52. Burgess WE. 1994 Scobinancistrus aureatus, a new species of loricariid catfish from the Rio Xingu (Loricariidae: Ancistrinae). *Tropical Fish Hobbyist* **43**, 236–242.

53. Burress ED, Muñoz MM. 2021 Ecological Limits on the Decoupling of Prey Capture and Processing in Fishes. *Integrative and Comparative Biology* **61**, 773–782. (doi:10.1093/icb/icab148)

54. Adriaens D, Geerinckx T, Vlassenbroeck J, Van Hoorebeke L, Herrel A. 2009 Extensive Jaw Mobility in Suckermouth Armored Catfishes (Loricariidae): A Morphological and Kinematic Analysis of Substrate Scraping Mode of Feeding. *Physiological and Biochemical Zoology* **82**, 51–62. (doi:10.1086/594378)

55. Armbruster JW. 2004 Phylogenetic relationships of the suckermouth armoured catfishes (Loricariidae) with emphasis on the Hypostominae and the Ancistrinae. *Zoological Journal of the Linnean Society* **141**, 1–80. (doi:10.1111/j.1096-3642.2004.00109.x)

56. Bright JA, Marugán-Lobón J, Cobb SN, Rayfield EJ. 2016 The shapes of bird beaks are highly controlled by nondietary factors. *Proc. Natl. Acad. Sci. U.S.A.* **113**, 5352–5357. (doi:10.1073/pnas.1602683113)

57. Felice RN, Goswami A. 2018 Developmental origins of mosaic evolution in the avian cranium. *Proc. Natl. Acad. Sci. U.S.A.* **115**, 555–560. (doi:10.1073/pnas.1716437115)

58. Navalón G, Bright JA, Marugán-Lobón J, Rayfield EJ. 2019 The evolutionary relationship among beak shape, mechanical advantage, and feeding ecology in modern birds*. *Evolution* **73**, 422–435. (doi:10.1111/evo.13655)

59. Bowen SH. 1983 Detritivory in neotropical fish communities. *Environmental Biology of Fishes* (doi:10.1007/BF00690858)

60. Hood JM, Vanni MJ, Flecker AS. 2005 Nutrient recycling by two phosphorus-rich grazing catfish: The potential for phosphorus-limitation of fish growth. *Oecologia* (doi:10.1007/s00442-005-0202-5)

61. Lujan NK, Winemiller KO, Armbruster JW. 2012 Trophic diversity in the evolution and community assembly of loricariid catfishes. *BMC Evolutionary Biology* **12**, 124. (doi:10.1186/1471-2148-12-124)

62. Black CR, Armbruster JW. 2021 New method of isotopic analysis: baseline-standardized isotope vector analysis shows trophic partitioning in loricariids. *Ecosphere* **12**. (doi:10.1002/ecs2.3503)

63. German DP. 2009 Inside the guts of wood-eating catfishes: Can they digest wood? *Journal of Comparative Physiology B: Biochemical, Systemic, and Environmental Physiology* **179**, 1011–1023. (doi:10.1007/s00360-009-0381-1)

64. Lujan NK, German DP, Winemiller KO. 2011 Do wood-grazing fishes partition their niche?: Morphological and isotopic evidence for trophic segregation in Neotropical Loricariidae. *Functional Ecology* **25**, 1327–1338. (doi:10.1111/j.1365-2435.2011.01883.x)

65. McCauley M, German DP, Lujan NK, Jackson CR. 2020 Gut microbiomes of sympatric Amazonian wood-eating catfishes (Loricariidae) reflect host identity and little role in wood digestion. *Ecol Evol*, ece3.6413. (doi:10.1002/ece3.6413)

66. Armbruster JW. 1998 Phylogenetic Relationships of the Suckermouth Armored Catfishes of the Rhinelepis Group (Loricariidae: Hypostominae). *Copeia* **1998**, 620. (doi:10.2307/1447792)

Tables

Table 1. Specimens used in this study.

Taxon	Abbr. in Fig.	Catalog Number	Morphosource ID/ARK ID	In Roxo et al. (congener)
Loricariidae				
Hypoptopomatinae				
Gymnotocinclus anosteos	*G. ano*	ANSP187156	M44337-80318 ark:/87602/m4/M80318	yes
Hirtella carinata	*H. car*	ANSP198032	M44346-80328 ark:/87602/m4/M80328	no
Hisonotus maculipinnis	*H. mac*	ANSP187011	M38996-70689 ark:/87602/m4/M70689	yes (*Hisonotus leucofrenatus* 10881)
Hypoptopoma spectabile	*H. spe*	ANSP133767	M38998-70693 ark:/87602/m4/M70693	yes (*Hypoptopoma psilogaster* 22980)
Hypoptopoma thoracatum	*H. tho*	ANSP198923	M37581-68823 ark:/87602/m4/M68823	yes (*Hypoptopoma thoracanthum* 63837)
Microlepidogaster perforatus	*M. per*	ANSP174117	M37975-69310 ark:/87602/m4/M69310	yes
Neoplecostomus microp	*N. mic*	ANSP174122	M37606-68859 ark:/87602/m4/M68859	yes (*Neoplecostomus franciscoensis* 7208)
Otocinclus vittatus	*O. vit*	ANSP174732	M39000-70695 ark:/87602/m4/M70695	yes
Otothyris lophophanes	*O. lop*	ANSP84381	M38995-70687 ark:/87602/m4/M70687	no
Oxyropsis ephippia	*O. eph*	ANSP177381	M44347-80330 ark:/87602/m4/M80330	no
Oxyropsis wrightiana	*O. wri*	ANSP193942	M37586-68830 ark:/87602/m4/M68830	no
Pareiorhaphis cameroni	*P. cam*	ANSP173796	M37986-69322 ark:/87602/m4/M69322	yes (*Pareiorhaphis* sp. 9685)
Pareiorhina rudolphi	*P. rud*	ANSP174125	M37990-69326 ark:/87602/m4/M69326	yes
Parotocinclus maculicauda	*P. mac*	ANSP168971	M44336-80317 ark:/87602/m4/M80317	yes (*Parotocinclus* cf. *bahiensis* 34692)
Hypostominae				
Baryancistrus xanthellus	*B. xan*	ANSP198216	M37989-69325 ark:/87602/m4/M69325	yes (*Baryancistrus beggini* 39227)

Taxon	Abbr. in Fig.	Catalog Number	Morphosource ID/ARK ID	In Roxo et al. (congener)
Chaetostoma milesi	*C. mil*	AUMXXXXX	M24790-48802 ark:/87602/m4/M48802	yes (*Chaetostoma jegui*)
Cordylancistrus torbesensis	*C. tor*	MCZ36170	M24040-47256 ark:/87602/m4/M47256	no
Dekeyseria pulcher	*D. pul*	ANSP185289	M37978-69314 ark:/87602/m4/M69314	no
Hypancistrus zebra	*H. zeb*	ANSP197839	M37572-68813 ark:/87602/m4/M68813	yes (*Hypancistrus* sp. 61759)
Leporacanthicus joselimai	*L. jos*	AUMXXXXX	M24526-48318 ark:/87602/m4/M48318	yes
Lithoxus lithoides	*L. lit*	ANSP177363	M37594-68841 ark:/87602/m4/M68841	no
Micracanthicus vandragti	*M. van*	ANSP199002	M37980-69316 ark:/87602/m4/M69316	yes
Panaqolus sp.	*P. sp.*	ANSP194642	M37593-68839 ark:/87602/m4/M68839	yes (*Panaqolus* sp. 61753)
Panaque nigrolineatus	*P. nig*	ANSP128682, AUMXXXXX	M37982-69318 ark:/87602/m4/M69318 M24791-48803 ark:/87602/m4/M48803	yes (*Panaque cochliodon* 19170)
Pseudolithoxus tigris	*P. tig*	YPM023896	M44257-80205 ark:/87602/m4/M80205	yes
Loricariinae				
Dentectus barbarmatus	*D. bar*	ANSP160860	M37577-68818 ark:/87602/m4/M68818	no
Farlowella acus	*F. acu*	ANSP191381	M37599-68848 ark:/87602/m4/M68848	yes (*Farlowella amazona* 26397)
Harttia loricariformis	*H. lor*	MCZ8121	M23563-46120 ark:/87602/m4/M46120	yes
Harttiella longicauda	*H. lon*	ANSP190961	M44340-80321 ark:/87602/m4/M80319	no
Hemiodontichthys acipenserinus	*H. aci*	ANSP192919	M37597-68845 ark:/87602/m4/M68845	no
Lamontichthys filamentosus	*L. fil*	ANSP181100	M37571-68812 ark:/87602/m4/M68812	yes

Taxon	Abbr. in Fig.	Catalog Number	Morphosource ID/ARK ID	In Roxo et al. (congener)
Loricaria clavipinna	*L. cla*	ANSP178472	M37573-68814 ark:/87602/m4/M69313	yes
Loricariichthys maculatus	*L. mac*	ANSP131614	M37590-68835 ark:/87602/m4/M68835	yes (*Loricariichthys* sp. 22778)
Planiloricaria cryptodon	*P. cry*	ANSP191512	M37604-68856 ark:/87602/m4/M68856	yes
Rhadinoloricaria macromystax	*R. mac*	TCWC15249.01	M30925-59120 ark:/87602/m4/M59120	no

Figures

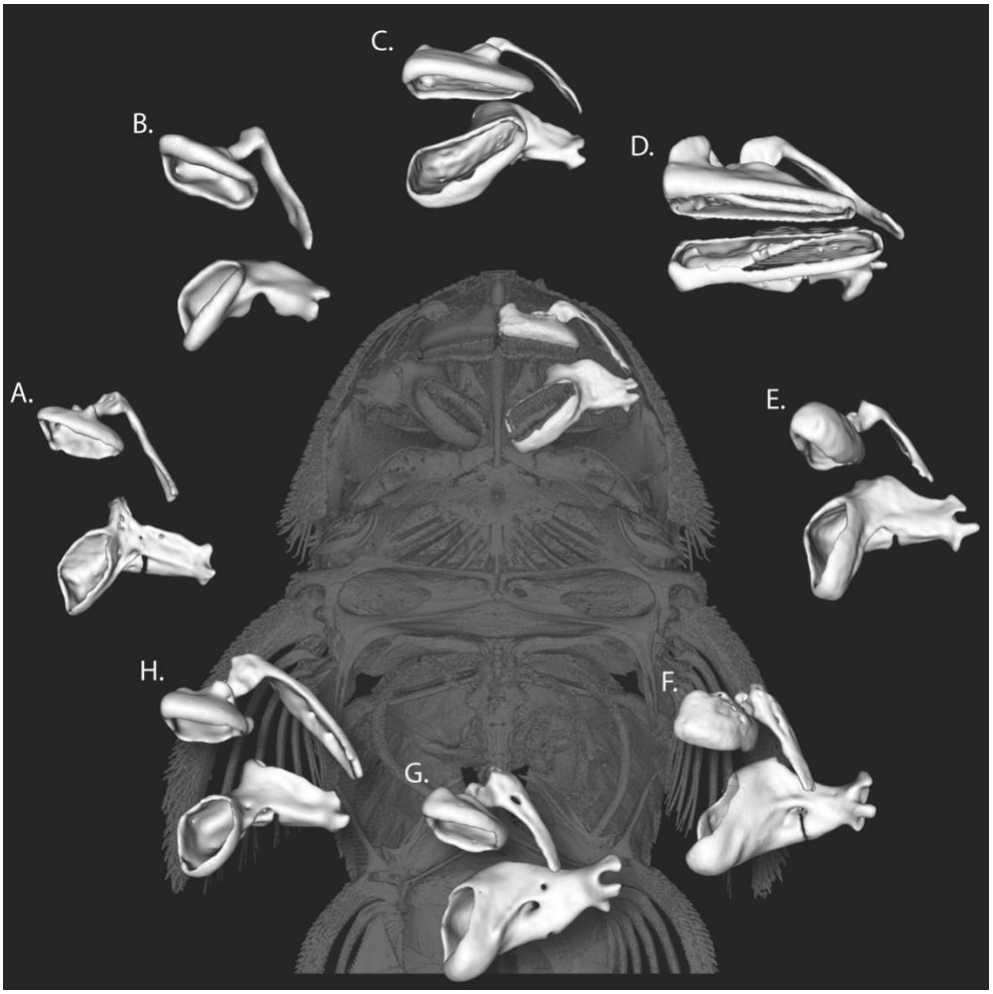

Figure 1. Oral jaw shape diversity in loricariid catfishes. The left oral jaws are shown in white. In the center, the placement of the oral jaws are shown for *Baryancistrus xanthellus*, MorphoSource ID: M37989-69325, Collection ID: ANSP 198216. Representatives of other species are as listed; A) *Otocinclus vittatus*, M39000-70695, ANSP 174732, B) *Farlowella acus*, M37599-68848, ANSP 191381, C) *Harttia loricariformis*, M44340-80321, ANSP 190961, D) *Chaetostoma milesi*, M24790-48802, AUM Unknown ID, E) *Panaqolus*, M37593-68839, ANSP 194642, F) *Hypancistrus vandragti*, M37980-69316, ANSP 199002, G) *Hypancistrus zebra*, M37572-68813, ANSP 197839, and H) *Microlepidogaster perforates*, M37975-69310, ANSP 174117. All CT scans were obtained from MorphoSource.

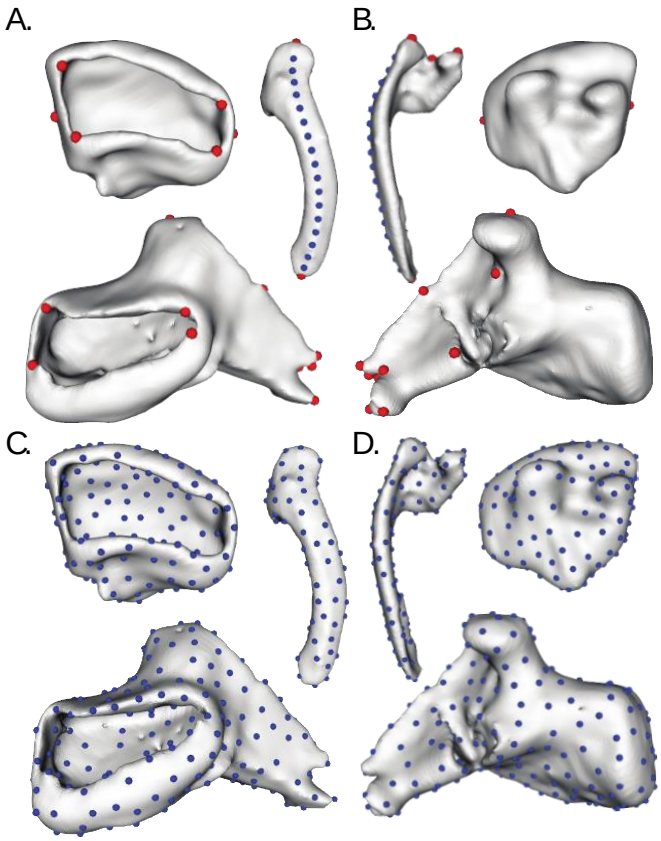

Figure 2. Traditional landmarks in the (A) ventral and (B) dorsal view, and automated landmarks in the (C) ventral and (D) dorsal view as shown on *Gymnotocinclus anosteos*.

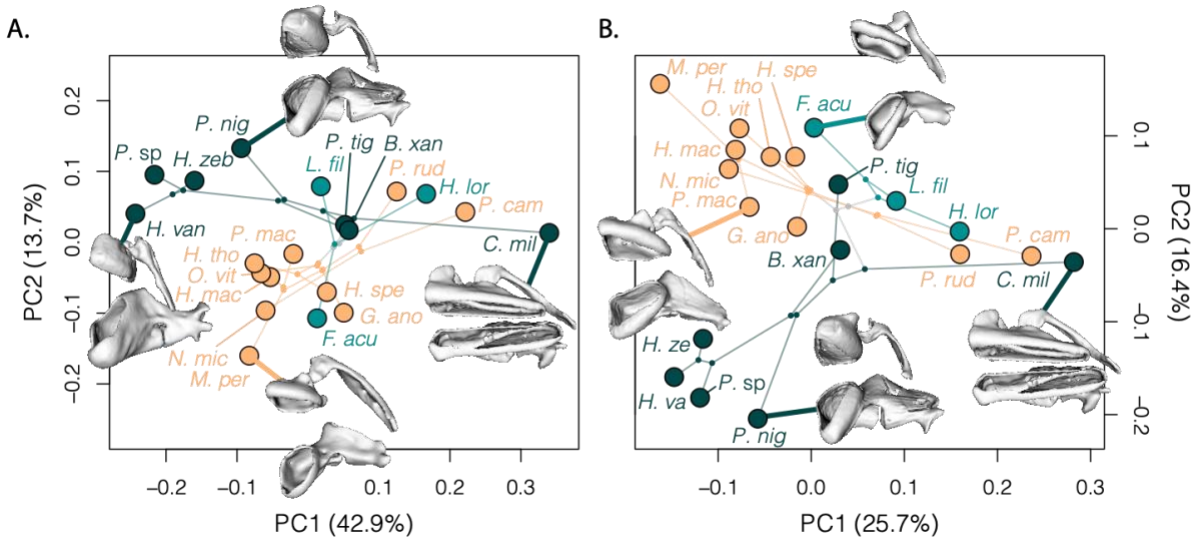

Figure 3. Phylomorphospaces for the combine shape (premaxilla, maxilla, and lower jaw) for loricariid species using (A) traditional and (B) automated landmarking. Subfamilies denoted by colors; Hypoptopomatinae in orange, Hypostominae in dark green, and Loricariinae in light green.

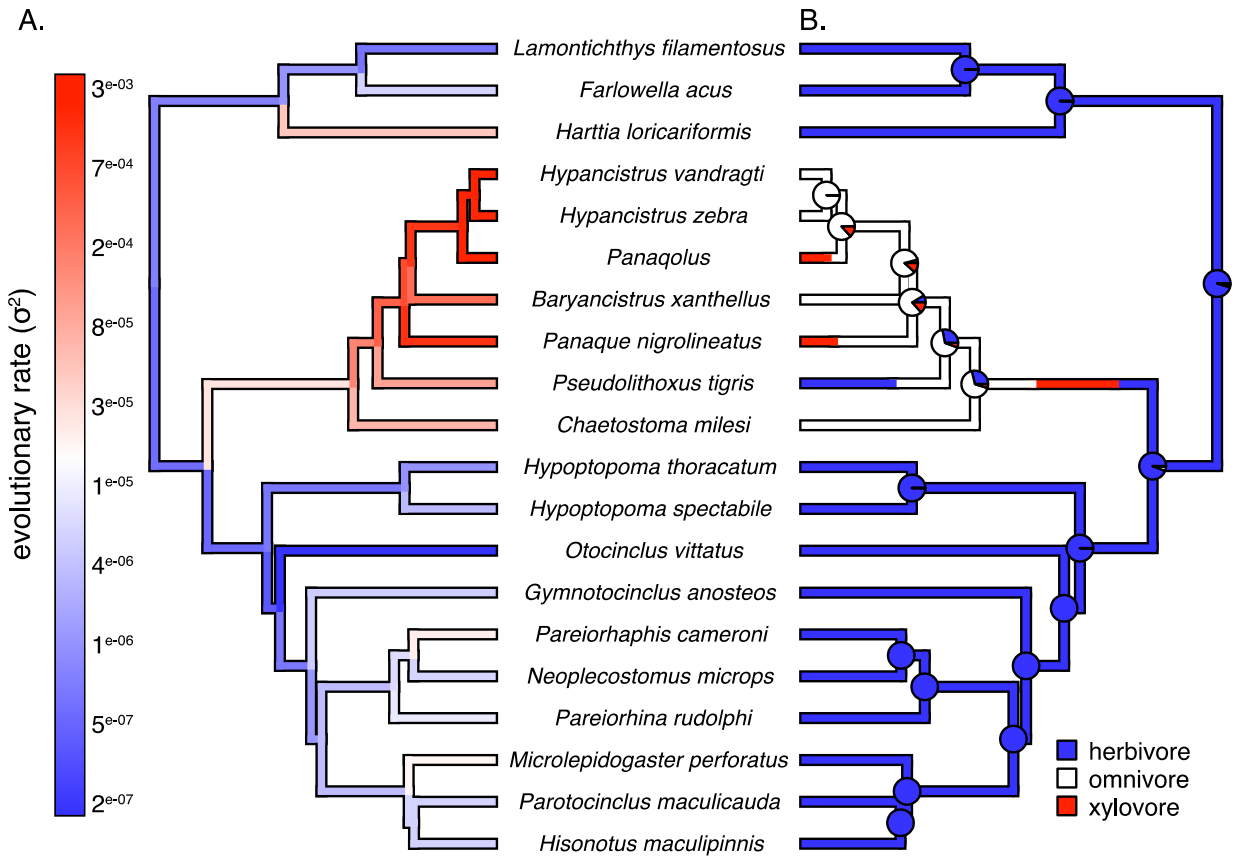

Figure 4. (A) Evolutionary rates of phylogenetically aligned components (PaCA) for combine dataset of automated landmarks along PC1 using a penalized-likelihood model compared to (B) the ancestral state reconstructions for diet type in loricariid species.

Chapter 2 Supplemental Materials

Supplemental Tables

Table S1. Significant axes and phylogenetic signal for phylomorphospaces.

Data Set		Sig. Axes	Phy Signal for Total Shape			Phy Signal for Sig. Axes		
			(K)	p-value	effect size	(K)	p-value	effect size
Traditional	Premaxilla	1	0.2334	0.918	-1.493	0.2460	0.860	-1.138
	Maxilla	3	0.3952	0.249	0.650	0.4780	0.066	1.516
	Lower Jaw	2	0.3502	0.612	-0.237	0.4228	0.319	0.458
	Combine Shape	1	0.3628	0.437	0.161	0.9452	0.005***	2.717
Automated	Premaxilla	2	0.3251	0.711	-0.521	0.5008	0.104	1.245
	Maxilla	2	0.3415	0.658	-0.353	0.5162	0.053	1.628
	Lower Jaw	2	0.3587	0.501	0.015	0.4206	0.255	0.678
	Combine Shape	3	0.4280	0.01***	2.287	0.7833	0.001***	3.983

Table S2. Phylogenetic generalized least squares for individual and combine oral jaw shape compared to diet type.

	PGLS Model	Df	SS	MS	Rsq	F	Z	Pr(>F)
Traditional Landmarks	Premaxilla~Diet	2	0.0035	0.0018	0.0541	0.4862	-0.3688	0.6360
	Maxilla~Diet	2	0.0029	0.0015	0.1312	1.5849	1.0812	0.1470
	Lower Jaw~Diet	2	0.0154	0.0077	0.1070	1.2579	0.6195	0.2780
	Combine Shape~Diet	2	0.0076	0.0038	0.1008	0.9530	0.1887	0.4290
Automated Landmarks	Premaxilla~Diet	2	0.0129	0.0064	0.1104	1.0553	0.3689	0.3430
	Maxilla~Diet	2	0.0126	0.0063	0.1368	1.6641	1.3436	0.0990
	Lower Jaw~Diet	2	0.0204	0.0102	0.1410	1.7229	1.2557	0.1190
	Combine Shape~Diet	2	0.0131	0.0065	0.1555	1.5646	1.3713	0.0820

Table S3. Evolutionary rates for automated landmarks on combine oral jaw shape for specimens and nodes.

	Phy-PCA			PaCA	
Specimen/Node#	PC1	PC2	PC3	PC1	PC2
Hisonotus_maculipinnis	3.3E-05	4.3E-05	8.5E-05	1.1E-05	1.3E-05
Parotocinclus_maculicauda	2.4E-05	4.1E-04	1.5E-03	1.3E-05	1.2E-05
Microlepidogaster_perforatus	1.4E-03	8.9E-04	7.9E-04	7.2E-05	1.0E-04
Pareiorhina_rudolphi	3.8E-03	8.3E-04	4.3E-05	2.8E-05	5.0E-04
Neoplecostomus_microp	8.1E-04	7.5E-05	5.8E-04	1.0E-05	1.7E-03
Pareiorhaphis_cameroni	1.0E-02	9.7E-04	1.4E-04	7.9E-05	1.8E-03
Gymnotocinclus_anosteos	2.0E-05	5.3E-04	6.8E-04	2.7E-05	2.7E-05
Otocinclus_vittatus	1.1E-04	7.2E-05	3.0E-04	1.6E-07	3.1E-05
Hypoptopoma_spectabile	3.6E-05	2.8E-09	6.7E-04	1.5E-05	1.3E-04
Hypoptopoma_thoracatum	1.9E-05	2.7E-09	7.6E-05	3.5E-06	2.2E-04
Chaetostoma_milesi	1.4E-02	2.9E-04	1.1E-05	4.6E-05	2.5E-04
Pseudolithoxus_tigris	3.6E-04	1.7E-04	1.7E-03	6.5E-05	4.6E-05
Panaque_nigrolineatus	8.7E-05	3.0E-03	1.1E-03	1.9E-03	1.0E-03
Baryancistrus_xanthellus	9.6E-04	3.4E-04	2.4E-04	2.1E-04	1.1E-04
Panaqolus	1.4E-04	6.5E-04	2.1E-03	1.8E-03	3.0E-04
Hypancistrus_zebra	1.7E-04	4.3E-04	6.3E-03	1.6E-03	8.3E-04
Micracanthicus_vandragti	2.6E-04	4.2E-04	3.9E-03	1.9E-03	4.2E-04
Harttia_loricariformis	2.7E-03	4.8E-04	1.1E-03	3.9E-04	7.4E-04
Farlowella_acus	2.7E-05	1.3E-04	4.5E-04	3.3E-05	1.7E-09
Lamontichthys_filamentosus	8.7E-04	1.6E-04	1.6E-04	1.0E-06	1.7E-09
Node 21	2.6E-05	5.3E-06	1.7E-05	1.3E-06	9.1E-06
Node 22	2.0E-05	6.0E-06	1.6E-05	2.1E-06	2.3E-04
Node 23	2.1E-05	3.8E-06	4.0E-05	1.1E-06	5.8E-04
Node 24	2.9E-05	7.9E-06	5.9E-05	1.2E-06	4.1E-04
Node 25	5.5E-05	3.0E-05	9.1E-05	3.4E-06	3.1E-04
Node 26	8.6E-05	3.7E-05	8.4E-05	4.2E-06	4.0E-04
Node 27	9.5E-05	1.2E-04	2.3E-04	1.4E-05	4.6E-05
Node 28	7.0E-05	1.1E-04	2.4E-04	1.3E-05	3.3E-05
Node 29	8.8E-04	1.8E-04	8.4E-05	1.4E-05	6.5E-04
Node 30	1.3E-03	1.8E-04	1.4E-04	1.7E-05	9.9E-04
Node 31	1.8E-05	6.4E-09	1.0E-04	3.5E-06	1.4E-04
Node 32	2.6E-04	4.8E-04	4.7E-05	2.3E-04	1.7E-04
Node 33	2.9E-04	6.5E-04	1.7E-04	3.5E-04	1.9E-04
Node 34	3.3E-04	1.2E-03	3.6E-04	8.2E-04	3.5E-04

Node 35	4.3E-04	1.1E-03	3.9E-04	8.0E-04	3.3E-04
Node 36	2.2E-04	6.4E-04	2.0E-03	1.8E-03	4.7E-04
Node 37	2.1E-04	4.6E-04	3.7E-03	1.7E-03	5.6E-04
Node 38	1.2E-04	3.3E-05	7.0E-05	4.0E-06	3.4E-07
Node 39	9.0E-05	6.8E-05	1.3E-04	3.4E-06	6.4E-09

Supplemental Figures

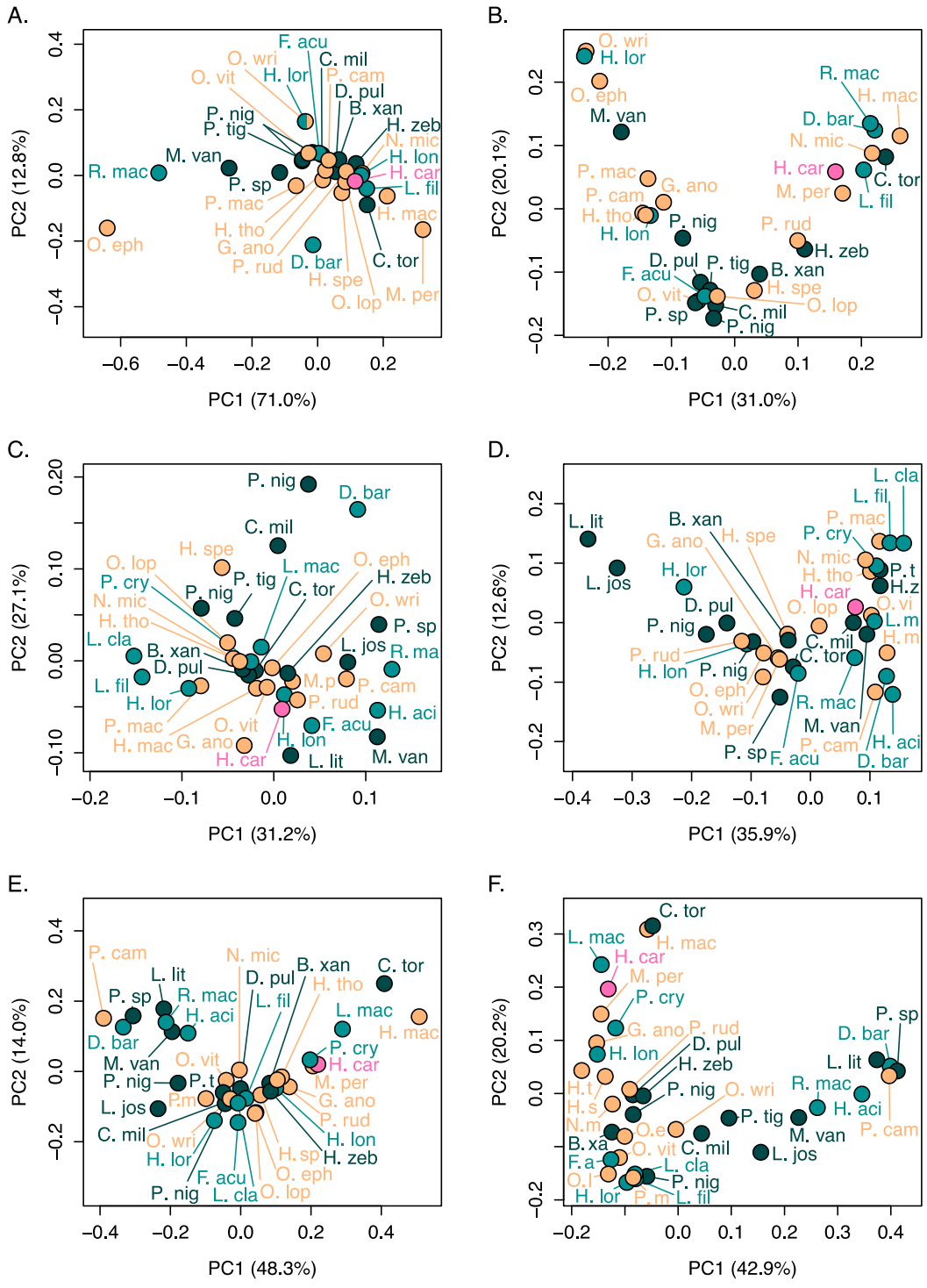

Figure S1. Morphospaces for individual bones using (A) traditional and (B) automated landmarks on the premaxilla, (C) traditional and (D) automated landmarks on the maxilla, and

(E) traditional and (F) automated landmarks on the lower jaw. Subfamilies denoted by colors; Hypoptopomatinae in orange, Hypostominae in dark green, Loricariinae in light green, and Neoplecostominae in pink.

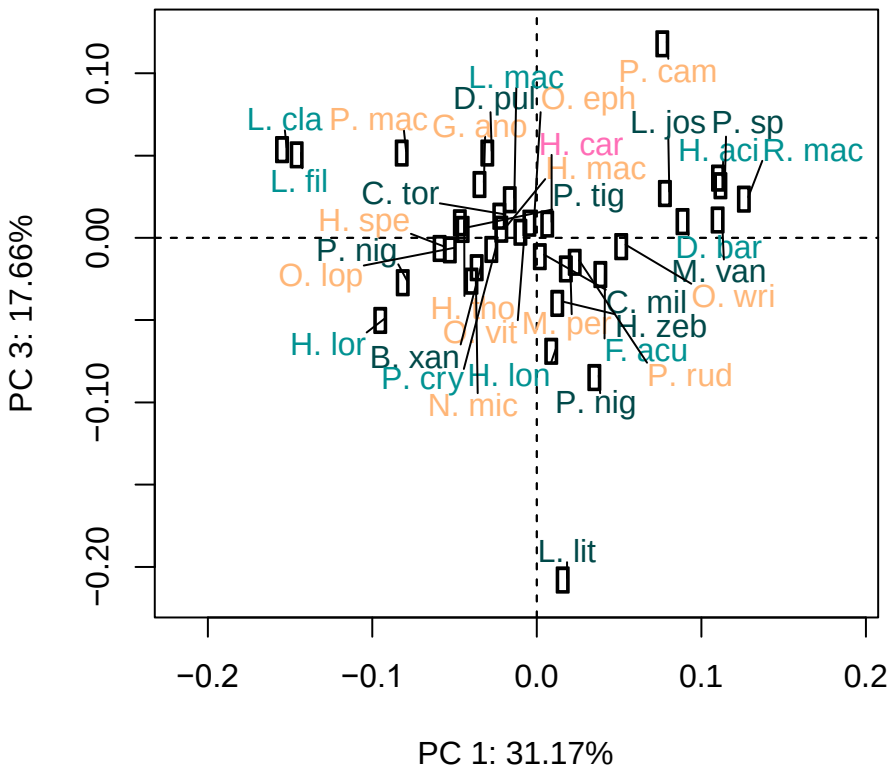

Figure S2. Morphospace of the maxilla using traditional landmarks for PC1 and PC3. Subfamilies denoted by colors; Hypoptopomatinae in orange, Hypostominae in dark green, Loricariinae in light green, and Neoplecostominae in pink.

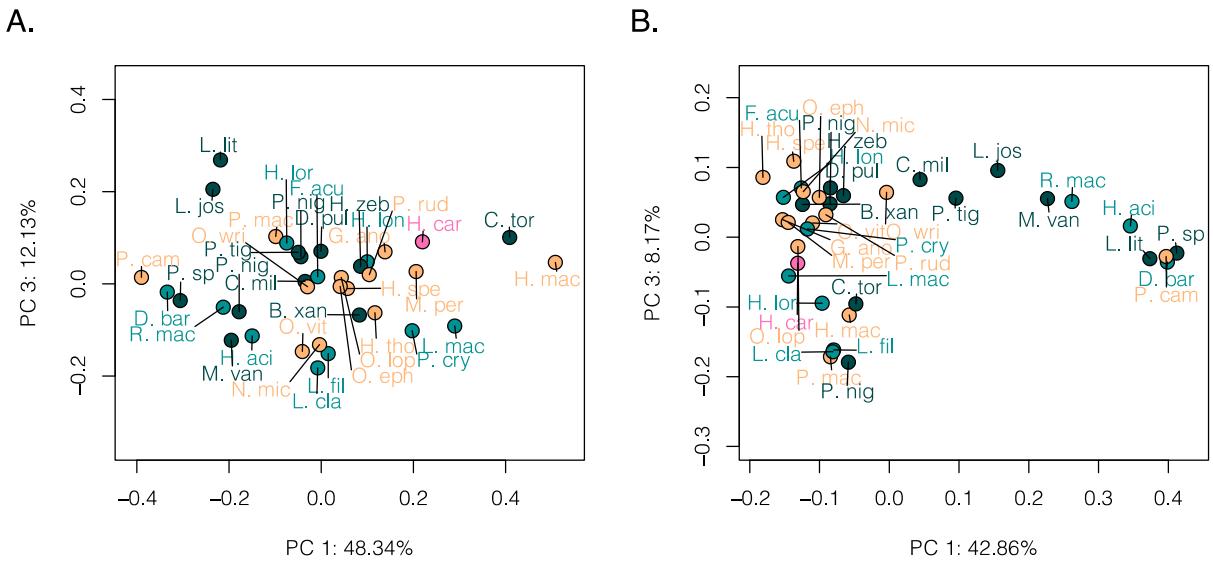

Figure S3. Morphospace for the lower jaw using (A) traditional landmarks and (B) automated landmarking methods for PC1 and PC3. Subfamilies denoted by colors; Hypoptopomatinae in orange, Hypostominae in dark green, Loricariinae in light green, and Neoplecostominae in pink.

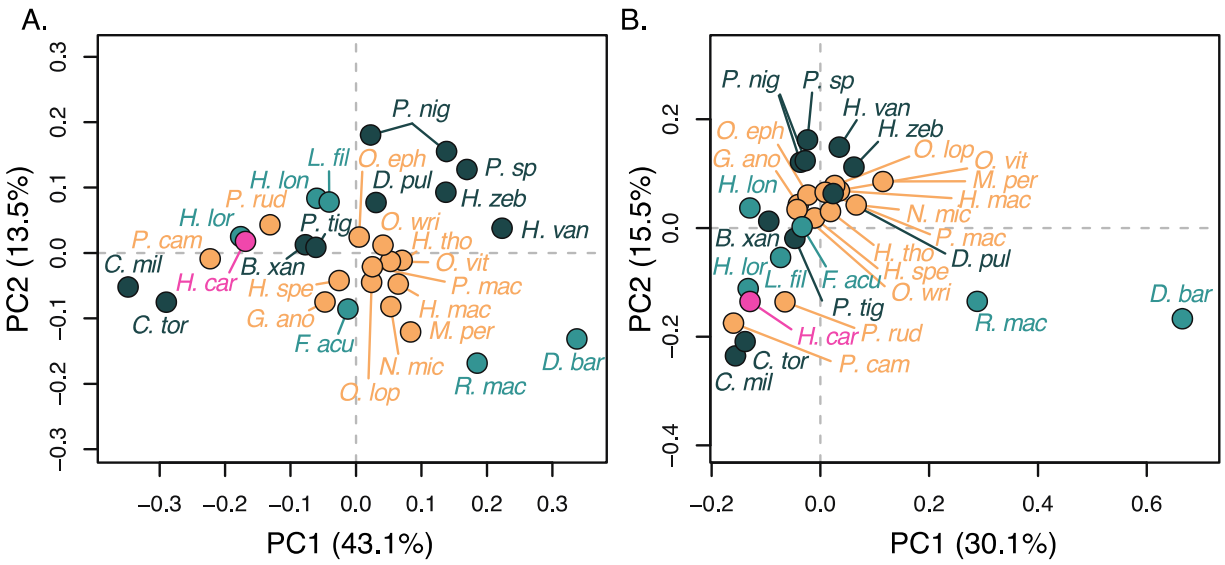

Figure S4. Morphospaces for the combine shape (premaxilla, maxilla, and lower jaw) for loricariid species using (A) traditional and (B) automated landmarking. Subfamilies denoted by colors; Hypoptopomatinae in orange, Hypostominae in dark green, Loricariinae in light green, and Neoplecostominae in pink.

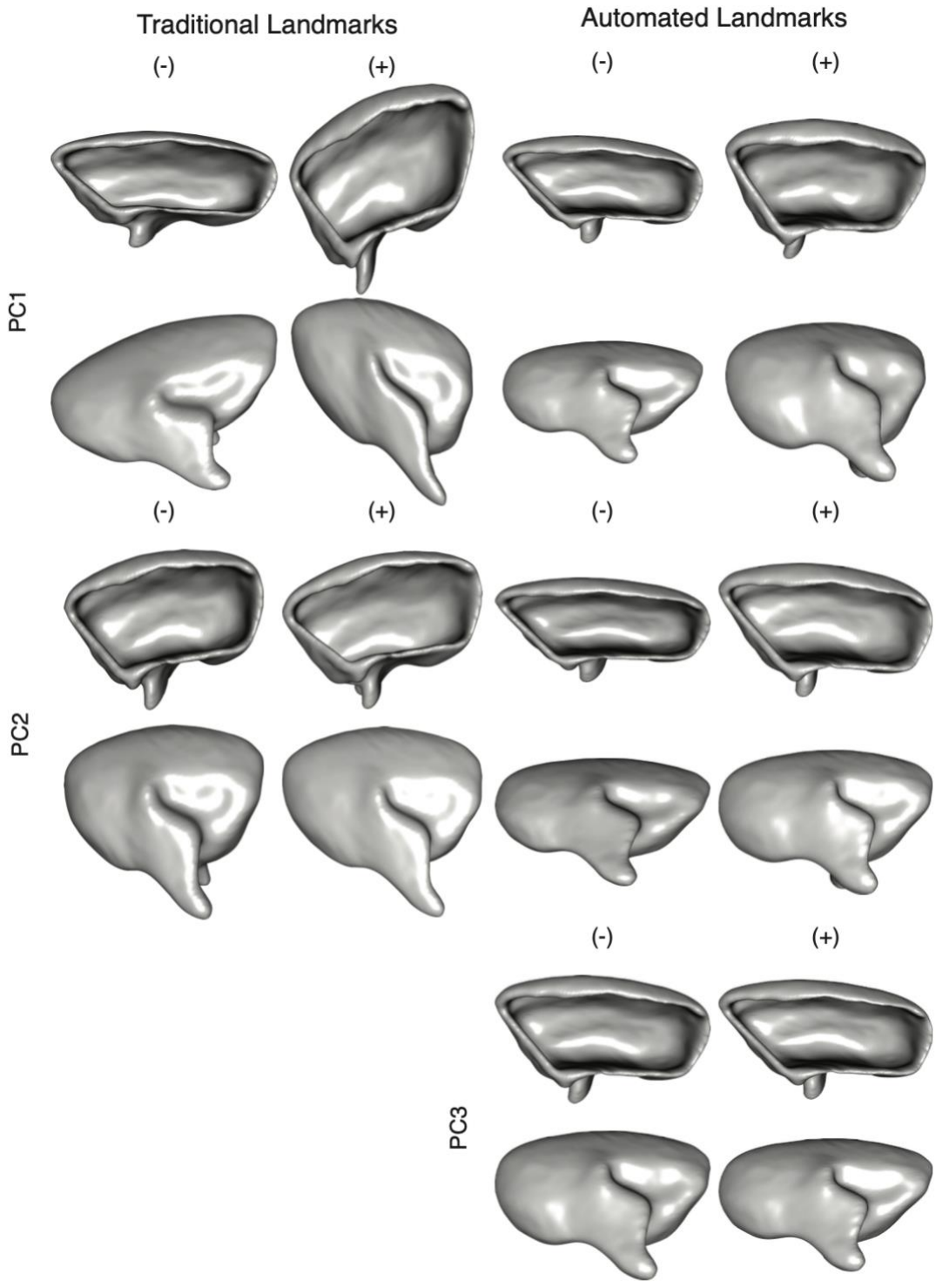

Figure S5. Warped 3D meshes for extreme shapes for the combine morphospace of the premaxilla.

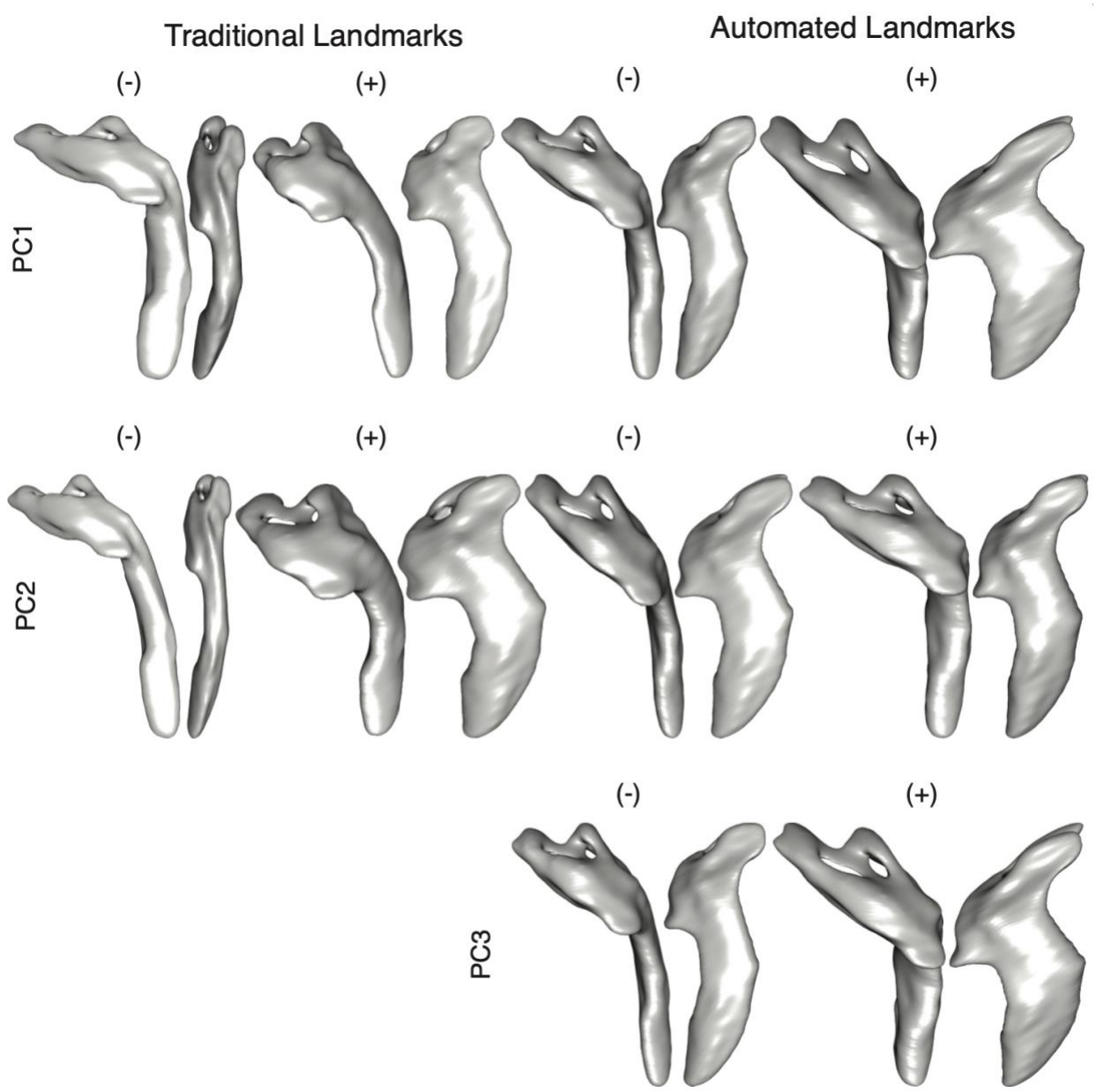

Figure S6. Warped 3D meshes for extreme shapes for the combine morphospace of the maxilla.

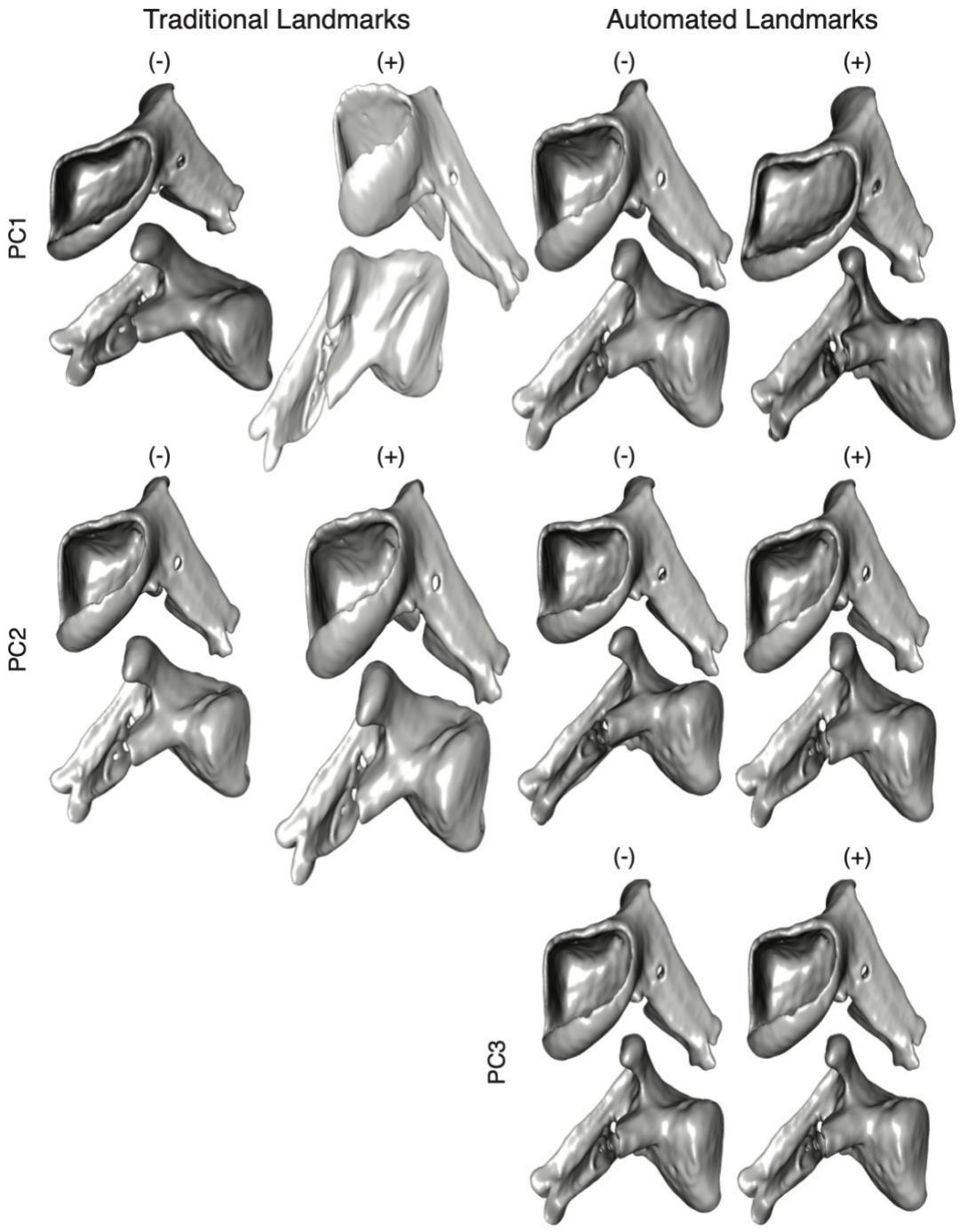

Figure S7. Warped 3D meshes for extreme shapes for the combine morphospace of the lower jaw.

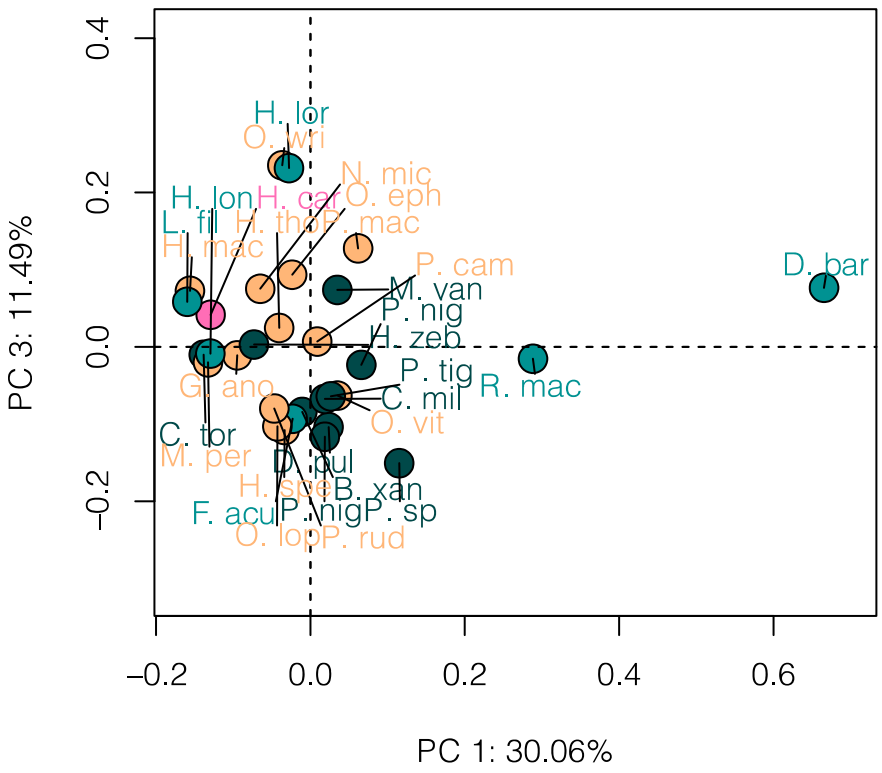

Figure S8. Morphospace of PC1 and PC3 for the combine shape (premaxilla, maxilla, and lower jaw) using automated landmarking. Subfamilies denoted by colors; Hypoptopomatinae in orange, Hypostominae in dark green, Loricariinae in light green, and Neoplecostominae in pink.

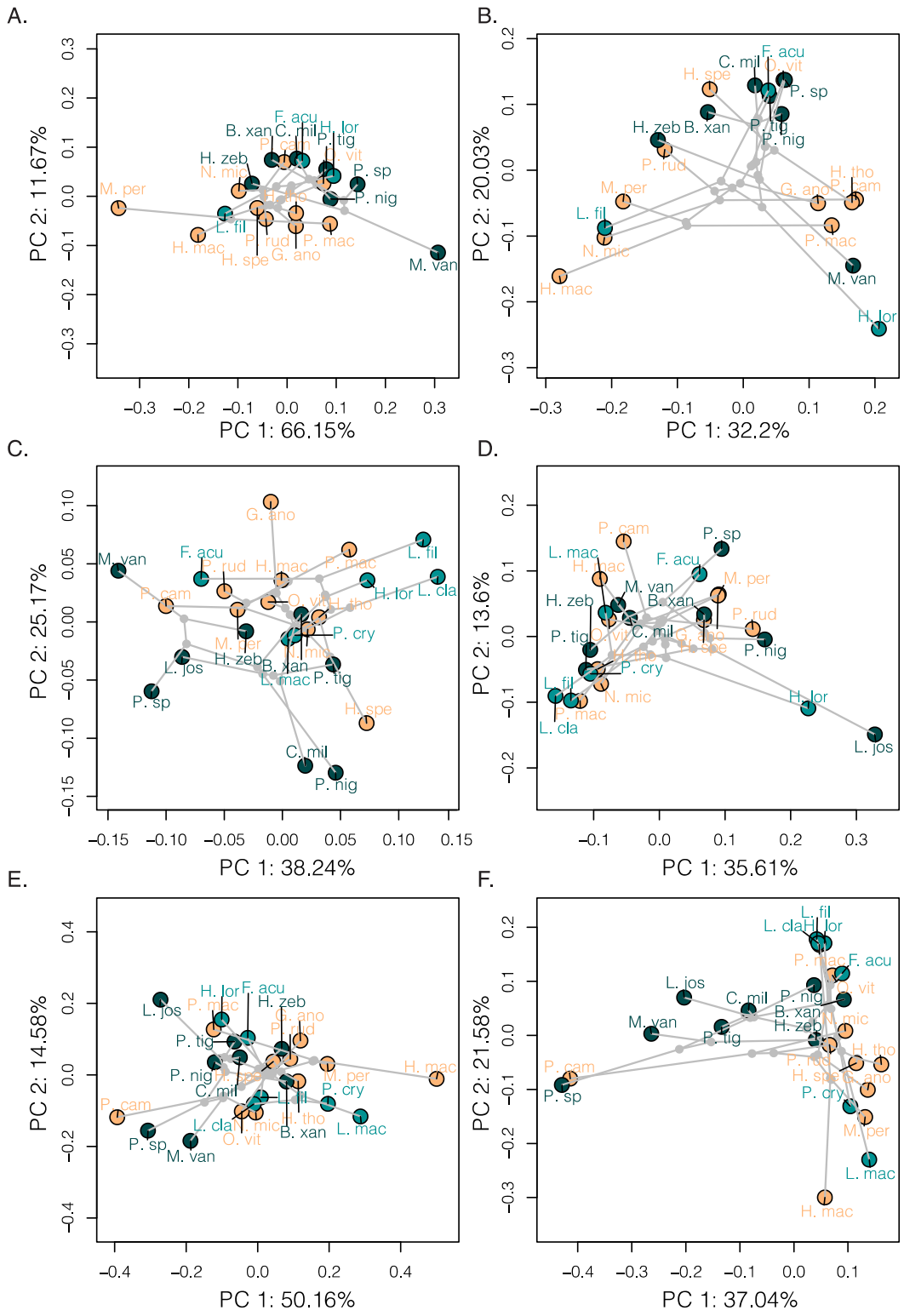

Figure S9. Phylomorphospaces for individual bones using (A) traditional and (B) automated landmarks on the premaxilla, (C) traditional and (D) automated landmarks on the maxilla, and

(E) traditional and (F) automated landmarks on the lower jaw. Subfamilies denoted by colors; Hypoptopomatinae in orange, Hypostominae in dark green, and Loricariinae in light green.

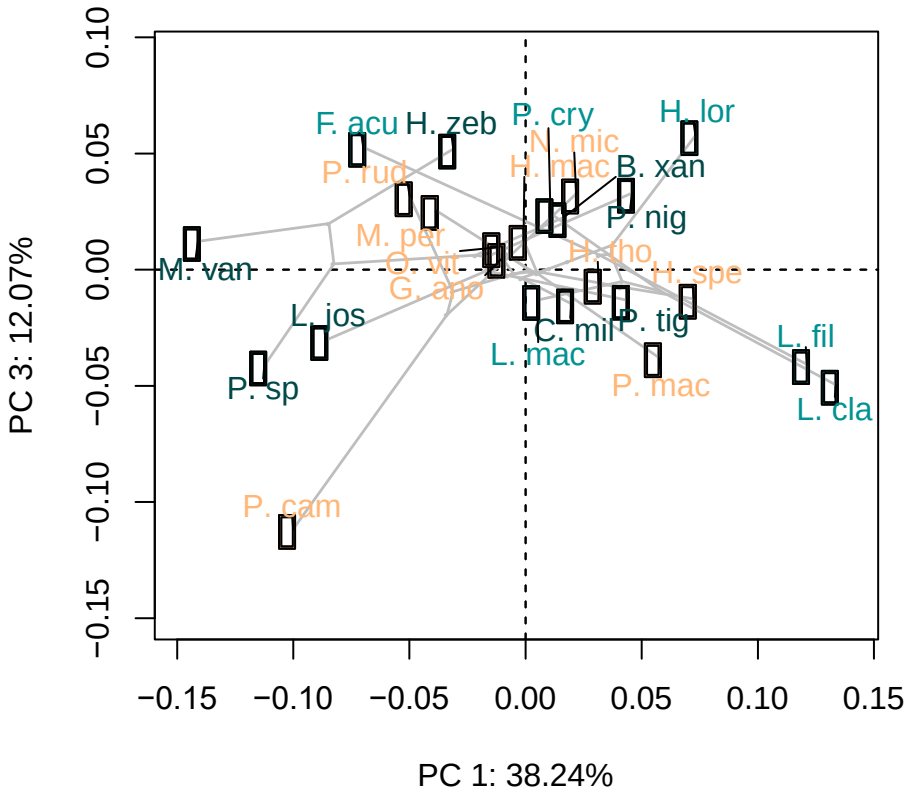

Figure S10. Phylomorphospace of PC1 and PC3 for the maxilla using traditional landmarks. Subfamilies denoted by colors; Hypoptopomatinae in orange, Hypostominae in dark green, and Loricariinae in light green.

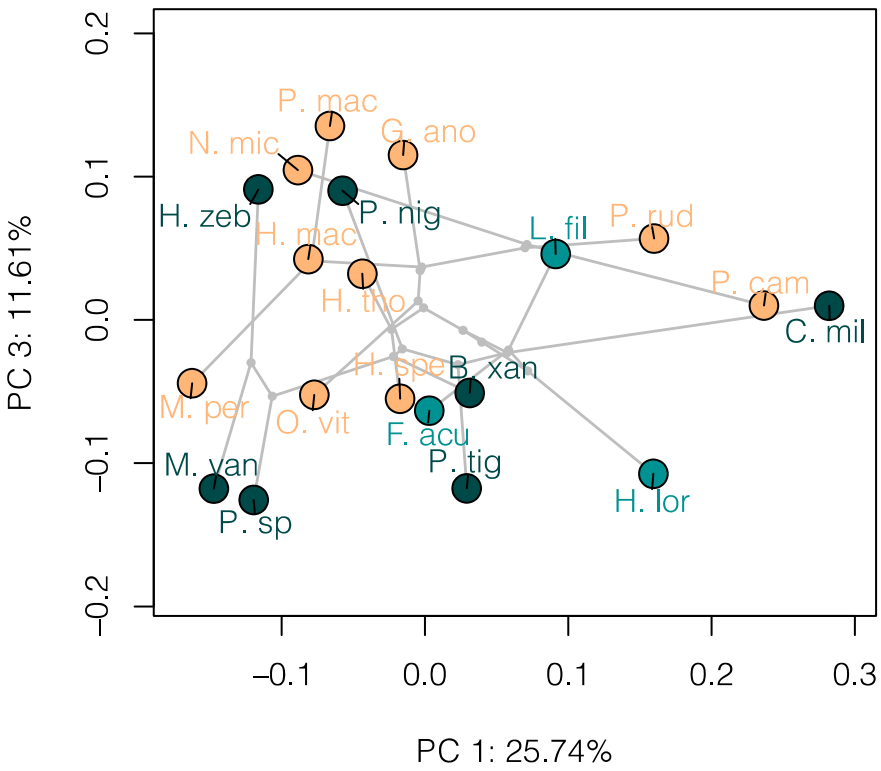

Figure S11. Phylomorphospace for the combine shape (premaxilla, maxilla, and lower jaw) of loricariid species using automated landmarking. Subfamilies denoted by colors; Hypoptopomatinae in orange, Hypostominae in dark green, and Loricariinae in light green.

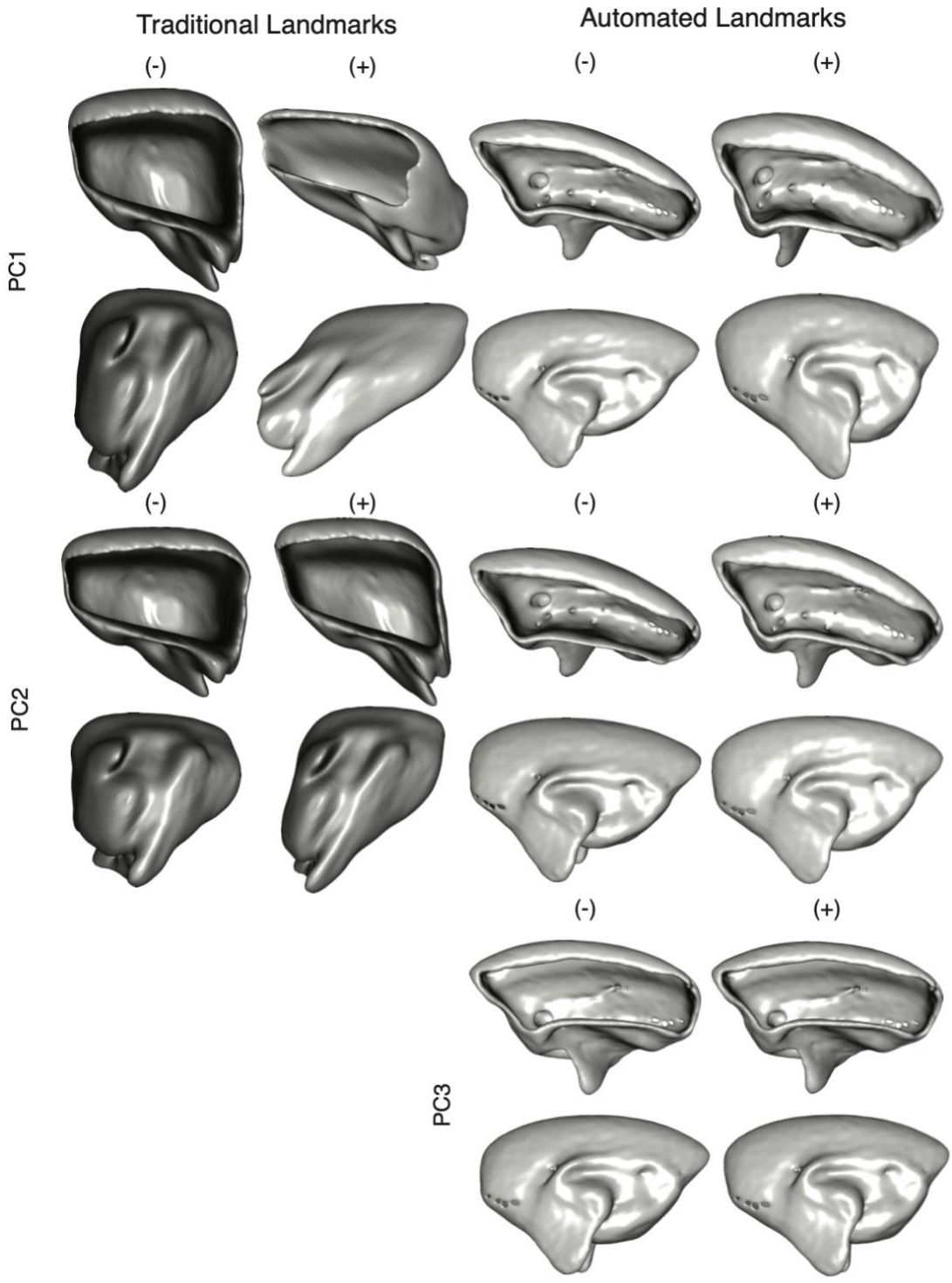

Figure S12. Warped 3D meshes for extreme shapes for the combine phylomorphospace of the premaxilla.

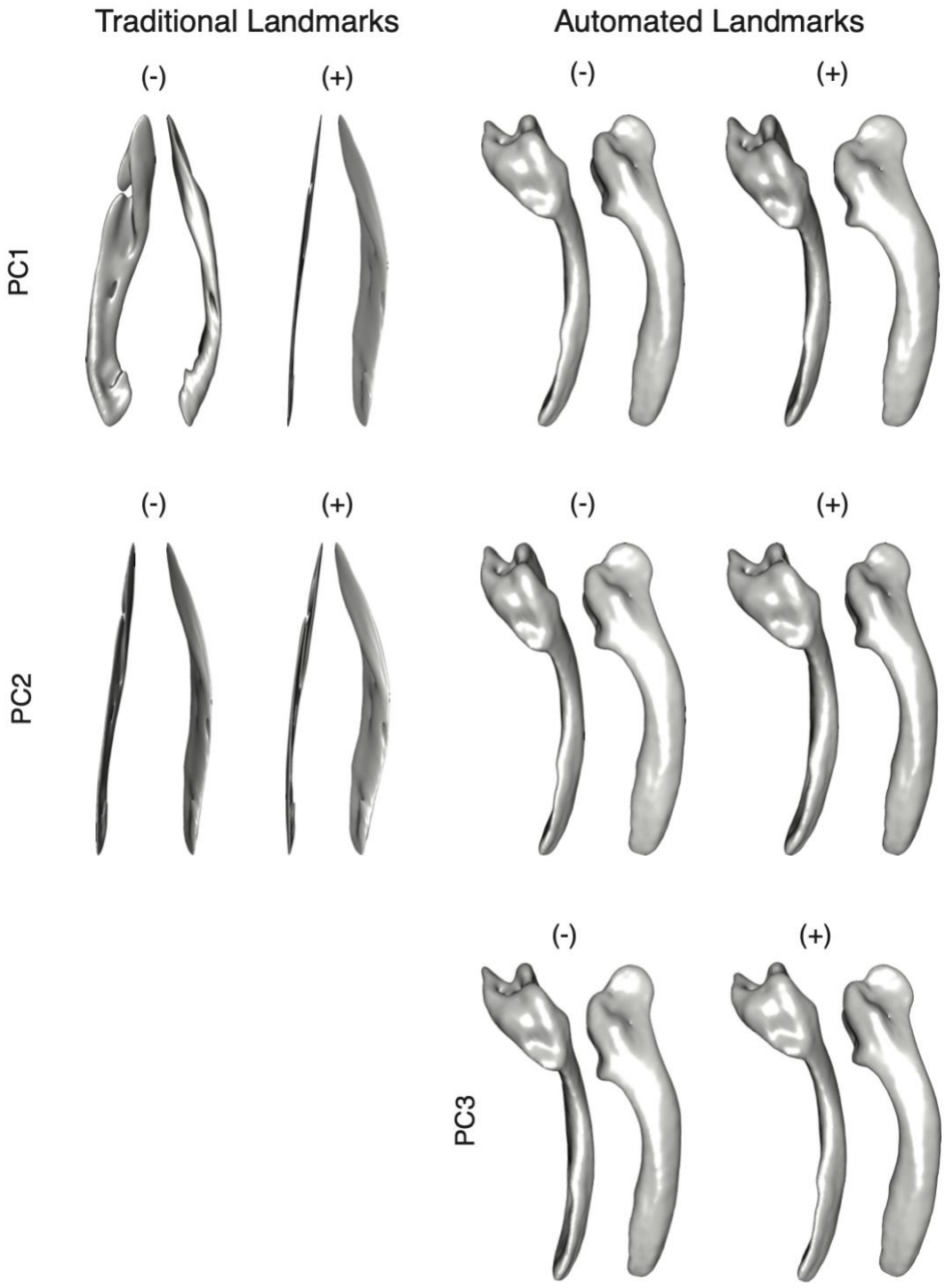

Figure S13. Warped 3D meshes for extreme shapes for the combine phylomorphospace of the maxilla.

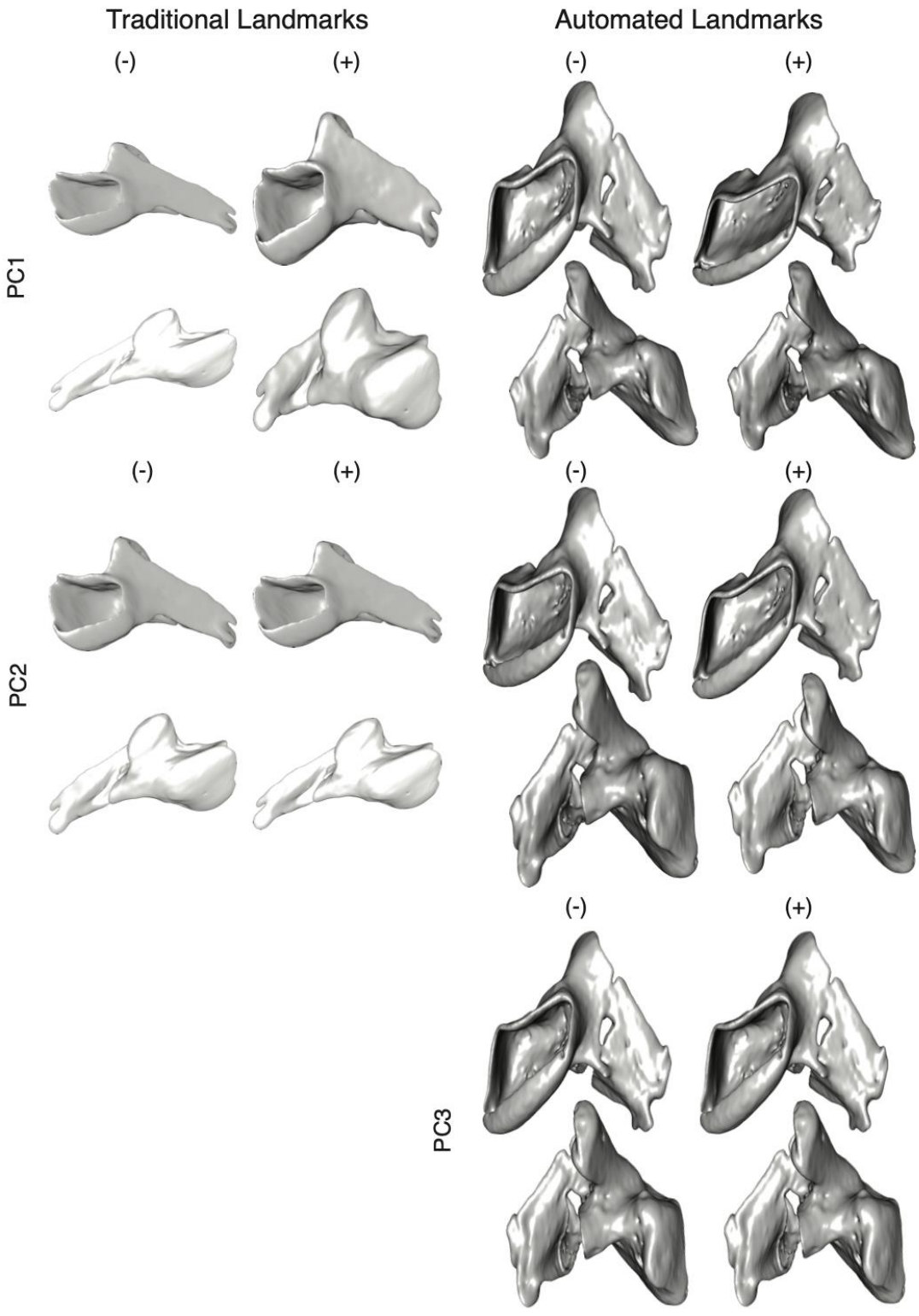

Figure S14. Warped 3D meshes for extreme shapes for the combine phylomorphospace of the lower jaw.

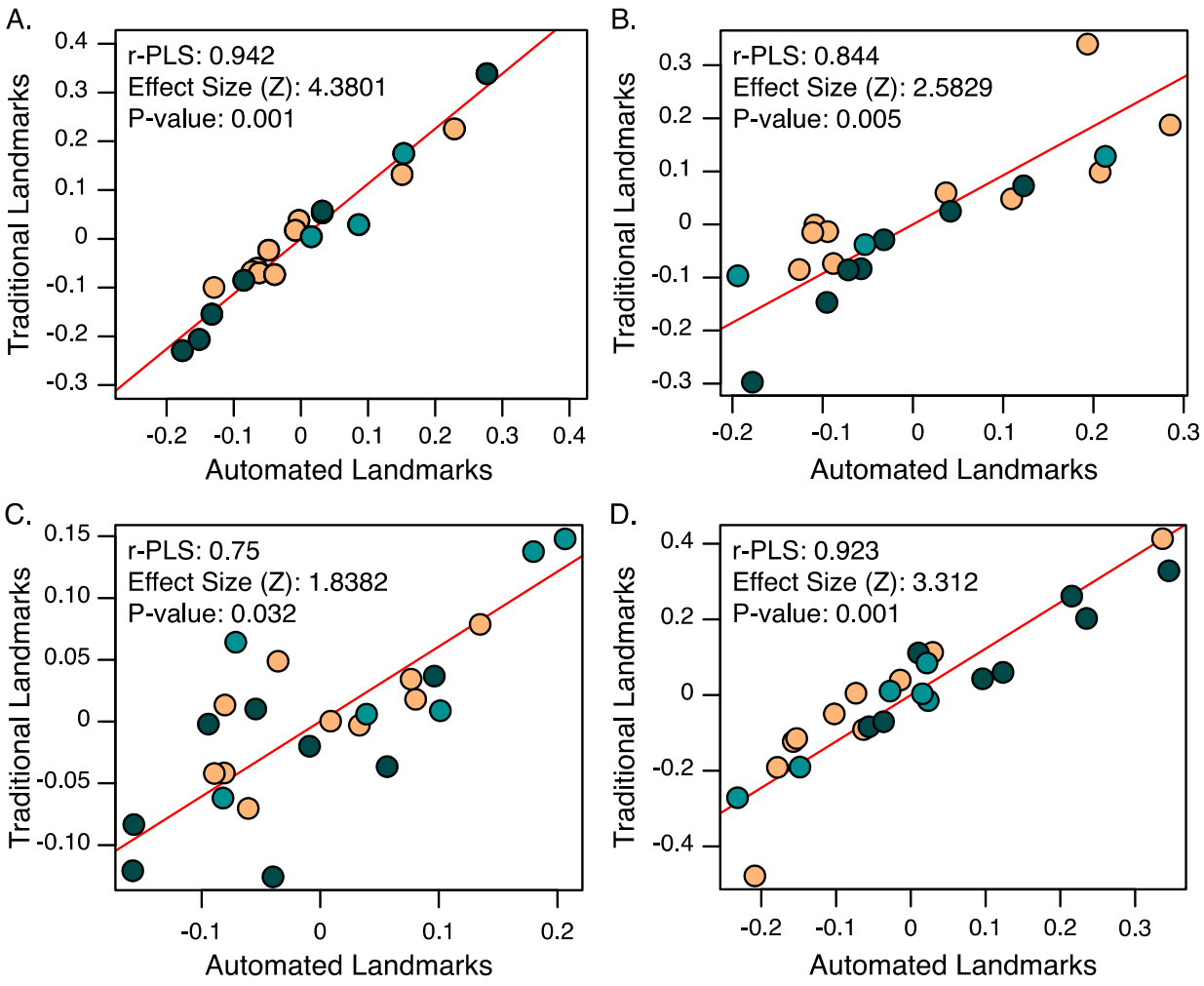

Figure S15. Partial least squares (PLS) comparing the traditional landmarking skeme to automated landmarking methods for (A) combine oral jaw shape, (B) the premaxilla, (C) the maxilla, and (D) the lower jaw for loricariid catfishes. Subfamilies denoted by colors; Hypoptopomatinae in orange, Hypostominae in dark green, and Loricariinae in light green.

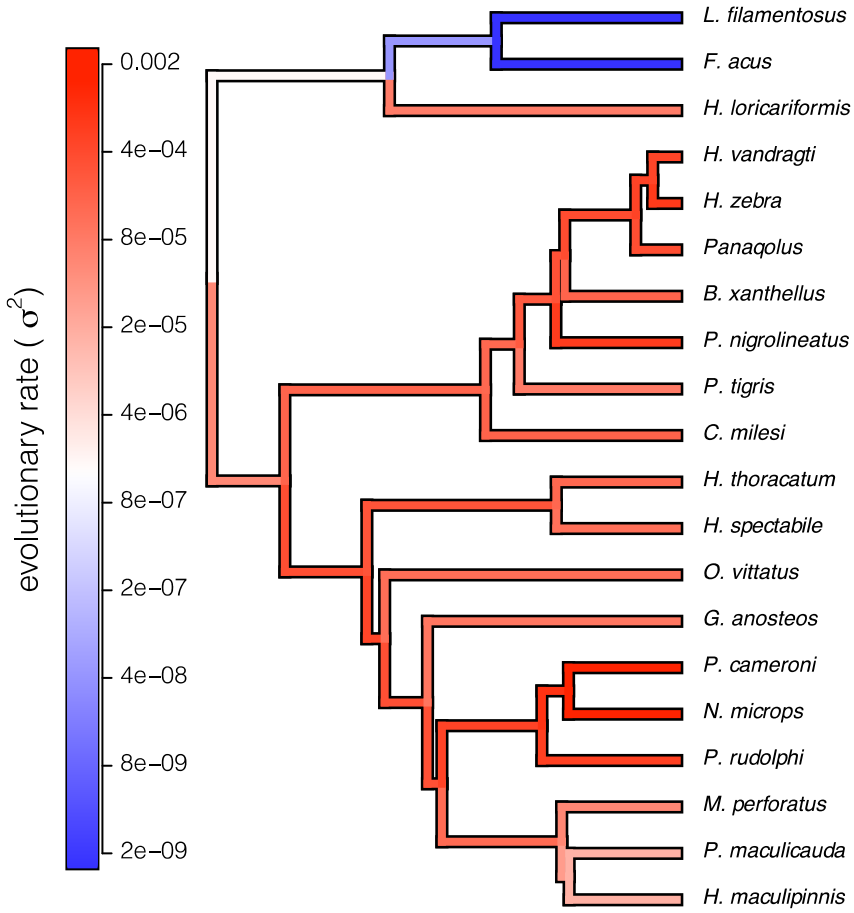

Figure S16. Evolutionary rates of phylogenetically aligned components (PaCA) for combine dataset of automated landmarks along using a penalized-likelihood model.

Chapter 3 – New method of isotopic analysis: Baseline-standardized isotope Vector analysis show trophic partitioning in loricariids

Published as: Black, CR and JW Armbruster. 2021. New method of isotopic analysis: Baseline-Standardized Isotope Vector Analysis show trophic partitioning in loricariids. Ecosphere, 12(5): e03503. DOI 10.1002/ecs2.3503.

Abstract

Stable isotope analyses have refined the study of trophic niche diversity within an ecosystem, yet traditional trophic partitioning methods may not be appropriate to identify variation among groups with similar dietary requirements. By building on vector-based analyses, we introduce a baseline-standardized isotopic vector analysis (BaSIVA) to visualize dietary variation while accounting for isotopic discrepancies between locations. To test the effectiveness of our new method, we collected muscle samples from eleven species of Loricarioidea in five assemblages in Northern Peru. Loricarioidea is a large, ecomorphologically diverse superfamily of scraping-feeding fishes. Most feed on an indistinguishable mix of detritus and algae, but some lineages have specialized diets of wood, seeds, and macroinvertebrates, making them an excellent group to study trophic variation. Isotopic data were collected using mass spectrometric isotope analyses, and communities were standardized by calculating a mean baseline (algae and periphyton) for each location. The entire community was shifted by subtracting the baseline of ^{15}N and ^{13}C from the consumers at each location, which allowed for comparison between assemblages. Incremental differences of ^{15}N and ^{13}C from the baseline were found via vector analysis, and the azimuth and module of each consumer were calculated. Standardization resulted in a significant shift of assemblages within the isotopic biplot, and vector analysis shows

three trophic groups primarily described by differences in carbon assimilation. Isotopic variation between species may account for some diversification in jaw shape within the Loricarioidea, but BaSIVA suggests several instances of trophic overlap in different jaw morphologies. Moreover, results from BaSIVA are better able to delineate trophic groups than traditional trophic positioning methods while accounting for variation in basal resources. We suggest a baseline-standardized vector analysis should be the standard for vector-based stable isotope analysis in riverine environments with similar baseline resources.
Keywords: Stable isotopes, armored catfishes, detritivores, local assemblage, trophic partitioning, trophic ecology

Introduction

Stable isotope ratios are useful to understand nutrient flow through ecosystems and can identify trophic niches within populations (Layman et al. 2007, Fry 2016). Yet, trophic partitioning among groups with similar dietary requirements can be difficult. For example, identifying variation between animals that feed primarily on algae and animals that feed primarily on detritus can be nearly impossible using traditional trophic partitioning methods. By building on vector-based analyses, we introduce a baseline-standardized isotopic vector analysis (BaSIVA) to visualize dietary variation within a group of fishes with similar diets, armored catfishes, and *Astroblepus*.

Loricariidae is a large, ecomorphologically diverse family of mainly scraping-feeding fishes and makes an excellent group to study the correlation between diet and morphology, yet inadequate evidence of trophic variability across the loricariids has made these studies difficult. The family, also called suckermouth armored catfishes, comprises ~1000 recognized species in

100 genera that have diverse morphologies, particularly of the jaws (Lujan and Armbruster 2012, Armbruster et al. 2018, Fricke et al. 2020). This species-rich family is easily recognized by ossified plates that cover the body, integumentary teeth known as odontodes that cover bony plates and fin rays, and ventrally located jaws with an oral disk (Adriaens et al. 2009, Garg et al. 2010 p. 201, Geerinckx et al. 2011, Lujan and Armbruster 2012). Within their range from southern Costa Rica, Panama, and tropical to subtropical South America, loricariids are found in all freshwater rivers, from rapid Andean rivers to quiet brackish estuaries (Covain and Fisch-Muller 2007, Armbruster et al. 2018). Most are obligate scrapers and are assumed to feed on an indistinguishable mix of detritus and algae, yet some lineages have specialized diets and feed on wood (*Hypostomus cochliodon* species group including *H. pyrineusi* examined here, *Panaqolus*, and *Panaque*), seeds, and macroinvertebrates (*Spatuloricaria* sp. examined here; Buck and Sazima 1995, Lujan and Armbruster 2012). Sister to the Loricariidae is the Astroblepidae, which is a much smaller family of 82 species. They are similar in appearance to loricariids but lack external plates. In contrast to the wide variety of habitats occupied by loricariids, astroblepids are found only in very swift water along the Andes from the río Chagres in Panama to central Bolivia. Unlike loricariids, *Astroblepus* are invertivores (Moody et al. 2019).

Until recently, trophic partitioning among detritivores was based solely on gut content analysis, which has proven challenging as detritivores have fast gut passage rates and feed on similar materials (Bowen 1983, Hood et al. 2005). Modern methods built from stable isotope analyses have refined trophic niche diversity of individuals within a local assemblage (Benedito-Cecilio et al. 2000, Layman et al. 2005, Atkinson et al. 2010, Lujan and Armbruster 2012). Stable isotope analyses quantify the accumulation of food items digested over a period of time by analyzing tissue samples for carbon and nitrogen isotopic signatures (German and Miles

2010). Tissues of consumers are generally measured in δ13C (the ratio of ^{13}C to ^{12}C isotopes) and $\delta^{15}N$ (the ratio of ^{15}N to ^{14}N isotopes). The accretion of basal sources, like plants and algae, is indicated by $\delta^{13}C$, whereas dietary protein and trophic-level variation are expressed by $\delta^{15}N$ (German and Miles 2010, Kelly and Martínez del Rio 2010). Isotopic data have been useful to determine what loricariids are digesting in an experimental setting. Studies have revealed that wood-eating species digest microbes, such as fungi and bacteria (or the materials they free), in the wood and not the wood itself (German 2009, Lujan et al. 2011).

Traditional isotopic studies visualize variation through biplots and trophic levels in comparison with basal resources. Because basal resources will vary among locations, it is difficult to compare between species from different assemblages. Vector analysis is useful in identifying minor differences by calculating the strength and direction from a reference point. Often used to detect speed and direction of moving fluid throughout a space, vector analyses have been applied to isotopic biplots to detect direction and magnitude of dietary affinity (Schmidt et al. 2007, Turner et al. 2010, Lujan et al. 2012). Previous attempts to use vector analysis lacked a method to standardize different localities which is necessary to correctly infer dietary affinity, as isotopic data can vary between sites (Post 2002).

To better visualize variation between species and compare across localities, we developed a baseline-standardized method. We tested the effectiveness by comparing our data to two types of analyses. The first analysis is vector-based, assemblage centroid-standardized isotope vector analysis (ACSIVA; Lujan et al. 2012). ACSIVA standardizes local assemblages by calculating the vector from the centroid of consumers at each locality; however, this method does not take into account the effect of basal resources which are essential to infer isotopic assimilation in consumers (Post 2002). The second analysis used as a comparison is a trophic-level analysis.

This analysis calculates the posterior distribution and trophic position with a two-baseline model in a Bayesian framework, yet this analysis does not identify directional changes between species. By standardizing various assemblages to a baseline, the mean of basal resources, our method identifies the direction and magnitude of isotopic assimilation across assemblages and time.

Materials and Methods

Tissue collection

We sampled eleven species of Loricarioidea in five assemblages (Figure 1) from the río Marañón, río Chinchipe, río Chimaya, río Utcubamba, and a tributary of río Tabacones in Northern Peru. Specimens were collected using a combination of seine and backpack electrofishing. Fishes were euthanized in a 1% solution of tricaine methanesulfonate (MS-222) and approximately one gram of epaxial muscle was cut from the caudal peduncle and preserved in about 10 cm^3 of table salt (NaCl) in small zipper-lock bags (Arrington and Winemiller 2002). Basal resources (Plant material included leaf and grass detritus, green filamentous algae and periphyton, green moss, wood, living grasses and leaves. Invertebrate material included dragonfly and mayfly larvae, freshwater shrimp, freshwater muscles, and snails) were collected from each location to be used as a baseline for stable isotope analysis. Samples were preserved in 10 cm^3 of table salt (NaCl) in small zipper-lock bags until they could be processed in the lab. We were unable to collect detritus and algae at site 16. Fish specimens were fixed in 10% formalin and deposited at museums in North and South America (Auburn University Museum of Natural History, AL; Royal Ontario Museum, Toronto, Ontario; and San Marcos University Natural History Museum, Lima, Peru). All animal handling was approved by Auburn University Institutional Animal Care and Use Committee protocol 2017-3134. Basal resources (47 samples)

and tissue samples (63 total samples) were processed following standard protocols (Lujan et al. 2011) and mass spectrometric isotope analyses for ^{15}N and ^{13}C were performed at the Analytical Chemistry Laboratory at the University of Georgia in Athens. Isotopic data was collected using a Carlo Erba CHN elemental analyzer and a Finnigan Delta C mass spectrometer.

Data analysis

To compare assemblages, communities were standardized by calculating a mean baseline for each location by averaging living green filamentous algae, periphyton, and moss for ^{15}N and ^{13}C. We restricted our baseline to living tissues to account for discrepancies that may occur due to unknown decomposition rates of detritus (the more a tissue decomposes, the more negative the carbon values are). Specifically, we used green filamentous algae, periphyton, and moss as a homologous baseline to remain consistent across assemblages, account for variation between basal resources, and because many loricariids specialize on algae. Locations that did not have stable isotope data for algae and periphyton were removed from the analysis. The mean baseline was used to shift the entire community by subtracting the baseline of ^{15}N and ^{13}C from all individuals which allowed for comparison between locations (Figure 2A). Following standardization of localities, the incremental difference of ^{15}N and ^{13}C from the baseline was calculated and the azimuth (vector trajectory) and module (strength of vector) for each consumer were calculated in the R package VecStatGraphs2D. To visualize vectors in the R package plotrix, radians were calculated using a simple equation ((degrees * pi) / 180) with the function deg2rad in the R package REdaS. Vector plots were then rotated in Adobe Illustrator to place 0° on the right-hand side to match typical presentation of stable isotopic data. All code and the raw data are available at github.com/corinthiablack/Black-and-Armbruster_BaSIVA. The assemblage centroid-standardized isotope vector analysis (ACSIVA) was calculated following ACSIVA

protocols (Lujan et al. 2012) to compare our method with an existing vector method. To test the effectiveness of our method, trophic position was calculated in the R package tRophicPosition (Quezada-Romegialli et al. 2018). Using the function multiSpeciesTP, we calculated posterior distribution and trophic position with a two-baseline model in a Bayesian framework for each location (Plant material and invertebrate material). Locations that were missing baseline 1 or baseline 2 were removed from the analysis.

Results

Standardization resulted in a significant shift within the isotopic biplot (Figure 2; Table 1). The average of $\delta^{15}N$ decreased from 8.97‰ to 5.26‰ ($p = 0.0003$) and the range expanded from 3.82‰ to 4.15‰ which is on the low end of controlled studies in Loricariidae (4.1–5.2‰) (German and Miles 2010). The average of $\delta^{13}C$ increased by from -20.35‰ to -0.61‰ ($p = 0.0004$) with the range expanding from 9.85‰ to 13.2‰ which is within the average range for entire Neotropical fish communities (10–17.5‰) (Kelly and Martínez del Rio 2010).

Our vector analysis resulted in dramatically different results than ACSIVA. Overall, the mean azimuth was 100.80° (circular standard deviation (CSD) = 0.67) with some variation in species means (range from 48.68° to 152.67°); whereas the ACSIVA method returned an overall mean of 215.51° (CSD = 2.18) with a wide range of species azimuth means (range from 1.93° to 320.91°) (Figure 3; Table 2). Within species, there was little variation using BaSIVA; *Ancistrus* sp. mean of 95.21° (CSD = 0.40; range = 82.17°–135.64°), *Astroblepus* sp. mean of 60.56° (CSD = 0.02; range = 59.26°–62.41°), *Chaetostoma breve* mean of 131.15° (CSD = 0.44; range = 88.23°–150.30°), *Chaetostoma microps* mean of 67.71° (CSD = 0.26; range = 48.68°–103.34°), *Cordylancistrus* sp. mean of 150.97° (CSD = 0.02; range = 149.66°–152.67°), *Hypostomus*

niceforoi mean of 61.47° (CSD = 0.07; range = 58.70°–68.77°), *Lamontichthys* sp. mean of 138.85° (CSD = 0.04; range = 135.53°–140.57°), *Spatoloricaria* sp. mean of 83.76° (CSD = 0.44; range = 64.39°–127.47°) (Figure 4). ACSIVA returned an extreme variance within species; *Ancistrus* sp. mean of 191.13° (CSD = 0.72; range = 116.83°–217.23°), *Astroblepus* sp. mean of 97.10° (CSD = 0.69; range = 68.19°–159.77°), *Chaetostoma breve* mean of 188.17° (CSD = 1.14; range = 1.89°–333.30°), *Chaetostoma microps* mean of 280.42° (CSD = 1.43; range = 159.72°–352.09°), *Cordylancistrus* sp. mean of 180.49° (CSD = 0.18; range = 168.01°–193.47°), *Hypostomus niceforoi* mean of 1.93° (CSD = 0.13; range = 5.49°–359.30°), *Lamontichthys* sp. mean of 320.91° (CSD = 0.16; range = 313.76°–333.90°), *Spatoloricaria* sp. mean of 28.74° (CSD = 0.55; range = 8.88°–85.08°) (Fig. S1). Additionally, our analysis allowed for comparison to the baseline through module distance whereas ACSIVA lacks baseline data and cannot compare communities to basal resources. The mean module length for all consumers was 5.30‰ (4.59‰–9.89‰) with species module means having very little variation; *Ancistrus* sp. at 6.28 ± 0.43, *Astroblepus* sp. at 7.51 ± 0.54, *Chaetostoma breve* at 7.27 ± 0.35, *Chaetostoma microps* at 6.29 ± 0.17, *Cordylancistrus* sp. at 9.12 ± 0.13, *Hypostomus niceforoi* at 7.23 ± 0.26, *Lamontichthys* sp. at 5.43 ± 0.42, *Spatoloricaria* sp. at 6.61 ± 0.47 (Figure 4, Table 2). Overall, three trophic groups were identified through BaSIVA; enriched δ13C‰ (*Astroblepus* sp., *Chaetostoma microps* and *Hypostomus niceforoi)*, balanced δ13C‰ (*Ancistrus* sp., *Spatoloricaria* sp.), and depleted δ13C‰ (*Chaetostoma breve*, *Cordylancistrus* sp., and *Lamontichthys* sp.) (See Table S1 for groups by location). There was little variation in δ15N; however, *Astroblepus* sp. was the most enriched in nitrogen values with an average of 6.53‰ and *Lamontichthys* sp. had the most depleted nitrogen values with an average of 3.55‰.

To compare our vector method to traditional methods, we calculated trophic positions for consumers at each location (Fig. S2-S5). Posterior trophic positions ranged from 2.85 to 5.06 with high error margins (Fig. S6, Table S2) and pairwise distances between species at specific locations showed no significant differences which suggests there is no variation in isotopic assimilation (Table S3). We were able to include one specimen of wood-eating catfish (*Hypostomus pyrineusi*) in this analysis, but because algae and periphyton were not collected from the site (PER 18-16), we could not include it in the BaSIVA approach.

Discussion

Baseline-standardized vector analysis is able to partition species with similar diets from within a single geographical region, suggesting that loricariids and astroblepids fall into three trophic groups. In contrast, assemblage centroid-standardized vector analysis (ACSIVA) suggests a small relative difference between species in resource use and should not be equated with typical trophic positioning. Furthermore, results of our vector analysis recovered more variation between species when compared to traditional trophic position methods. As our method accounts for basal resources and adheres to conventional stable isotopic methods, we suggest BaSIVA should be the standard for vector-based stable isotope analysis in riverine environments with similar baseline resources. BaSIVA further provides values that can be examined in a phylotrophospace approach (Burress et al. 2016), which cannot be done with traditional isotopic methods. This approach may allow for the examination of evolutionary ecology across a phylogeny of fishes within similar environments to study changes in resource use. Assumptions of BaSIVA are that 1) species vary linearly from the primary food consumed, 2) basal resources are similar at different localities, and 3) nutrient assimilation is similar across organisms studied.

Three trophic groups were identified by BaSIVA and describe variation in carbon isotopes. Surprisingly there was little variation in nitrogen, which suggests dietary protein consumption is similar across loricariids, with the exception of *Astroblepus* sp. which had the most enriched $\delta^{15}N$ and *Lamontichthys* sp. which had the most depleted $\delta^{15}N$ (Kelly and Martínez del Rio 2010). This is interesting as loricariids are thought to feed on a mix of detritus and algae which have depleted nitrogen levels (Buck and Sazima 1995), yet *Astroblepus* and *Spatuloricaria* are known insectivores and did not show much variation from the remainder of the species. This suggests that detritus-feeding loricariids are capable of assimilating similar levels of nitrogen as insectivores.

Major isotopic differences were seen were in carbon assimilation. ^{13}C is typically used to separate ultimate carbon sources within a food web. For example, particulate organic matter is often the most negative followed by C3 and C4 plants, yet algae has a unique carbon content to vascular plants and relationships between basal resources can vary from location to location (Post 2002). Although carbon variation between species was identified using BaSIVA (Figure 4), a more comprehensive collection of basal resources is necessary to infer differences in dietary affinity among consumers.

Isotopic variation between species (Figure 4) may account for some diversification in jaw shape and function within the armored catfishes (Lujan and Armbruster 2012). However, we found several species with different jaw morphologies that fell into the same trophic category (Table S1). For example, *Astroblepus* sp. and *Chaetostoma microps* had enriched δ13C signatures, yet *Astroblepus* sp. has a relatively short jaw with eight to ten asymmetrical bifid teeth and *Chaetostoma microps* has long jaws with over one-hundred asymmetrical bicuspid teeth (Schaefer et al. 2011, Lujan et al. 2015). Most loricariid species scrape algae and detritus

from rocks; however, it is unknown as to how *Astroblepus* forages for insect larvae. Despite some correlation of morphotypes to dietary specializations, few species-poor studies have statistically examined the relationship between jaw shape and diet type (Delariva and Agostinho 2001, Fugi et al. 2005, de Mérona et al. 2008). As we found several species with differing jaw morphologies within a trophic group (Table S1), our study suggests that variation in jaw morphology is not associated with what loricariids are eating, but rather the surface they are eating from. The correlation of diversification and habitat type has been demonstrated in a clade of armored catfishes, where Neoplecostomini fishes displayed an increased body size and changes in head shape when found in fast-flowing, rocky riverine habitats (Roxo et al. 2017). As we found overlap of species with varying jaw morphologies within each trophic group and previous studies have suggested that habitat type is correlated to shape variation, we suggest that variation in jaw shape is most likely associated with how and where loricariid catfishes are feeding rather than what they are feeding upon.

Furthermore, gut content analyses show that armored catfishes consume other items in addition to algae and detritus; including wood, seeds, and macroinvertebrates (Lujan et al. 2012). Yet, a study in wood-eating armored catfishes suggests that what is consumed is not always what is assimilated. Laboratory experiments show that wild-caught *Pterygoplichthys disjunctivus* and *Panaque nigrolineatus* from the aquarium trade poorly digest wood cellulose and lose weight when fed wood exclusively (German 2009). This, in addition to digestive enzyme activity profiles and fermentation levels in the gastrointestinal tract, suggests that wood-eating armored catfishes are consuming detritus rather than wood (German 2009). Further, the microbiomes of wood-eating loricariids suggest minimal digestion of wood, meaning these fishes may rely on microbes in the environment to degrade wood fiber (McCauley et al. 2020). This further

supports our hypothesis that jaw shape in armored catfishes is associated with the surface type they are feeding on and items that are assimilated are similar.

The question of habitat partitioning among basal consumers is not unique to loricariid catfishes. It had long been wondered how African savannahs can support up to twenty-five large herbivorous mammals. This diversification in mammals has been partly explained through observation, stable isotopic analysis, and metabarcoding of feces. Some specialization is suggested to be the result of specialization on browsing (leaves) vs. grazing (grasses); however, multiple species feed upon the same things. Other factors such as body size, ruminant vs. non-ruminant, spatio-temporal partitioning, microhabitat selection, grazing succession (feeding on different height grasses for example), and browsing stratification (feeding at different heights) explain how African savannahs can support so many species (Kartzinel et al., 2015). Similar patterns in habitat partitioning have been found in coral reef environments where parrotfishes feed on a wide variety of substrates (Clements et al. 2016). Instead of feeding on macroscopic algae as formerly believed, the parrotfishes were found to be microphages feeding on cyanobacteria and autotrophic microorganisms. These studies provide insight on how ecomorphologically diverse loricariids can include thirty or more species in an assemblage. It is likely that different species feed in different flow regimes, and based on this study and Lujan et al. (2012), could be focusing on unknown resources similar to the parrotfishes. The longest-jawed loricariid species tend to prefer the fastest flow, and some loricariid species specialize on particular substrates like rocks, wood, and loose gravel. Similar to grazing succession, wood-scraping species include species with relatively generalized jaws that feed on the surfaces of the logs (e.g. *Hypostomus niceforoi*) to species with robust jaws with spoon-shaped teeth that dig into the wood (e.g. *Hypostomus pyrineusi*). Further research is required to better understand the

relationship of jaw shape to substrate type and whether loricariids are seeking out dietary resources other than the main materials in their guts.

ACSIVA provided a unique means to compare disparate populations that lack basal resources to present results providing a richer comparative palate than traditional stable isotopic methods; however, we found the method to have some flawed reasoning in the populations that we examined (Figure 3). Although ACSIVA did demonstrate a small amount of variation between species, it could lead to overstating the relative contributions of nitrogen and carbon in the diet; however, ACSIVA correctly shows insectivorous species (*Astroblepus* sp. and *Spatuloricaria* sp.) to be more enriched in relative nitrogen than all other species. Our method of baseline-standardized isotopic vector analysis (BaSIVA) is an intellectual successor to ACSIVA and maintains a means of visualizing differences in diet while allowing for comparisons across communities and, like ACSIVA, the ability to understand the evolution of resource use in a phylotrophospace approach across multiple communities (Burress et al. 2016). Additionally, BaSIVA was able to recover three distinct groups that traditional trophic positioning was unable to separate (Fig. S6). As our method accounts for variation between sites, we are better able to compare isotopic assimilation in species across assemblages and time than in traditional analyses. There are potential limitations to the utility of BaSIVA across other organisms. For example, BaSIVA assumes environments are driven by similar basal resources and that species vary linearly from the average of those resources. If ecosystems are dominated by different basal resources (for example, allochtonous vs. autochronous resources), analyses may be biased. However, as long as environments are comparable, BaSIVA can still be used by adjusting baseline resources to account for systems driven by other resources. Additional analyses, such as fatty acid profiling, may be required to differentiate trophic variability when stable isotope

analyses are unable to address these differences (Piché et al. 2010, Clements et al. 2016). The utility of the method across greater geographic scales and greater ecological diversity remains to be tested.

The method, BaSIVA, introduced in this paper accounts for changes in basal resources between sites which makes it useful for identifying variation across species in different assemblages. Our results were better able to separate species which gut content analysis and traditional trophic partitioning could not. This suggests that loricariid catfishes consume more than just a mixture of detritus and algae and that digestive processes may have a greater impact in isotopic resource assimilation. Furthermore, overlap of species with varying morphologies in trophic groups may suggest that the diversity in jaw shape is correlated to surface types and flow regime rather than food items consumed.

References

Adriaens, D., T. Geerinckx, J. Vlassenbroeck, L. Van Hoorebeke, and A. Herrel. 2009. Extensive Jaw Mobility in Suckermouth Armored Catfishes (Loricariidae): A Morphological and Kinematic Analysis of Substrate Scraping Mode of Feeding. Physiological and Biochemical Zoology 82:51–62.

Armbruster, J. W., P. van der Sleen, and N. K. Lujan. 2018. Family Loricariidae - Suckermouth Armored Catfishes. Pages 253–254 *in* P. van der Sleen and J. S. Albert, editors. Field Guide to the Fishes of the Amazon, Orinoco, & Guianas. Princeton University Press.

Arrington, D. A., and K. O. Winemiller. 2002. Preservation Effects on Stable Isotope Analysis of Fish Muscle. Transactions of the American Fisheries Society 131:337–342.

Atkinson, C. L., S. P. Opsahl, A. P. Covich, S. W. Golladay, and L. M. Conner. 2010. Stable isotopic signatures, tissue stoichiometry, and nutrient cycling (C and N) of native and invasive freshwater bivalves. Journal of the North American Benthological Society 29:496–505.

Benedito-Cecilio, E., C. A. R. M. Araujo-Lima, B. R. Forsberg, M. M. Bittencourt, and L. C. Martinelli. 2000. Carbon sources of Amazonian fisheries. Fisheries Management and Ecology 7:305–315.

Bowen, S. H. 1983. Detritivory in neotropical fish communities. Environmental Biology of Fishes.

Buck, S., and I. Sazima. 1995. An assemblage of mailed catfish (Loricariidae) in southeastern Brazil: distribution, activity and feeding. Ichthyological Exploration of Freshwaters 6:325–332.

Burress, E. D., J. M. Holcomb, M. Tan, and J. W. Armbruster. 2016. Ecological diversification associated with the benthic-to-pelagic transition by North American minnows:1–12.

Clements, K. D., D. P. German, J. Piché, A. Tribollet, and J. H. Choat. 2016. Integrating ecological roles and trophic diversification on coral reefs: multiple lines of evidence identify parrotfishes as microphages. Biological Journal of the Linnean Society.

Covain, R., and S. Fisch-Muller. 2007. The genera of the Neotropical armored catfish subfamily Loricariinae (Siluriformes: Loricariidae): a practical key and synopsis. Zootaxa 1462:1–40.

Delariva, R. L., and A. A. Agostinho. 2001. Relationship between morphology and diets of six neotropical loricariids. Journal of Fish Biology 58:832–847.

Fricke, R., W. N. Eschmeyer, and J. Fong. 2020. Eschmeyer's Catalog of Fishes. http://researcharchive.calacademy.org/research/ichthyology/catalog/SpeciesByFamily.

Fry, B. 2016. Stable Isotope Ecology. Pages E1–E1 Stable Isotope Ecology. Springer New York, New York, NY.

Fugi, R., A. A. Agostinho, and N. S. Hahn. 2005. Trophic morphology of five benthic-feeding fish species of a tropical floodplain. Revista Brasileira de Biologia.

Garg, T. K., F. X. Valdez Domingos, V. M. F. Almeida-Val, and A. L. Val. 2010. Histochemistry and functional organization of the dorsal skin of Ancistrus dolichopterus (Siluriformes: Loricariidae). Neotropical Ichthyology.

Geerinckx, T., A. Herrel, and D. Adriaens. 2011. Suckermouth armored catfish resolve the paradox of simultaneous respiration and suction attachment: a kinematic study of Pterygoplichthys disjunctivus. Journal of Experimental Zoology Part A: Ecological Genetics and Physiology.

German, D. P. 2009. Inside the guts of wood-eating catfishes: Can they digest wood? Journal of Comparative Physiology B: Biochemical, Systemic, and Environmental Physiology 179:1011–1023.

German, D. P., and R. D. Miles. 2010. Stable carbon and nitrogen incorporation in blood and fin tissue of the catfish Pterygoplichthys disjunctivus (Siluriformes, Loricariidae). Environmental Biology of Fishes 89:117–133.

Hood, J. M., M. J. Vanni, and A. S. Flecker. 2005. Nutrient recycling by two phosphorus-rich grazing catfish: The potential for phosphorus-limitation of fish growth. Oecologia.

Kelly, L. J., and C. Martínez del Rio. 2010. The Fate of Carbon in Growing Fish: An Experimental Study of Isotopic Routing. Physiological and Biochemical Zoology 83:473–480.

Layman, C. A., D. A. Arrington, C. G. Montaña, and D. M. Post. 2007. Can stable isotope ratios provide for community-wide measures of trophic structure? Ecology 88:42–48.

Layman, C. A., K. O. Winemiller, D. A. Arrington, and D. B. Jepsen. 2005. Body size and trophic position in a diverse tropical food web. Ecology 86:2530–2535.

Lujan, N. K., and J. W. Armbruster. 2012. Morphological and functional diversity of the mandible in suckermouth armored catfishes (Siluriformes: Loricariidae). Journal of Morphology 273:24–39.

Lujan, N. K., D. P. German, and K. O. Winemiller. 2011. Do wood-grazing fishes partition their niche? Morphological and isotopic evidence for trophic segregation in Neotropical Loricariidae. Functional Ecology 25:1327–1338.

Lujan, N. K., V. Meza-Vargas, V. Astudillo-Clavijo, R. Barriga-Salazar, and H. López-Fernández. 2015. A Multilocus Molecular Phylogeny for *Chaetostoma* Clade Genera and

Species with a Review of *Chaetostoma* (Siluriformes: Loricariidae) from the Central Andes. Copeia 103:664–701.

Lujan, N. K., K. O. Winemiller, and J. W. Armbruster. 2012. Trophic diversity in the evolution and community assembly of loricariid catfishes. BMC Evolutionary Biology 12:1.

McCauley, M., D. P. German, N. K. Lujan, and C. R. Jackson. 2020. Gut microbiomes of sympatric Amazonian wood-eating catfishes (Loricariidae) reflect host identity and little role in wood digestion. Ecology and Evolution: ece3.6413.

de Mérona, B., B. Hugueny, F. L. Tejerina-Garro, and E. Gautheret. 2008. Diet-morphology relationship in a fish assemblage from a medium-sized river of French Guiana: the effect of species taxonomic proximity. Aquatic Living Resources.

Moody, E. K., N. K. Lujan, K. A. Roach, and K. O. Winemiller. 2019. Threshold elemental ratios and the temperature dependence of herbivory in fishes. Functional Ecology 33:913–923.

Piché, J., S. Iverson, F. Parrish, and R. Dollar. 2010. Characterization of forage fish and invertebrates in the Northwestern Hawaiian Islands using fatty acid signatures: species and ecological groups. Marine Ecology Progress Series 418:1–15.

Post, D. M. 2002. Using Stable Isotopes To Estimate Trophic Position: Models, Methods, and Assumptions. Ecology 83:703–718.

Quezada-Romegialli, C., A. L. Jackson, and C. Harrod. 2018. tRophicPosition: Bayesian trophic position calculation with stable isotopes.

Roxo, F. F., N. K. Lujan, V. A. Tagliacollo, B. T. Waltz, G. S. C. Silva, C. Oliveira, and J. S. Albert. 2017. Shift from slow-to fast-water habitats accelerates lineage and phenotype

evolution in a clade of Neotropical suckermouth catfishes (Loricariidae: Hypoptopomatinae). PLoS ONE 12:4–6.

Schaefer, S. A., P. Chakrabarty, A. J. Geneva, and M. H. Sabaj Pérez. 2011. Nucleotide sequence data confirm diagnosis and local endemism of variable morphospecies of Andean astroblepid catfishes (Siluriformes: Astroblepidae): Molecular diagnosis of astroblepid species. Zoological Journal of the Linnean Society 162:90–102.

Schmidt, S. N., J. D. Olden, C. T. Solomon, and M. J. V. Zanden. 2007. Quantitative approaches to the analysis of stable isotope food web data. Ecology 88:2793–2802.

Turner, T. F., M. L. Collyer, and T. J. Krabbenhoft. 2010. A general hypothesis-testing framework for stable isotope ratios in ecological studies. Ecology 91:2227–2233.

Tables

Table 1. Raw and standardized stable isotope data used in this study.

Source	n	Location	d15N	Standardized d15N	d13C	Standardized d13C
Chaetostoma breve	5	río Chinchipe	8.8 ± 0.37	4.50 ± 0.37	-21.84 ± 1.08	-7.29 ± 1.08
Cordylancistrus sp.	3	río Chinchipe	8.72 ± 0.11	4.42 ± 0.11	-22.52 ± 0.31	-7.97 ± 0.31
Ancistrus sp.	1	río Marañón	9.99	5.28	-24.93	5.40
Chaetostoma breve	4	río Marañón	8.41 ± 0.34	3.70 ± 0.34	0.72 ± 0.2	-5.40 ± 0.20
Lamontichthys sp.	3	río Marañón	8.27 ± 0.29	3.55 ± 0.29	-23.64 ± 0.72	-4.10 ± 0.72
Spatoloricarid sp.	1	río Marañón	8.87	4.16	-22.72	-3.19
Ancistrus sp.	3	río Utcubamba	9.27 ± 0.12	5.81 ± 0.12	-23.8 ± 0.05	0.74 ± 0.05
Chaetostoma breve	4	río Utcubamba	9.78 ± 0.42	6.32 ± 0.42	-24.91 ± 0.5	-0.36 ± 0.5
Chaetostoma microps	4	río Utcubamba	9.4 ± 0.21	5.93 ± 0.21	-23.28 ± 1.76	1.27 ± 1.76
Hypostomus niceforoi	4	río Utcubamba	9.79 ± 0.35	6.33 ± 0.35	-21.08 ± 0.71	3.46 ± 0.71
Spatoloricaria sp.	3	río Utcubamba	10.09 ± 0.11	6.62 ± 0.11	-22.17 ± 0.83	2.38 ± 0.83
Astroblepus sp.	3	Tributary of río Tabacones	8.22 ± 0.47	6.09 ± 1.08	-17.04 ± 0.85	3.49 ± 0.64
Chaetostoma microps	4	Tributary of río Tabacones	6.98 ± 0.76	5.69 ± 0.89	-17.31 ± 0.59	3.58 ± 0.66

Table 2. Circular statistics among Loricarioidea species for BaSIVA and ACSIVA.

Species	n	New Azimuth Mean	New Circular SD	New Module Mean	ACSIVA Azimuth Mean	ACSIVA Circular SD	ACSIVA Module Mean
Ancistrus sp.	4	95.21	0.40	6.28 ± 0.43	191.13	0.72	1.05 ± 0.32
Astroblepus sp.	3	60.56	0.02	7.51 ± 0.54	97.10	0.76	1.02 ± 0.69
Chaetostoma breve	13	131.15	0.44	7.27 ± 0.35	188.17	1.14	1.17 ± 0.69
Chaetostoma microps	8	67.71	0.26	6.29 ± 0.17	280.42	1.43	1.08 ± 0.78
Cordylancistrus sp.	3	150.97	0.02	9.12 ± 0.13	180.49	0.18	0.43 ± 0.32
Hypostomus niceforoi	4	61.47	0.07	7.23 ± 0.26	1.93	0.13	0.36 ± 0.73
Lamontichthys sp.	3	138.85	0.04	5.43 ± 0.42	320.91	0.16	0.72 ± 0.76
Spatoloricaria sp.	4	83.76	0.44	6.61 ± 0.47	28.74	0.55	1.16 ± 0.59

Figures

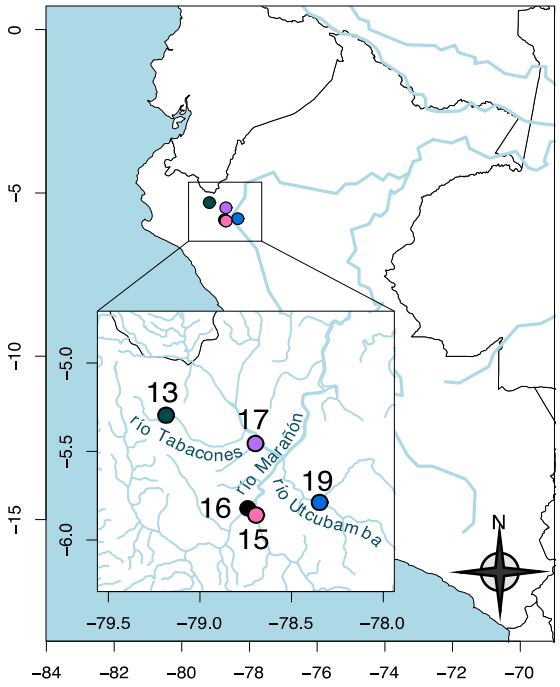

Figure 1. Map of Peru. Inset box depicts the sampling localities: (13) tributary of río Tabacones, (15) río Marañón, (16) río Chimaya, (17) río Chinchipe, and (19) río Utcubamba.

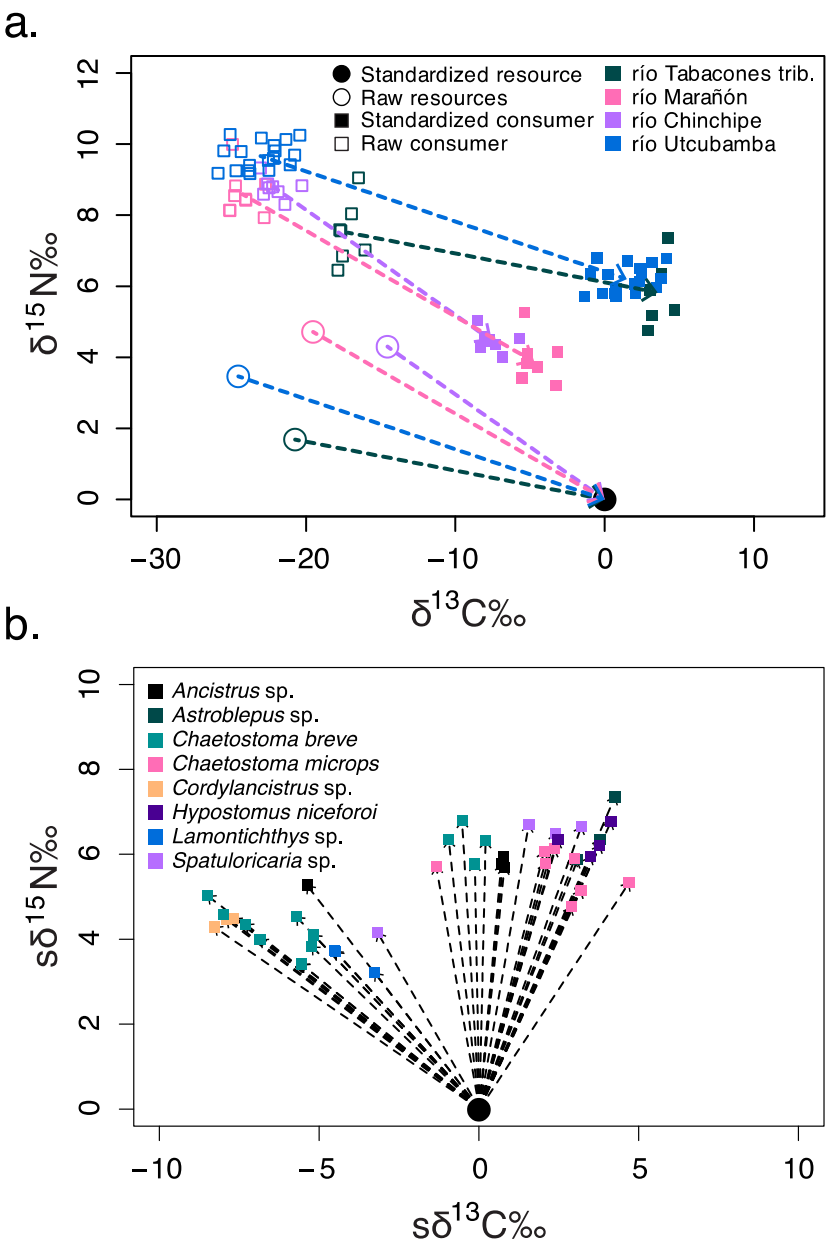

Figure 2. (a) Circles are the mean of detritus and algae and squares are individuals. (b) Vectors point to individuals from the mean of detritus and algae.

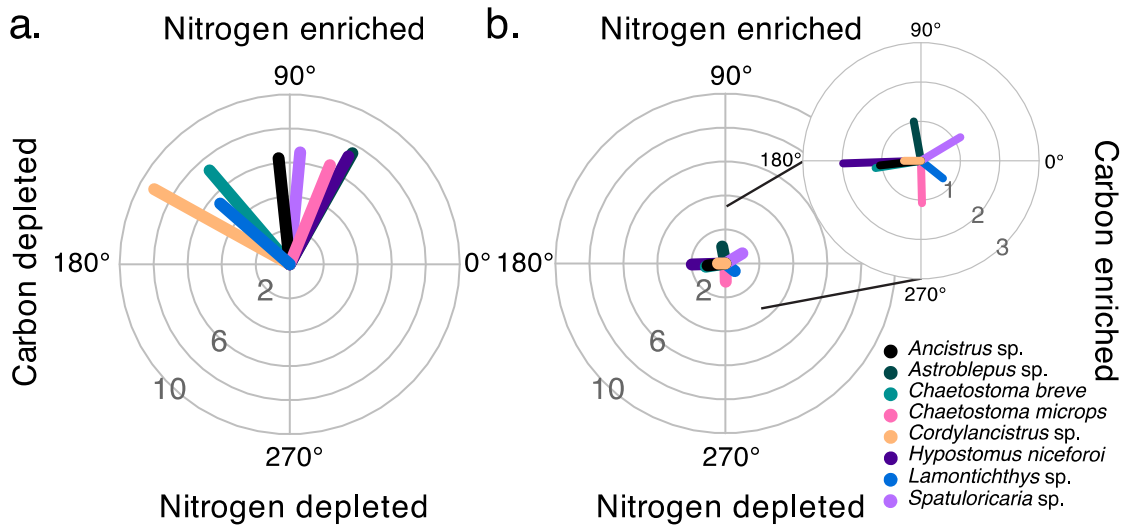

Figure 3. (a) BaSIVA shows species deviate from the mean of basal resources and have very little variation between each other vs. (b) ACSIVA which deviates from the mean of the population and emphasizes relative differences between species in resource use, but has a small degree of variation (inset).

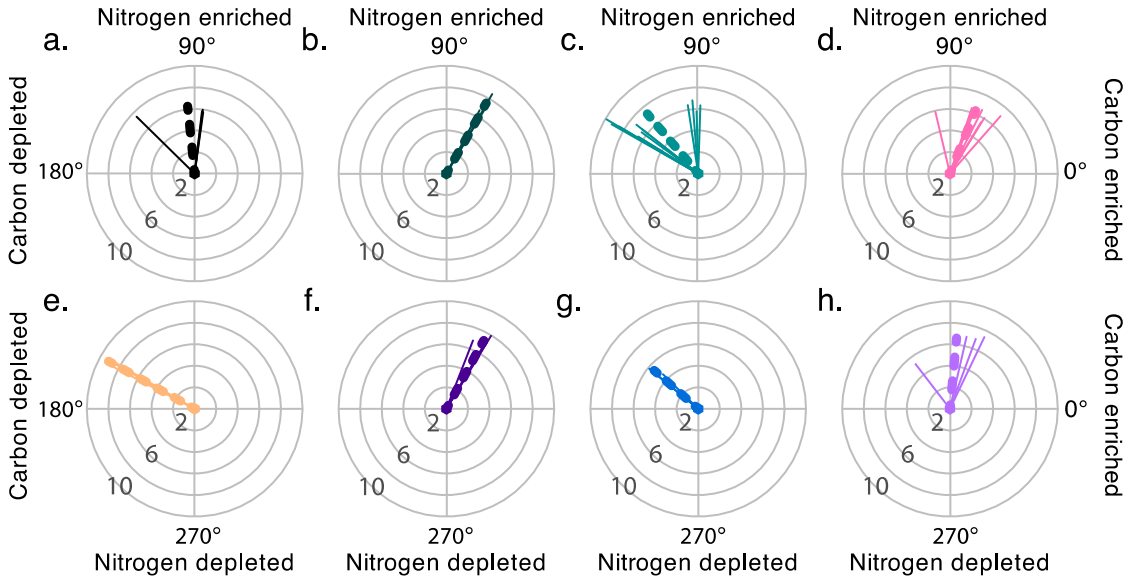

Figure 4. Details for each species using BaSIVA. Means are thicker dotted lines, thinner lines are individuals. Vector and Module (strength of trajectory) for (a) *Ancistrus* sp. (b) *Astroblepus* sp. (c) *Chaetostoma breve* (d) *Chaetostoma microps* (e) *Cordylancistrus* sp. (f) *Hypostomus niceforoi* (g) *Lamontichthys* sp. (h) *Spatoloricaria* sp.

Chapter 3 Supplemental Materials

Supplemental Tables

Table S1. Locations and trophic groups as identified by BaSIVA.

Location (Figure 1)	Enriched δ13C‰	Average δ13C‰	Depleted δ13C‰
río Tabacones tributary	*Astroblepus* sp., and *Chaetostoma microps*		
río Marañón		*Ancistrus* sp., and *Spatoloricaria* sp.	*Chaetostoma breve, and Lamontichthys* sp.
río Chinchipe			*Chaetostoma breve*, and *Cordylancistrus* sp.
río Utcubumba	*Chaetostoma microps*, and *Hypostomus niceforoi*	*Ancistrus* sp., and *Spatoloricaria* sp.	*Chaetostoma breve*

Table S2. Posterior trophic positions for each species at specific locations.

Species and Location (Figure 1)	Posterior Mode	2.50%	50%	97.50%
Chaetostoma microps 13	3.46	2.17	3.97	9.30
Astroblepus sp. 13	3.82	2.20	4.36	9.53
Spatoloricaria sp. 16	3.04	2.16	3.35	8.81
Hypostomus niceforoi 16	2.71	2.14	2.85	5.82
Lasiancistrus schomburgkii 16	2.93	2.11	3.11	6.73
Chaetostoma trimaculineum 16	3.12	2.16	3.27	7.06
Hypostomus pyrineusi 16	2.71	2.13	5.06	9.70
Chaetostoma breve 16	3.16	2.16	3.37	7.70
Cordylancistrus sp. 17	3.69	2.35	3.60	5.13
Chaetostoma breve 17	3.61	2.30	3.55	4.77
Chaetostoma breve 19	4.02	2.82	4.00	5.75
Chaetostoma microps 19	3.90	2.61	3.88	5.60
Ancistrus sp. 19	3.85	2.67	3.83	5.15
Spatoloricaria sp. 19	3.98	2.74	3.95	4.94
Hypostomus niceforoi 19	3.86	2.47	3.81	5.67

Table S3. Pairwise distances where values below the diagonal are the proportion of posterior samples that are less than or equal to the posterior samples of the model in the column, and above the diagonal are the proportion of posterior samples that are higher than posterior samples of the model in the row.

	***C. bre* 17**	***C. sp.* 17**	***C. bre* 16**	***H. pyr* 16**	***C. tri* 16**	***L. sch* 16**	***H. nic*16**	***S. sp.* 16**	***A. sp.* 13**	***C. mic* 13**
***C. microps* 13**	0.4	0.37	0.36	0.63	0.32	0.35	0.23	0.35	0.56	0
***Astroblepus* sp. 13**	0.32	0.29	0.32	0.58	0.26	0.32	0.2	0.29	0	0.44
***Spatoloricaria* sp. 16**	0.61	0.6	0.54	0.74	0.51	0.51	0.35	0	0.71	0.65
***H. niceforoi* 16**	0.77	0.74	0.68	0.82	0.67	0.64	0	0.65	0.8	0.77
***L. schomburgkii* 16**	0.61	0.58	0.53	0.72	0.5	0	0.36	0.49	0.68	0.65
***C. trimaculineum* 16**	0.64	0.6	0.54	0.75	0	0.5	0.33	0.49	0.74	0.68
***H. pyrineusi* 16**	0.29	0.27	0.28	0	0.25	0.28	0.18	0.27	0.42	0.38
***C. breve* 16**	0.58	0.55	0	0.72	0.47	0.47	0.32	0.46	0.69	0.64
***Cordylancistrus* sp. 17**	0.55	0	0.45	0.73	0.4	0.42	0.26	0.4	0.71	0.63
***C. breve* 17**	0	0.45	0.42	0.71	0.36	0.39	0.23	0.39	0.68	0.61
***C. breve* 19**	0.28	0.23	0.29	0.66	0.22	0.3	0.15	0.28	0.58	0.51
***C. microps* 19**	0.4	0.34	0.36	0.7	0.28	0.34	0.18	0.34	0.63	0.55
***Ancistrus* sp. 19**	0.37	0.33	0.34	0.67	0.3	0.32	0.21	0.32	0.61	0.55
***Spatoloricaria* sp. 19**	0.32	0.27	0.33	0.67	0.24	0.3	0.16	0.29	0.59	0.51
***H. niceforoi* 19**	0.36	0.29	0.33	0.65	0.27	0.33	0.17	0.31	0.59	0.53

	***H. nic* 19**	***S.* sp. 19**	***A.* sp. 19**	***C. mic* 19**	***C. bre* 19**	
***C. microps* 13**	0.47	0.49	0.45	0.45	0.49	***C. microps* 13**
***Astroblepus* sp. 13**	0.41	0.41	0.39	0.37	0.43	***Astroblepus* sp. 13**
***Spatoloricaria* sp. 16**	0.69	0.71	0.68	0.66	0.72	***Spatoloricaria* sp. 16**
***H. niceforoi* 16**	0.83	0.84	0.79	0.82	0.85	***H. niceforoi* 16**
***L. schomburgkii* 16**	0.68	0.7	0.68	0.66	0.7	***L. schomburgkii* 16**
***C. trimaculineum* 16**	0.74	0.76	0.7	0.72	0.78	***C. trimaculineum* 16**
***H. pyrineusi* 16**	0.35	0.34	0.33	0.3	0.34	***H. pyrineusi* 16**
***C. breve* 16**	0.67	0.67	0.66	0.64	0.71	***C. breve* 16**
***Cordylancistrus* sp. 17**	0.71	0.73	0.67	0.66	0.77	***Cordylancistrus* sp. 17**
***C. breve* 17**	0.65	0.68	0.63	0.6	0.72	***C. breve* 17**
***C. breve* 19**	0.46	0.49	0.41	0.38	0	***C. breve* 19**
***C. microps* 19**	0.57	0.61	0.53	0	0.62	***C. microps* 19**
***Ancistrus* sp. 19**	0.53	0.56	0	0.47	0.59	***Ancistrus* sp. 19**
***Spatoloricaria* sp. 19**	0.47	0	0.44	0.39	0.51	***Spatoloricaria* sp. 19**
***H. niceforoi* 19**	0	0.53	0.47	0.43	0.54	***H. niceforoi* 19**

Supplemental Figures

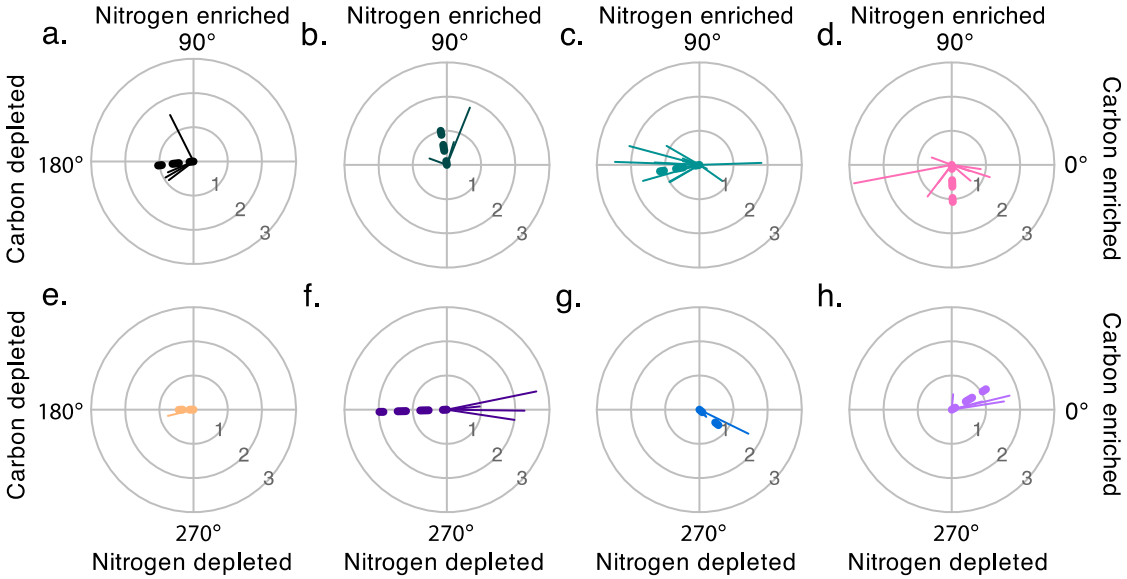

Fig. S1. Details for each species using ACSIVA. Means are thicker dotted lines, thinner lines are individuals. Vector and Module (strength of trajectory) for (a) *Ancistrus* sp. (b) *Astroblepus* sp. (c) *Chaetostoma breve* (d) *Chaetostoma microps* (e) *Cordylancistrus* sp. (f) *Hypostomus niceforoi* (g) *Lamontichthys* sp. (h) *Spatoloricaria* sp.

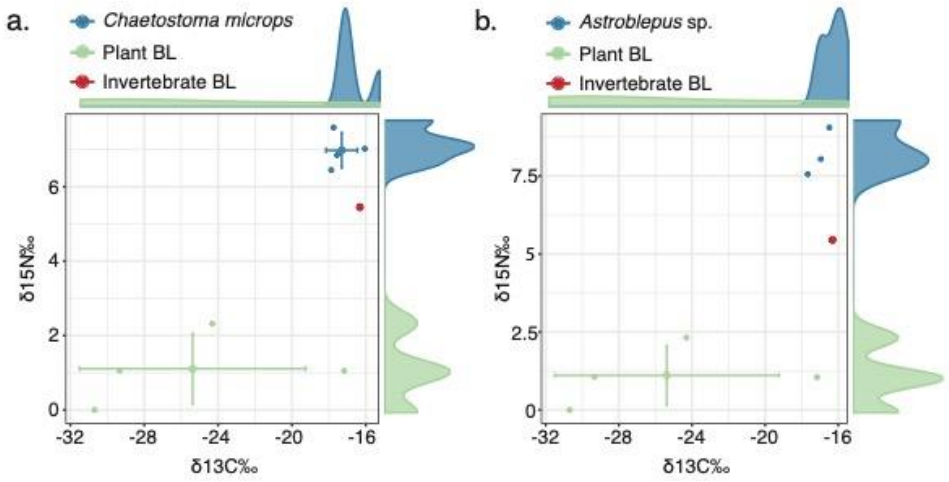

Fig. S2. Isotopic biplot of (a.) *Chaetostoma microps* and (b.) *Astroblepus* sp. for individuals from a tributary of río Tabacones. Shading above and to the right of the plot show distribution of individuals.

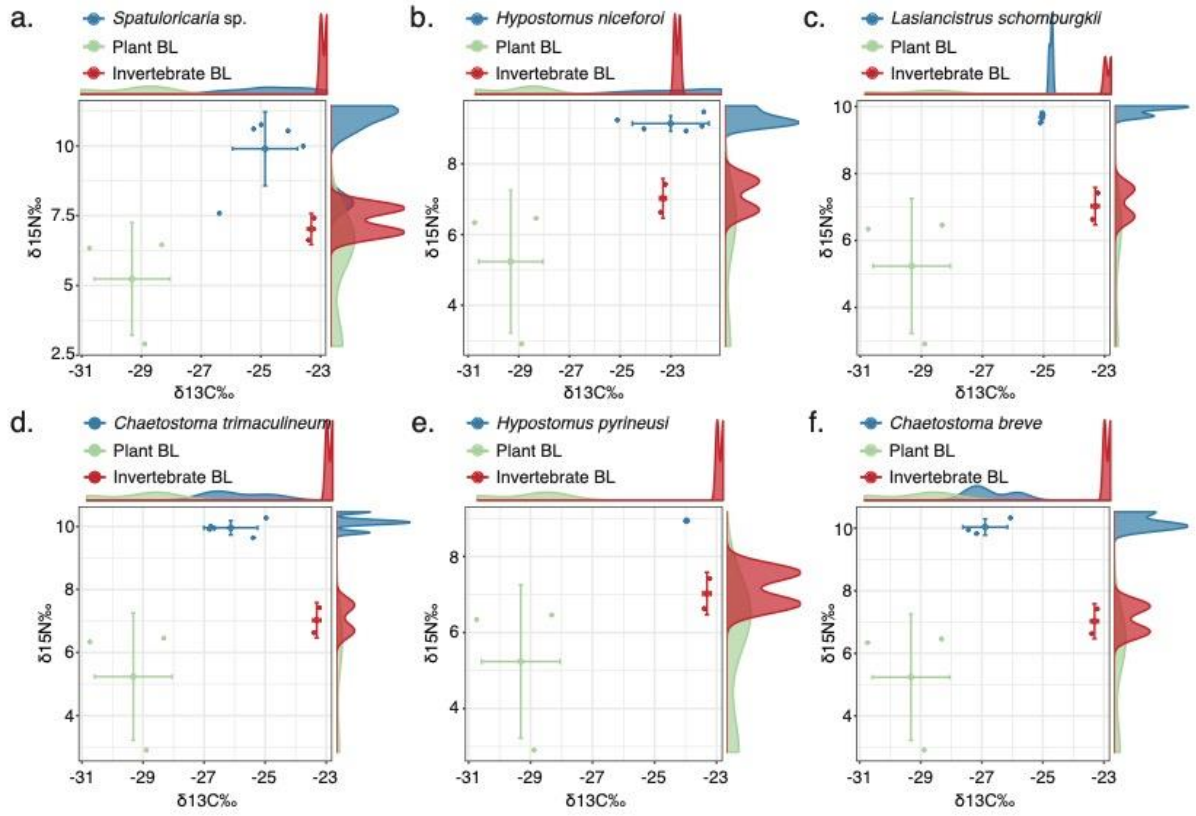

Fig. S3. Isotopic biplot of (a.) *Spatoloricaria* sp. (b.) *Hypostomus niceforoi* (c.) *Lasiancistrus schomburgkii* (d.) *Chaetostoma trimaculineum* (e.) *Hypostomus pyrineusi* and (f.) *Chaetostoma breve* for individuals from río Chimaya. Shading above and to the right of the plot show distribution of individuals.

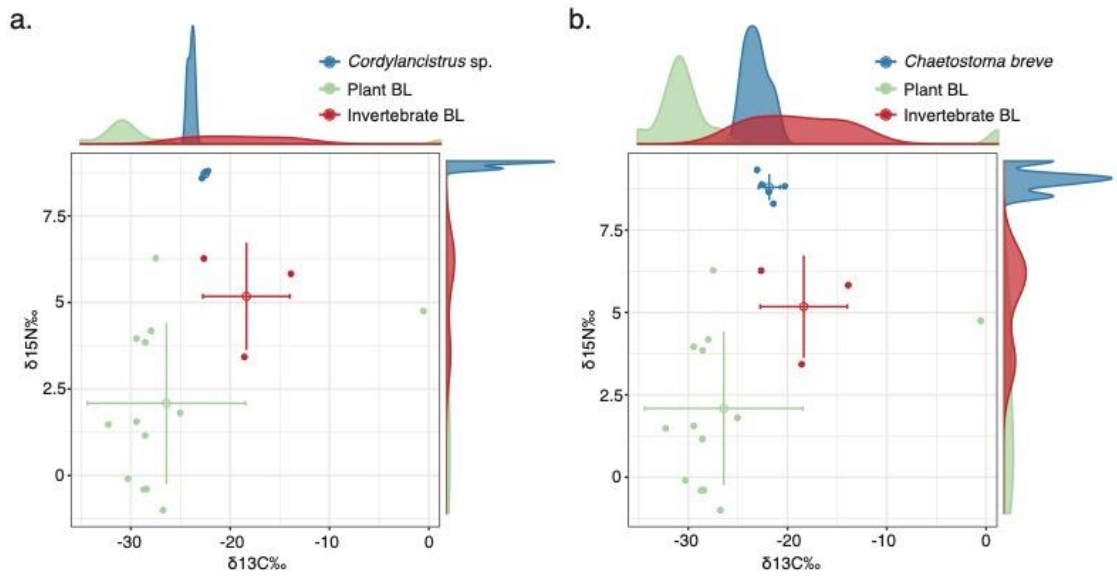

Fig. S4. Isotopic biplot of (a.) *Cordylancistrus sp.* and (b.) *Chaetostoma breve* for individuals from río Chinchipe. Shading above and to the right of the plot show distribution of individuals.

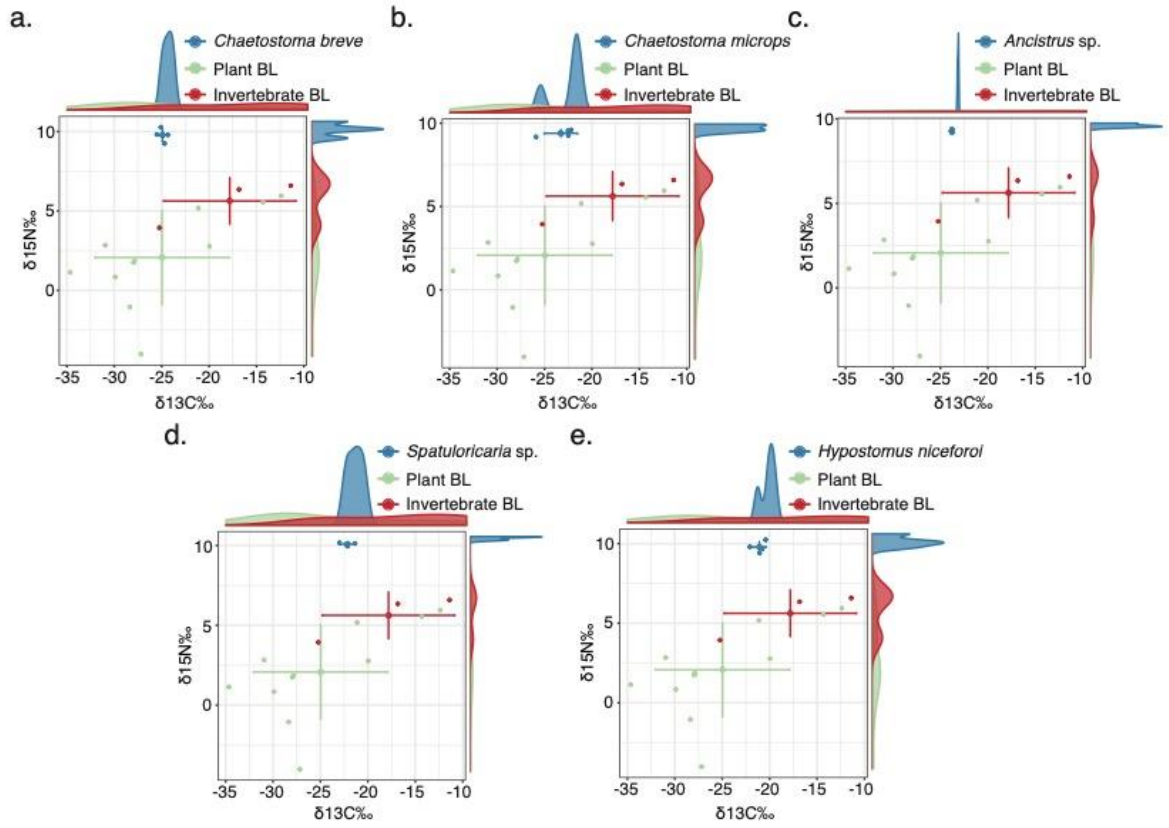

Fig. S5. Isotopic biplot of (a.) *Chaetostoma breve* (b.) *Chaetostoma microps* (c.) *Ancistrus* sp. (d.) *Spatoloricaria* sp. and (e.) *Hypostomus niceforoi* for individuals from río Utcubamba. Shading above and to the right of the plot show distribution of individuals.

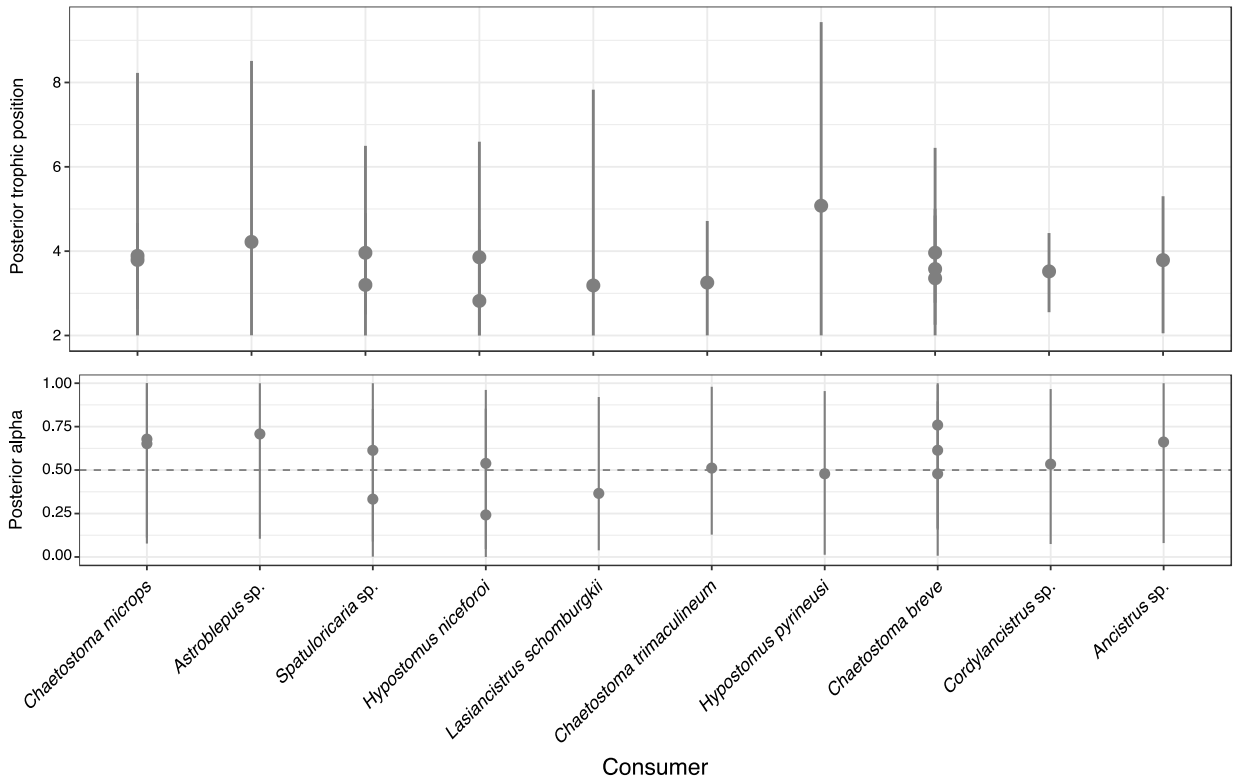

Fig. S6. Posterior trophic position and posterior alpha for consumers. Each point represents an individual with bars as credibility intervals (± 95%).